NASA
Technical
Memorandum

NASA TM-108434

DETAILED STUDY OF OXIDATION/WEAR MECHANISM IN LOX TURBOPUMP BEARINGS

By T.J. Chase and J.P. McCarty

Propulsion Laboratory
Science and Engineering Directorate

December 1993

NASA
National Aeronautics and
Space Administration

George C. Marshall Space Flight Center

MSFC - Form 3190 (Rev. May 1983)

REPORT DOCUMENTATION PAGE

Public reporting burden for this collection of information is estimated to average 1 hour per response, including the time for reviewing instructions, searching existing data sources, gathering and maintaining the data needed, and completing and reviewing the collection of information. Send comments regarding this burden estimate or any other aspect of this collection of information, including suggestions for reducing this burden, to Washington Headquarters Services, Directorate for Information Operations and Reports, 1215 Jefferson Davis Highway, Suite 1204, Arlington, VA 22202-4302, and to the Office of Management and Budget, Paperwork Reduction Project (0704-0188), Washington, DC 20503.

1. AGENCY USE ONLY (Leave blank)	2. REPORT DATE December 1993	3. REPORT TYPE AND DATES COVERED Technical Memorandum

4. TITLE AND SUBTITLE

Detailed Study of Oxidation/Wear Mechanism in Lox Turbopump Bearings

5. FUNDING NUMBERS

6. AUTHOR(S)

T.J. Chase* and J.P. McCarty

7. PERFORMING ORGANIZATION NAME(S) AND ADDRESS(ES)

George C. Marshall Space Flight Center
Marshall Space Flight Center, Alabama 35812

8. PERFORMING ORGANIZATION REPORT NUMBER

9. SPONSORING/MONITORING AGENCY NAME(S) AND ADDRESS(ES)

National Aeronautics and Space Administration
Washington, DC 20546

10. SPONSORING/MONITORING AGENCY REPORT NUMBER

NASA TM-108434

11. SUPPLEMENTARY NOTES
Prepared by Propulsion Laboratory, Science and Engineering Directorate.

*National Research Council

12a. DISTRIBUTION/AVAILABILITY STATEMENT

Unclassified—Unlimited

12b. DISTRIBUTION CODE

13. ABSTRACT (Maximum 200 words)

Wear of 440C angular contact ball bearings of the phase II high pressure oxygen turbopump (HPOTP) of the space shuttle main engine (SSME) has been studied by means of various advanced nondestructive techniques (NDT) and modeled with reference to all known material, design, and operation variables. Three modes dominating the wear scenario were found to be the adhesive/sheer peeling (ASP), oxidation, and abrasion. Bearing wear was modeled in terms of the three modes. Lacking a comprehensive theory of rolling contact wear to date, each mode is modeled after well-established theories of sliding wear, while sliding velocity and distance are related to microsliding in ball-to-ring contacts. Microsliding, stress, temperature, and other contact variables are evaluated with analytical software packages of SHABERTH™/SINDA™ and ADORE™. Empirical constants for the models are derived from NIST experiments by applying the models to the NIST wear data. The bearing wear model so established precisely predicts quite well the average ball wear rate for the HPOTP bearings. The wear rate has been statistically determined for the entire population of flight and development bearings based on Rocketdyne records to date. Numerous illustrations are given.

14. SUBJECT TERMS

angular contact bearings, wear modeling, cryogenic bearings, lox turbopump bearings, wear modes/mechanisms

15. NUMBER OF PAGES 115

16. PRICE CODE NTIS

17. SECURITY CLASSIFICATION OF REPORT	18. SECURITY CLASSIFICATION OF THIS PAGE	19. SECURITY CLASSIFICATION OF ABSTRACT	20. LIMITATION OF ABSTRACT
Unclassified	Unclassified	Unclassified	Unlimited

PAGE __ii__ INTENTIONALLY BLANK

TABLE OF CONTENTS

LIST OF ILLUSTRATIONS

LIST OF ILLUSTRATIONS (Continued)

LIST OF TABLES

TECHNICAL MEMORANDUM

DETAILED STUDY OF OXIDATION/WEAR MECHANISM IN LOX TURBOPUMP BEARINGS

I. PURPOSE OF THE STUDY AND MAJOR OBJECTIVES

The purpose of this study was to scientifically establish a viable wear model for the angular contact ball bearings operating in the liquid oxygen (lox) environment of the phase II (current flight configuration) high-pressure oxidizer turbopump (HPOTP) of the space shuttle main engine (SSME). This purpose has been accomplished in the three stages outlined below.

The goal of the first stage was to gain insight into physical phenomena occurring in these cryogenic bearings in flight service and to establish modes (mechanisms) of wear. Wear phenomenon of 440C angular contact ball bearings of the phase II HPOTP has been studied by means of various experimental analytical nondestructive techniques (NDT) described in detail elsewhere.[1] While most of the known modes of rolling contact bearing wear were evident on the ball and ring surfaces, the three modes dominating the wear scenario were found to be the adhesive/sheer peeling (ASP), oxidation, and abrasion.

The aim of the second stage was to mathematically model operation of the bearings in order to derive all static, kinematic, thermal, and dynamic quantities pertaining to wear modeling. This has been accomplished utilizing mathematical and numerical modeling shown below. Microsliding, stress, temperature, and other contact variables were evaluated with analytical software of SHABERTH™/ SINDA™ and ADORE™, all supplemented with pertinent engineering analyses.

In the third stage of this study, the aim was to propose a mathematical model of wear for the bearings and verify the model on the basis of fit with the statistical wear record. Bearing wear has been modeled in terms of the three modes named above and is shown in figures 1 through 4. Lacking a comprehensive theory of rolling contact wear to date, each mode has been modeled after well-known and established theories of sliding wear, while sliding velocity and/or distance has been related to microsliding in ball-to-ring contacts. Empirical constants for the models have been derived from the National Institute of Standards and Technology (NIST) experiments[2] by applying the models to the NIST wear data.

The bearing wear model, so established, predicts quite well the ball wear rate for the HPOTP bearings. The wear rate has been statistically determined for the entire population of flight and development bearings, based on Rocketdyne records to date.

II. BACKGROUND

There are ambiguities in tribology literature[3][4] regarding classification of wear. Wear terminology quite often reflects this situation by not having well-defined boundaries for such commonly used terms as "mode," "mechanism," and sometimes "process" of wear. Hereunder, the wear mechanism is a

means of removal of wear debris from the surface, and wear mode is a broader term which classifies wear with reference to its mechanism(s), occurrence, appearance, etc.

This study has confirmed the existence of the following generic wear modes acting simultaneously in phase II HPOTP bearings:

1. ASP

2. Oxidation

3. Abrasion

4. Fatigue

    a. Spalling (pitting)

    b. Flaking (delamination)

5. Gauging (plastic deformation)

6. Corrosion.

Preloaded angular contact ball bearings are commonly used in a variety of spacecraft applications, ranging from very light duties of controlling movement of shutters or pointing antennas, to the very heavy duty of supporting turbine rotors. Under the best of circumstances, these bearings can reliably support the combined radial and axial loads and accommodate the unavoidable thermal distortions of the space hardware over a wide range of operational variables in a light duty service, wherein loads and/or speeds are low.

Lubrication in rocket motors, and in outer space in general, is difficult because of the weight limitations which virtually eliminate all heavy auxiliary lubrication equipment like pumps, motors, sumps, etc., as well as the limitations imposed by the vacuum environment. With a few exceptions, liquid lubricants cannot be used. The most successful solid lubricants used in outer space are the filled polytetrafluoroethylene (PTFE), sputtered MoS_2, and ion-plated soft metals (e.g., Pb). Since solid lubricants cannot prevent the solid-solid interaction of the load bearing surfaces, a surface distress and resulting mechanical wear are unavoidable. Successful applications under these circumstances are the ones which result in manageable wear rates, in addition to satisfying various other requirements.

The phase II HPOTP bearings are lubricated with PTFE contained within the glass fiber reinforced cages. They operate at nearly 2 million DN (bearing pitch diameter (mm) by shaft speed (revolutions/minute)) in an environment of lox which precludes effective liquid film lubrication and imposes cryogenic temperatures, high thermal gradients, and heavy transient loads. In most other space applications, bearings operate well below 1 million DN.

Wear may be low in applications characterized by a low DN value and short or infrequent operation. However, a high DN value, heavy use, and a corrosive or contaminated environment tend to produce heavy wear. The useful life of phase II HPOTP bearings is limited to only two (or three) flights of the space shuttle, due to excessive wear.

2

Many technical issues related to the HPOTP bearings have been studied recently, ranging from performance and materials to a new cage design, testing, and optimization of race curvatures for heat generation and stress. Naerheim, et al.[5] have evaluated the maximum operating surface temperature of the bearings to be in the range of 600 °C, based upon the postmortem Cr/Fe ratio of oxides found on the wear tracks.

Failures of lubricated rolling bearings have been studied very extensively. Consequently, the combined body of knowledge on pitting, smearing, fretting, etc., is usually sufficient to design reliable bearing systems. However, wear of rolling element bearings remains largely unexplored in general, wear dynamics in particular, and participation of recognized modes of surface wear and effects of variables remained unknown until this publication.

III. BEARING ENVIRONMENT AND OPERATING CONDITIONS

A simplified cross section of the phase II HPOTP showing the main shaft support configuration is shown in figure 5. The bearings are of the type of separable angular contact ball bearings made of 440C stainless steel, have a customized internal geometry, and work in a back-to-back preloaded tandem. The bearing studied in this report is the second bearing from the left (marked 2). A carefully controlled axial preload is exerted by a custom design beam-spring placed between the outer rings of the bearings, as shown. Both bearings are cooled by the same steady stream of lox passing axially through them from the pump end, left to right.

Operating conditions for the No. 2 bearing of the phase II HPOTP are shown in table 1. The data listed in it are believed to average and approximate the overall conditions of operation. They do not represent a coherent set of recorded "test data," as most readers are accustomed to seeing in strictly controlled experiments, because each test specimen in this study comes from a different turbopump and a different flight of the space shuttle and not from a controlled tribology experiment.

Direct measurements for some variables listed in table 1 were impractical (e.g., loads) or even impossible (e.g., ball temperatures) to accomplish due to a lack of access to these bearings in the flight service and/or their explosive environment (lox). Also, there is no single source of information on which to rely in re-creating the conditions of operation. In various contractors reports, particular features are usually related to bearing malfunction and/or proposed remedies, while operational variables are treated as incidental information to the issues. Consequently, there is a considerable disagreement among experts on the operating conditions. This is an open issue in itself, too broad for an exhaustive treatment, and out of scope in this context. The "best" plausible estimates are shown, considering all the available information, in order to provide a feel for the extraordinary severity of this application. The following comments are offered in order to provide more insight.

The high power (30,000 hp), high speed (30,000 r/min), and short duration of the HPOTP work cycle renders many important variables of its operation highly time dependent due to thermal transients inherent in the turbopump and/or those which are generated in the bearing itself. Likewise, bearing operating conditions, except for the shaft speed, are transient. Also, individual variations in some component dimensions of the HPOTP, despite a strict scrutiny and individual certification, are probably sufficient to substantially influence bearing loads, especially if thermal effects are considered. Thus, a considerable scatter of bearing operation variables is unavoidable.

The angular velocity and acceleration of the bearing's inner ring are virtually certain and precise, although they vary with the power level. The oxygen environment is believed to locally change from liquid (lox) to gas (gox) on and near the hot surface tracks of balls. This upsets the heat balance within the bearing and is believed a major cause of a potential thermal instability.

Surface temperatures (table 1) of the race tracks and balls may reach 600 °C,[5] while the outer race surface temperature in contact with the seat may remain at –150 °C. A thermally induced radial expansion of the inner ring and balls may cause a loss of a bearing operational clearance, resulting in an interference overload which generates more heat, and further thermal expansion, until the ongoing and thus accelerated wear processes restore the bearing clearance.

The initially applied coating of dry lubricant film wears away very rapidly, within a few seconds perhaps, and the PTFE transfer film produced by attrition from the ball retainer seats is not quite sufficient to keep the ball wear in check. Since solid lubricants cannot prevent the solid-solid interaction of the load bearing surfaces, a surface distress and the resulting mechanical wear are unavoidable. This is a favorite wear scenario for the HPOTP bearings related to their cooling and lubrication.

The radial load consists of constant and alternating parts (fig. 5). The constant radial load is due to the rotor weight and static fluid pressure. The alternating part is induced by the fluctuating fluid pressure and a dynamic unbalance. The axial load consists of a design preload component (approximately 1,000 lb) which is superposed on the load components due, primarily, to differential axial displacements of the bearing caused by the combined actions of the balance piston (fig. 5), thermal expansion, and changes in fluid pressure.

IV. MATERIALS

Cryogenic applications like this one require careful selection of materials for rolling bearing components. High strength, hardness, fracture toughness, and stress corrosion resistance are the usual prerequisites for rolling elements and rings which must withstand repetitive applications of high contact stresses and the resulting wear and rolling contact fatigue. In addition, dimensional stability at cryogenic and elevated temperatures, corrosion resistance, and compatibility with the lox environment, as measured by the NASA auto-ignition test, are required. The AISI 440C martensitic stainless steel (table 2) satisfies these requirements reasonably well except for the wear resistance. All bearings analyzed here are made of the 440C steel.

Other materials involved include Armalon™ ball retainers, solid lubricants, and lox. They influence lubrication and cooling and, thereby, affect all tribological features of this very unique and technologically critical application. The phase II HPOTP bearings are prelubricated with a coating of dry lubricant and dry lubricated with a transfer film of PTFE from the ball retainers. The retainers are made of Armalon™, a composite material mode of polytetrafluoroethylene (PTFE, Teflon™) which is reinforced with glass fibers whose chemistry is composed of the following oxides: 54.3 percent Si, 17.2 percent Ca, 15.2 percent Al, 8 percent Bo, 4.7 percent Mg, and 0.6 percent Na. Load-bearing surfaces of these bearings are initially sputter-coated and cured with a dry lubricant composed of 65 percent MoS_2 and 35 percent Sb_2O_3.

Undesirable, yet present on most bearing surfaces, as shown by the EDT diagrams, are the contaminant particles carried by the stream of lox flowing through the bearings. Lox is the process fluid of the HPOTP as well as the coolant for the bearings.

V. ANALYTICAL MODELING OF MAJOR WEAR MODES

A. On Wear Modeling in General

Wear and friction are not intrinsic material properties. They are both interrelated and both depend on conditions and environment at contact. More often than not, operating conditions in a microscale define the tribological behavior of a mechanical contact subjected to friction and wear, i.e., made to sustain external or internal load and relative motion simultaneously. Wear relies upon three phases of particle generation[6] whose relative duration, and importance to modeling, varies from one engineering application to another. These are:

Phase I – particle detachment

Phase II – third body life

Phase III – particle ejection.

Particle detachment mechanisms, and related wear modes which are usually named after these mechanisms, are relatively well known, and mathematical models exist for these few situations in which particle detachment dominates the wear scenario. Modeling wear from first principles, i.e., from the basic laws of physics, is not yet possible for the majority of engineering applications in which all the three phases named above participate to a significant degree. Empirical models are successfully used to predict wear rates in these situations, but their applicability must always be ascertained and experimentally derived constants obtained before these models can render reliable predictions. Wear maps have become quite fashionable recently[2] since wear modes significantly influence the wear rates.

B. Major Wear Modes Established for the Phase II Turbopump Bearings

The initial stage of this study[7] revealed that wear of the turbopump bearings involves several modes whose dynamics varies with time of a work cycle. While most of the known modes of rolling contact bearing wear were evident on the ball and ring surfaces, the three modes dominating the wear scenario were found to be ASP, oxidation, and abrasion. Thus, the dominant modes are modeled according to the well-known empirical equations, and allowance is made for wear dynamics by incorporating intermediate dimensional, friction, and other changes into the operational SHABERTH™/SINDA™ model of a representative bearing. Averaged operational variables derived with SHABERTH™ are then used to model the bearing wear.

C. Adapting Models of Sliding Wear for Ball Bearings Operating in Lox

Wear of rolling element bearings is a marginal issue in general tribology[8] because ample fluid film lubrication and cleanliness, in the sense of exclusion of contaminants, are the usual prerequisites of most engineering applications, and consequently, rolling contact wear is very low. Rolling contact wear should not be confused with rolling contact fatigue[9] which continues to receive a lot of attention as a major and unavoidable problem of rolling bearings. There has been no model available for rolling contact wear applicable to the case under consideration, but, fortunately, suitable models for the particular wear modes of sliding wear corresponding to those established for the turbopump bearings have been identified and subsequently adapted, as shown below.

1. <u>ASP Mode—Microfatigue</u>. The ASP mode relies upon propagation of cracks in a direction parallel to the surface of contact and wear debris generated[7] in contact resembles microscopic flakes (fig. 4). Thus, it is a form of microfatigue wear whose best mathematical model to date has been given by Kragelsky.[10] His original equation is shown below:

$$I = K \, 15^{0.4 \, t^*} \, aK'pE^{0.5 \, t^*-1} \, (t/a')^{0.5} \, (kf'/s)^{t^*}$$

I = linear wear rate in meters per meter of sliding distance

K = contact geometry/fatigue factor, usually = 0.2

K' = correction factor for load variation

k = contact stress/frictional fatigue parameter, usually = 3 for elastic materials

t = molecular component of friction stress (normal load extrapolated to 0)

t^* = exponent of Wohler's equation, empirical variable

a = asperity overlap coefficient, usually = 0.5 for run-in surfaces

a' = hysteretic loss factor, evaluated = 0.05 for the case

p = average contact pressure

E = Young's modulus of elasticity

f' = molecular component of the coefficient of friction, empirical variable

s = ultimate tensile stress .

This equation has been modified using the original Kragelsky's intermediate forms and nomenclature in order to better suit this study. The modified equation is shown below. It renders similar results in this case, and it is simpler to use.

$$I = K \, 15^{1/2} \, 2^{1/2V} \, \theta^{3/8} \, a^{2+1/2V} \, (t/a')^{3/8} \, p^{-1/4} \, (kf'p'/s)^{t^*} \, ,$$

where

V = asperity interaction parameter, empirical variable evaluated = 3.5

p' - real average contact pressure, statistical surface roughness variable

$\theta = (1-u^2)/E$, composite elastic constant

u = Poisson's ratio .

All remaining symbols are identical to those in the original equation.

A number of variables and constants for the successful application of Kragelsky's model to the ASP mode have been derived from the NIST report by Slifka[11] whose experimental setup, extent of study, and a representative worn specimen are shown in figure 6.

Kinematic relations of wear scar growth on the ball in Slifka's experiment (fig. 7) have been studied in order to prorate various variables entering Kragelsky's equations for the ASP mode. Also, a coherent wear scenario has been created in order to make Slifka's wear rates compatible with those of Kragelsky, as shown below.

Wear scenario of NIST experiment to evaluate A, q, and I

- With $U = 0.5$ m/s and $N = 150.6$ N, both constant, the final wear scar area A and pressure q depend on sliding distance L. The linear rate of wear I stays nearly independent of q.

- A coherent wear scenario for the entire matrix of empirical variables is produced by assuming the same sliding distance L. Let $L = 240$ m.

- A, q, and I have been computed using Slifka's figure 5(c) and the kinematic relations of wear scar growth shown earlier.

- The selected data for U and N are the closest values for the variables in the operational range of the HPOTP pump end bearing.

From Slifka's figure 5(c):

Ball Temperature (°C)	–200	0	200	400	600
Volume Wear (mm³/m) ($\times 10^{-3}$)	0.8	1.2	3.6	10	30
Computed:					
Scar Area (mm²)	2.396	2.935	5.083	8.472	14.674
Final Pressure (MPa)	62.847	51.314	29.628	17.776	10.263
Linear Wear Rate "I" (multiply by 10^{-7})	6.67	8.18	14.17	23.61	40.89

Contact pressures p^* (Hertzian), q (final), p (average), and p' (real) evaluated for the ASP mode from Slifka's experimental data using the wear scenario are shown below.

Load (kg(N)	4.56 (44.7)	15.36 (150.6)	36.40 (357)
p^* (kg/mm²)	280.4	420.8	561.1
q (kg/mm²)	2.0	3.3	4.4
p (kg/mm²)	94.5	141.9	189.2
p' (kg/mm²)	136.6	144.6	196.1

$$p^* = 0.616\ (P(E/d)^2)^{(1/3)}\ ,\quad q = P/A\ ,\quad p = (2p^*/3+q)/2$$

$$p' = 0.616\ (R^*/r^*\theta^{-2})(/4)^{0.43}\,p^{0.14}$$

where

R^* = combined roughness parameter in μm

r' = combined waviness parameter in μm

P = normal load

E = Young's modulus

d = ball diameter .

The molecular component of friction stress "t" has been derived using the Kragelsky's definition and methodology in application to Slifka's frictional data as shown in figure 8. The average value in the range interest is

$$t = 19.84\ \text{kg/mm}^2\ .$$

The molecular component of the coefficient of friction "f' (T)" for the range most applicable to turbopump bearings under consideration has been derived using the Kragelsky's definition and Slifka's experimental data as shown in appendix A. The average value in the range of interest is

$$f' = 0.12\ .$$

The frictional fatigue component "t^*" in Kragelsky's equation for the ASP mode has been evaluated from the Slifka's data as shown below. The average value in the range of interest is:

$$t^* = 6.71\ .$$

With

$$K^* = K15^{(1/2)}2^{(1/(2v))}\theta^{(3/8)}a^{(2+1/(2v))}(t/a')^{(3/8)}\ ,$$

the modified Kragelsky's equation for the ASP mode is

$$I = K^*p^{(-1/4)}\ ((kf'/s)p')^{t^*}\ .$$

Solve for

$$t^* = (\ell n l)+(\ell n p)/4-\ell n K^*)/(\ell n k-\ell n s+\ell n f'+\ell n p')\ ,$$

K^* = 0.0360485, constant in Slifka's experiment

T	–200	0	200	400	600
t^*	17.50	10.48	7.11	5.23	4.02

Average value for the range 0 to 600 °C:

$$t^* = 6.71$$

This value is within the range quoted by Kragelsky for hard steel. No other data are available.

2. Oxidation Mode. Oxidation wear has been modeled by Quinn,[12] and although this study[7] did not show explicit "oxidative only" wear debris as such, due to technical limitations of the available microscopy, it nevertheless provided enough secondary evidence to include oxidation as one of the three dominant modes of wear for the HPOTP bearings which operate in the lox environment.

Using Slifka's experimental data and Quinn's model for the range of operational variables of interest (appendix B), the final equations are:

$$w' = 8.1224 \times 10^{-7} \times (A/V) \exp(-64.896/T), \text{ for } T < 350 \text{ °C} ,$$

$$w'' = 25.9631 \times 10^{-6} \times (A/V) \exp(-1{,}613.71/T), \text{ for } T > 350 \text{ °C} ,$$

where

w ($m^3 m$) = volumetric wear per unit sliding distance

T (K) = contact temperature at asperity level

V (m/s) = sliding velocity

A (m^2) = real area of contact.

3. Abrasion Mode. Abrasion has been confirmed in many forms on ball and ring surfaces of the HPOTP bearings.[7] This mode was first introduced by Holm and Archard.[13] Using Slifka's data (appendix C) for the range of variables of interest in this study, the wear coefficient is:

$$k = 3.10 \times 10^{-6} .$$

D. Conversion of Linear Wear Rate "*l*" and Average Pressure "*p*"

Empirical wear rate equations are directly applicable to the configurations resembling those for which they were derived, i.e., pin-on-disk in which the wear scar area remains constant and so does the average pressure. In ball bearings, wear surface is spread over the entire ball surface, contact area continuously varies, and so does the contact pressure. Linear wear "*l*" and average pressure "*p*" are therefore prorated as shown in figure 9.

E. Evaluating Operational Variables With SHABERTH™/SINDA™

1. What SHABERTH™ is All About. SHABERTH™ is a mainframe computer program for the analysis of steady-state and transient thermal performance of shaft-bearing systems. It was developed in 1976 by SKF, Inc., for the U.S. Air Force/Navy under contract No. F33615–76–C–2061/N62376–76–MP–00005.[14] A PC version[15] of the program (adapted for NASA-MSFC by SRS Technologies of

Huntsville, AL, under contract No. NAS8-37350) was used in this project, with due consideration for correctness and accuracy by referencing the mainframe SHABERTH™.

PC/SHABERTH™ proved to be as potent a tool for the analysis of bearing statics and kinetics versus the operational, design, and materials variables as its mainframe predecessor as far as requirements of this project are concerned. However, modeling of ball/separator contact with either version of SHABERTH™ produced unrealistically high contact forces because of the intrinsic inaccuracies of the "quasi-static" modeling concept utilized in the program. SHABERTH™ has been coupled with SINDA™, a software package for fluid and thermal analysis, in order to more precisely model bearing operating temperatures.

2. <u>Input Data and Related Matters</u>. SHABERTH™ requires a great deal of input data on bearing/shaft/housing design, tolerances, materials, surface finish, friction, lubricant, elastic and thermal properties, loading and operating conditions, etc. Depending on the application, the number of these input data varies from about 70 upwards, and all of them affect SHABERTH™ operation, accuracy, and eventually output, just as they do operation of bearings, but to a varying degree.

Detailed discussion of the input data is omitted here for brevity. It can be found in reference 14, but all data which were used here are listed in appendix D, explicitly on the front page of each computer printout and again at the end of the printout in a coded "card input" form. Input data are compatible with NASA and its contractor's reports, including reference 15. Printouts have been curtailed to the essential information only because their original version runs into an excessive number of pages, exceeding 50 per case studied. Although many more cases were run in order to gain confidence in the system as well as to get the feel for the relative importance of specific variables, only the three cases representative of the study are shown in appendix D and discussed in detail below.

3. <u>Computational Modes</u>. Solution level 2 has been chosen because friction effects on ball position in the track envelope are important in this case. One degree of freedom mode for the inner ring has been used because it provided the most reliable and consistent results.

4. <u>Input Variables</u>. Most of the input data remained invariable in this study, except for bearing loads, clearance, ball size, raceway curvatures, temperatures, friction coefficient, and contact angle, all of which were varied in accordance with bearing wear history, which was interactively customized until proper convergence. For example, decrease of bearing preload due to wear of balls and raceways has been accounted for.

5. <u>Input Sensitivity and Output Verification</u>. A large number of computer trials had to be run before loads converged to the desired magnitude, as can be seen in tables 3 and 4 and in figure 10. This anomaly is caused by the sensitivity of SHABERTH™ to the load input when it is operated in a "single bearing" mode which was chosen here for the simplicity of interpretation of results, free of destructive design influences. The case selected as valid has been highlighted in the tables and pointed to in the figure. The selection is based on two criteria in effect simultaneously, i.e., minimum departure from the assigned loads after conversion and minimum frictional energy dissipation in both ball/ring contacts combined. The second criterion is related to the authors' understanding of dynamic simulation of mechanical systems, namely that a numerical solution to this "quasi-static" formulation of bearing dynamic equilibrium in SHABERTH™ has to be more accurate for a case with lower energy dissipation for a given set of input data.

10

6. **Results and Their Relevance to Modeling**. Computer printouts shown in appendix D contain most of the information on static, kinematic, and kinetic quantities describing operational characteristics of the modeled bearings, but they are not easy to read unless augmented with graphical illustrations and direct comparisons. The following figures and tables are provided in order to make up for this deficiency.

Table 5 gives a direct comparison of the two distant cases regarding wear modeling, namely the one right after the start of work cycle (named "base isothermal") and the other after 100 min of cycling (named "worn thermal"). The effect of wear is visible in all quantities. The quantities listed in the table heading from left to right are the following:

Azimuth in degrees (AZIM) = peripheral coordinate of the ball

Spin/roll ratio × 1,000 (SPIN/R)

Ball excursion in micrometers (B.EXC.)

Cage force in Newtons (CAGE F.)

Ball angular velocity about x axis in rad/s (WX)

Ball angular velocity about y axis in rad/s (WY)

Cage angular velocity in rad/s (Wcage)

Contact angle at the outer ring in degrees (C.NGL./O)

Contact angle at the inner ring in degrees (C.NGL./I)

Contact force at the outer ring in Newtons (C.F./O)

Contact force at the inner ring in Newtons (C.F./I)

Hertzian contact stress at the outer ring in MPa (HRTZ/O)

Hertzian contact stress at the inner ring in MPa (HRTZ/I).

Figure 11 shows variation of contact angles for inner and outer rings around the bearing. The range of variation exceeds 30° for the inner contact and 25° for the outer. The effect of wear lowers contact angles and the range of variation.

Figure 12 shows variation of ball angular velocity components with reference to the cage around the bearing. It can be seen that a ball slows down rolling and accelerates spinning directly under the load vector on the "unloaded" side (180°). The effect of wear decreases the range of variation.

Figure 13 shows variation of contact load and contact stress in the outer ring/ball contact around the bearing. Both quantities have two relative maximums on the load vector of which the one on the loaded side (0°) is larger. The range of variation is insignificantly lower for the worn bearing.

Figure 14 shows variation of contact load and contact stress in the inner ring/ball contact around the bearing. Both quantities have two relative maximums on the load vector of which the one on the loaded side (0°) is larger. The range of variation is insignificantly lower for the worn bearing. It can be seen that both stress and load are higher in the inner contact in comparison to the outer (fig. 13).

Figure 15 shows variation of cage force, ball excursion, and spin-to-roll ratio around the bearing. The effect of wear is a lowering of all these quantities, especially ball excursion as expected. It is worthy of note that cage force reaches the same order of magnitude as the contact force at the races, which is incorrect and due to obvious shortcomings of the SHABERTH™ model. When modeled with the ADORE™ software, cage pocket/ball contact forces are lower by nearly two orders of magnitude.

Figure 16 shows maximum variation of "pV," the pressure and sliding velocity product, along the major axis of the ellipse of contact with the outer ring of a ball located directly under the load vector on the loaded size (azimuth 0). Since contact pressure has a semielliptic distribution with a maximum at the center of contact, it can be envisioned that microsliding in contact is mostly due to the symmetric interfacial rolling slip (Heathcote effect, compare with reference 16). This distribution pattern is typical for the outer ring.

Figure 17 shows maximum variation of "pV," the pressure and sliding velocity product, along the major axis of the ellipse of contact with the inner ring of a ball located directly under the load vector on the "unloaded" side (azimuth 180). Since contact pressure has a semielliptic distribution with a maximum at the center of contact, it can be envisioned that microsliding in contact is mostly due to spin (compare references 17 and 18). This distribution pattern is typical of the inner ring.

Figure 18 shows a "pV" profile along the major axis of contact with the outer ring of a ball located at 150° from the load vector for a "new" and a "worn" bearing. The effect of wear is significant, as can be seen by a direct comparison, at 150° but not elsewhere (compare fig. 19).

Figure 19 shows a "pV" profile along the major axis of contact with the inner ring of a ball located at 150° from the load vector for a "new" and a "worn" bearing. The effect of wear is visible but small as can be seen in comparison to figure 18.

Power dissipation in the outer ring/ball contact along the major axis of contact ellipse due to friction and microsliding is shown for seven consecutive ball positions around the bearing in figures 20 and 26 and again, combined, in figure 27. As mentioned earlier in the context of the "pV," interfacial slip friction is dominant here which creates a peculiar symmetric double-hump distribution. Figure 28 shows a pie chart comparison of power dissipation in contact with the inner ring of a ball traveling around the bearing. It can be seen that balls located along the load vector dissipate most of the frictional energy (because they carry most of the bearing load).

Effect of wear on frictional power dissipation in contact of ball No. 1 with the outer ring is shown in figure 29. It is visible.

Power dissipation in the inner ring/ball contact along the major axis of contact ellipse due to friction and microsliding is shown for seven consecutive ball positions around the bearing in figures 30 to 36 and again, combined, in figure 37. As mentioned earlier in the context of the "pV," spin friction is predominant here which creates a peculiar asymmetric double-hump distribution. Figure 38 shows a pie chart comparison of power dissipation in contact with the inner ring of a ball traveling around the

bearing circumference. It can be seen that balls located along and near the load vector on the "loaded" side dissipate most of the frictional energy.

Effect of wear on frictional power dissipation in contact of ball No. 1 with the inner ring is shown in figure 39. It is visible.

Figure 40 shows combined frictional power dissipation in contact due to interfacial (Heathcote) slip and spin around the bearing for the inner and the outer contacts. It can be seen that most energy is dissipated in the inner contact and directly under the load vector, i.e., at 0° (360°) and 180°.

Combined frictional losses for all balls on one side of the bearing are laid out at their respective locations along the track for the outer ring in figure 41, and for the inner ring in figure 42. Since wear volume is to a certain scale proportional to the frictional power loss for the particular location, the outer envelope of this graph can be shown to represent a wear path profile for the location on the ring, inner or outer, assuming that operating conditions of a bearing remain unchanged over the course of the entire work cycle. Measured wear profiles[19] seem to show the same characteristic features as those shown in figures 41 and 42. The same cannot be said about the wear path profile on a ball because it can roll and spin simultaneously, thereby exposing a new part of its surface with each passage. However, the authors' own experience[1] and literature[20] strongly suggest that a wear path does stabilize on the ball surface. Thus, to a different scale, these graphs can be representative of ball wear track profiles as well.

A computed wear track developed along the bearing circumference for both inner and outer rings is shown in figure 43. Together with an appropriately scaled wear profile from figures 41 and 42, it can be used to compute the volume of wear debris removed from the rings if there is no back and forth transfer of wear debris between balls and rings.

F. Averaged Data for the Three Representative Cases

Not all the data presented so far enter analytical expressions for computation of wear, and none can be applied directly. Since balls rotate, spin, and revolve simultaneously while remaining in contact with both rings, average rather than instantaneous values of pressure, sliding distance, and sliding velocity are needed for the final wear analysis. The average values have been computed by integration over the contact areas of a ball with the inner and outer rings, and averaging them for the 12 ball positions around the bearing. These data are shown in table 6.

G. Computing Ball Wear According to the Combined Model

Wear of balls has always been so much greater than wear of rings of the HPOTP flight bearings that the latter has usually been ignored. This model pertains to diametral ball wear due to all the three dominant modes, i.e., ASP, oxidation, and abrasion, simultaneously acting in contact of all balls with both rings of a bearing. Wear of balls due to their contact with pockets of the ball retainer is not considered here because it is insignificant under typical circumstances.

The most essential features of the combined model of ball bearing wear are summarized below:

1. Arithmetic average of all three modes computed independently of each other is assumed representative of ball wear.

2. Empirical constants come from modeling the NIST experimental data with applicable theories of sliding wear for the wear modes experimentally established.[7]

3. Data entering mathematical models of the modes come from SHABERTH™/SINDA™ and/or analytical modeling of bearing operational variables as shown in this study.

4. No field data on actual bearing wear or statistical correction factors are used to predict ball wear.

The predicted diametral ball wear for phase II HPOTP No. 2 bearing in micrometers is shown below versus the flight time, i.e., service time in minutes of operation at the nominal speed of 30,000 inner ring rotations per minute. In the tabulation, all the three modes of wear are shown in vertical columns, next to each other, with the arithmetic average of the three being shown in the last column.

Time (min)	Abrasion	Oxidation	ASP	Average
1	0.5	0.1	0.1	0.2
10	3.8	3.3	6.7	4.6
100	38.0	48.9	70.2	52.4

Since it was not feasible to experimentally determine actual participation of the individual modes in the overall wear picture, the average value of all the three modes has been taken as representative. Also, in deriving empirical coefficients from the NIST data, each mode has been treated as acting alone and therefore representative of the entire wear process in NIST experiments, each time.

Interestingly, each of the mathematical models used to describe the particular modes modeled here, in the literature[10 12 19] have been shown as the models, although it is obvious[2] that various modes always contribute in the overall wear processes.

VI. STATISTICAL ANALYSIS OF FIELD DATA AND APPRAISAL OF BALL WEAR MEASUREMENT METHODOLOGY

A. Statistical Analysis of Field Data

A complete wear record for all flight (F) and development (D) bearings of standard phase II HPOTP configuration and design, and covering a period of 1987 to 1993 is shown in table 7. It is based on the Rocketdyne data for the same period. Bearings whose ball wear record was incomplete are not included in table 7, and not considered in the subsequent analysis.

For the purpose of visual comparisons, the wear record of flight bearings, development bearings, and combined (F and D) bearings is displayed in figures 44, 45, and 46, respectively. It can be seen that flight bearings show diametral ball wear ranging from zero (replaced with 0.1 for graphical purposes) to 20 micrometers. Seemingly, wear is independent of service time, but these bearings were not allowed to work more than two or three flight cycles, and wear was low so measurement errors were large. It should be obvious that zero wear corresponding to a flight time of up to 35 min of service is anomalous and inconsistent with the nature of wear processes. It can possibly be explained in terms of measurement

14

errors and related metrology, as shown later in this report. Development bearings, in contrast to flight bearings, show a wide spread of diametral wear which is quite clearly dependent on the flight time. The combined record of flight and development bearings will be used as background to wear modeling later.

Histograms on diametral wear data of the phase II HPOTP bearings and the standard configuration development bearings are shown in figures 47 and 48, respectively. Table 8 gives numerical values of the quantities displayed in figures 47 and 48. It can be seen that wear histograms are representative of the bearing population shown in table 7 and figures 44 to 46. A trend of wear growth with service time is also quite clearly visible despite the logarithmic scale for the ordinate axis.

Statistical and linear regression analysis of the bearing wear record has been carried out with a commercial package provided with QUATTRO PRO™ and checked for the accuracy of its most relevant findings. The results are displayed in tables 9 and 10. The latter is for the "forced 0" mode, meaning that a regression line is required to pass through 0, as expected for the type of physical phenomenon being modeled (i.e., wear is zero at service time being zero). It can be seen that for the most meaningful case of combined flight and development bearings, the "X coefficient" is nearly 0.91 with the "standard error of coefficient" equal to 0.16 (case of "forced 0"). All this can be translated into a nearly straight proportionality of diametral ball wear in micrometers to service time in minutes with an error margin of 16 percent. However, the analytical expressions relating ball wear to service time are nonlinear, as can be seen in the preceding sections.

B. Appraisal of Ball Wear Measurement Methodology

Diametral ball wear is a minute quantity to measure, it is not easy to establish a common reference basis for measurements, balls are difficult to position relative to a common reference basis, and wear patterns vary from ball to ball.[7] Also, in the case of bearings which were examined after only a few minutes of service time, wear can be visible on a microscopic scale quite well, but it cannot be detected with a standard micrometer because it is not uniform over the ball surface. These and other difficulties of wear measurement and their reflection in the wear record have prompted the authors to take a closer look at some of the available bearing specimens whose wear record was available from the existing data bases.

Ball diameter of worn bearings has been measured with a mechanical micrometer accurate to within 0.00001 inch immediately following careful calibration at room temperature. An average of three measurements for each ball taken at three approximately perpendicular axes, related to the wear pattern on the ball, was considered to represent ball diameter, just as it was supposed to have been done at Rocketdyne, whose ball wear record is shown in table 7. All balls have also been weighed using a digital scale of 0.01-mg resolution, an average of five measurements considered as the weight.

Results of these measurements are shown in figures 49 through 52 for representative bearings whose wear record was extremely low (0.0000 inch), medium (0.0003 inch), heavy (0.0004 inch), and very heavy (exceeding 0.0010 inch). For ease of plotting only, ball diameter in micrometers minus 11,000 was multiplied by five to be of magnitude compatible with ball weight in milligrams minus 5,000.

It can be seen that "diameter/weight" correlation is pretty good, except for the case of very heavy wear. A relatively poor correlation in the last case is caused by the uneven wear pattern (a single wide

wear track on the ball) whose effect upon diametral wear measurement is obscured by the wear metrology outlined above although its effect on ball weight is not.

This simple experiment indicates that diametral ball wear record may not be a very accurate measure of ball wear. Also, it seems that weight measurement is less prone to errors caused by uneven wear, effects of thermal distortions, and linear resolution of the available micrometers.

VII. COMPARISON OF RESULTS OF WEAR MODELING TO WEAR STATISTICS

Combined results of wear modeling for the No. 2 bearing of the phase II HPOTP of the space shuttle main engine are shown in figure 53 in the form of bars on the background of actual statistical data for the bearing. It can be seen that there is excellent agreement of the two, considering that usually prediction of wear differs from the actual field data on wear by an order of magnitude or more. It seems that such good agreement was possible to achieve only because of the availability of the NIST data on wear of the 440C under the conditions closely resembling those of the phase II HPOTP.

REFERENCES

1. Chase, T.J.: "Wear Modes Active in Angular Contact Ball Bearings Operating in Liquid Oxygen Environment of the Space Shuttle Turbopumps." Lubrication Engineering, vol. 49, No. 4, 1993, pp. 313–322.

2. Slifka, A.J., Morgan, T.J., Compos, R., and Chaudhuri, D.K.: "Wear Mechanism Maps of 440C Martensitic Stainless Steel." Wear, vol. 162–164, 1993, pp. 614–618.

3. Lancaster, J.K.: "Material Specific Wear Mechanisms: Relevance to Wear Modeling." Wear, vol. 141, 1990, pp. 159–183.

4. Keer, L.M., and Worden, R.E.: "A Qualitative Model to Describe the Microchipping Wear Mode in Ceramic Bearings." Tribology Trans., vol. 33, 1990, pp. 411–417.

5. Naerheim, Y., Stocker, P.J., and Lumsden, J.B.: "Determination of the SSME High Pressure Oxidizer Turbopump Bearing Temperature." Advanced Earth-to-Orbit Technology, NASA, Huntsville, AL, CP 3012, vol. 1, 1988, pp 88–101.

6. Godet, M., Bertier, Y., Lancaster, J., and Vincent, L.: "Wear Modeling: Using Fundamental Understanding or Practical Experience?" Wear, vol. 149, 1991, pp. 325–340.

7. Chase, T.J.: "Wear Mechanisms Found in Angular Contact Ball Bearings of the SSME's Lox Turbopumps." NASA TM-103596, Marshall Space Flight Center, AL, July 1992.

8. Quinn, T.J.F.: "Role of Wear in Failure of Common Tribosystems." Wear, vol. 100, 1984, pp. 399–436.

9. Czyzewski, T.: "Influence of a Tension Stress Field Introduced in the Elastohydrodynamic Contact Zone on the Rolling Contact Fatigue." Wear, vol. 34, 1975, pp. 201–212.

10. Kragelsky, I.V., and Alisin, V.V.: "Friction, Wear, and Lubrication (Tribology Handbook)." Mir Publishers (in English), Moscow, 1981.

11. Slifka, A.J.: "Coefficient of Sliding Friction of 440C as a Function of Temperature." NIST progress report to Materials and Processes Laboratory of NASA-MSFC, December 18, 1990, Boulder, CO.

12. Hong, H., Hochman, R.F., and Quinn, T.J.F.: "A New Approach to the Oxidational Theory of Mild Wear." STLE Transactions, vol. 31, 1988, pp. 71–75.

13. Archard, J.F.: "Wear Theory and Mechanisms." Wear Control Handbook, ASME, Eds. M.B. Peterson and W.D. Winer, New York, NY, 1980.

14. "Computer Program Operational Manual on SHABERTH™, a Computer Program for the Analysis of the Steady-State and Transient Thermal Performance of Shaft-Bearing Systems." Technical Report AFAPL-TR-76-90, SKF Industries, Inc., King of Prussia, PA, October 1976.

15. "SSME Bearing and Seal Tested Data Compilation, Analysis and Reporting, and Refinement of the Cryogenic Bearing Analysis Mathematical Model." Report SRS/STD-PR92-5891, SRS Technologies, Huntsville, AL, August 1992.

16. Leveille, A.R., Zupkus, C.J., and Ludwig, H.R.: "Prediction of Ball-Spin and Interfacial Slip Friction From Room to 2,500 °F." ASLE Transactions, vol. 9, 1966, pp. 361–371.

17. Jones, A.B.: "Ball Motion and Sliding Friction in Ball Bearings." ASME Trans., Journal of Basic Engineering, vol. 81, 1959, pp. 1–12.

18. Halling, J.: "The Microslip Between a Ball and Its Track in Ball-Thrust Bearings." ASME Trans., Journal of Basic Engineering, vol. 88, 1966, pp. 213–220.

19. Bunting, B.G.: "Wear in Dry-Lubricated, Silicon Nitride, Angular-Contact Ball Bearings." Lubrication Engineering, vol. 46, 1990, pp. 745–751.

20. Kawamura, H., and Touma, K.: "Motion of Unbalanced Balls in High-Speed Angular Contact Ball Bearings." Journal of Tribology, vol. 112, 1990, pp. 241–247.

Table 1. Operating conditions.*

Radial load	2.56 to 7.13 (kN)
Axial load	6.46 to 10.24 (kN)
Angular velocity, inner ring (IR)	3,141.6 (rad/s)
Angular acceleration (IR) (average, start to FPL)	785.4 (rad/s^2)
Environmental (coolant) 2.1 kg/s axial mass flow rate, pressure, and temperature	lox 2 MPa and −162 °C
Lubricant: transfer film from ball separator seats dry film lube coating on race tracks	solid PTFE Mo-S$_2$/Sb$_2$O$_3$
Hertz contact stress (IR)	2.5 to 3.5 (GPa)
Surface temperture: ball and inner race track	up to 600 °C
outer ring on O.D., approximately	−150 °C

*Compiled by the author from NASA and contractors' files.

Table 2. AISI 440C stainless steel.

	Fe	Cr	C	Mo	Mn	Si	Ni	Cu	P
Composition* (in percent weight)	80.25	16.95	1.04	0.50	0.36	0.49	0.28	1.04	0.02

Properties† (hardened and tempered)	
Tensile strength	1.965 GPa (285 ksi)
0.2-percent yield strength	1.896 GPa (275 ksi)
Percent elongation (in 50 mm)	2
Percent reduction of area	10
Hardness (Rockwell C)	57 (to 61)

*Supplier information.
†T. Baumeister (editor): "Marks' Standard Handbook for Mechanical Engineers," (eighth edition).

Table 3. SHABERTH™ convergence to target loads "M," an example.

SHABERTH™ Convergence to Target Loads "M" $FX = 8,230$ (N), $FR = 4,760$ (N), OP.CL. = 148 (μm), C.NGL. = 25.19						
Run No.	Input Fx	Input Fy	Output Fx	Output Fr	Fr.loss/OR	Fr.loss/IR
1	8,230	4,760	8,253	4,824	2,025	5,281
2	8,230	4,759.9	8,131	5,083	4,966	6,395
3	8,230	4,759.99	8,307	4,737	2,280	5,371
4	8,230	4,760.1	7,846	5,052	1,989	5,279
5	8,230	4,760.11	8.094	4,879	2,663	5,040
6	8,229.99	4,760	7,983	4,938	3,072	6,292
7	8,229.9	4,760	8,033	4,978	2,462	5,477
8	8,230.1	4,760	8,362	4,733	1,777	5,187
9	8,230.11	4,760	8,289	4,864	4,213	6,428
10	8,229.99	4,759.99	8,252	4,803	2,016	5,119
11	8,230	4,699	8,099	4,841	3,266	5,679
12	8,230	4,700	8,026	4,301	64,170	46,650
13	8,230	4,701	8,210	4,758	2,200	5,558
14	8,230	4,700.9	7,990	4,850	2,159	5,151
15	8,231	4,699	8,387	4,648	2,843	5,689
16	8,231	4,700	8,534	4,600	3,685	7,190
17	8,231	4,701	8,248	4,747	1,955	5,137
18	8,231	4,702	7,058	5,050	32,490	20,790
19	8,232	4,699	8,068	4,790	4,655	5,377
20	8,232	4,700	8,256	4,730	2,007	5,124
21	8,232	4,701	8,239	4,734	2,164	5,098
22	8,232	4,702	8,208	4,824	1,975	5,166
23	8,232	4,700.9	8,513	4,650	1,899	5,384
24	8,230.8	4,699	7,999	4,767	3,648	7,112
25	8,230.8	4,700	8,141	4,808	2,119	5,090
26	8,230.8	4,701	8,238	4,755	1,820	5,135
27	8,230.8	4,702	8,182	4,850	2,244	5,508
UNITS	(N)	(N)	(N)	(N)	(W)	(W)

Table 4. SHABERTH™ convergence to target loads "*M*," listing of data for quantities displayed in figure 9.

Const. is 4,760 for lines 1 to 10, and 4,700 for lines 11 to 27					
INPUT		OUTPUT			
Fx-8,230	Fy-Const.*	delFx(%)	delFr(%)	Pwr.loss/OR (kW)	Pwr.loss/IR (kW)
0	0	0.28	1.34	2.025	5.281
0	−0.1	−1.2	6.79	4.966	6.395
0	−0.01	0.94	−0.48	2.28	5.371
0	0.1	−4.67	6.13	1.989	5.279
0	0.11	−1.65	2.54	2.663	5.04
−0.01	0	−3	3.74	3.072	6.292
−0.1	0	−2.39	4.58	2.462	5.477
0.1	0	1.6	−0.57	1.777	5.187
0.11	0	0.72	2.18	4.213	6.428
−0.01	−0.01	0.27	0.9	2.016	5.119
0	−1	−1.59	1.7	3.266	5.679
0	0	−2.48	−9.64	64.17	46.65
0	1	−0.24	−0.04	2.2	5.558
0	0.9	2.92	1.89	2.159	5.151
1	−1	1.91	−2.35	2.843	5.689
1	0	3.69	−3.36	3.685	7.19
1	1	0.22	−0.27	1.955	5.137
1	2	−10	6.09	32.49	20.79
2	−1	−1.97	0.63	4.655	5.377
2	0	0.33	−0.63	2.007	5.124
2	1	0.11	−0.5	2.164	5.098
2	2	−0.27	1.34	1.975	5.166
2	0.9	3.44	−2.31	1.899	5.384
0.8	−1	−2.81	0.15	3.648	7.112
0.8	0	−1.08	1.04	2.119	5.09
0.8	1	0.1	−0.11	1.82	5.135
0.8	2	0.58	1.89	2.24	5.508

Table 5. Comparison of the "base isothermal" and "worn thermal" cases.

BASE ISOTHERMAL, CASE "M"

AZIM.	SPIN/R	B.EXC.	CAGE F.	WX	WY	Wcage	C.NGL/O	C.NGL/I	C.F/O	C.F/I	HRTZ/O	HRTZ/I
0	138.3	-31.9	19	8,632	2,600	1,320	19.9	21.8	3,294	3,002	2,610	3,513
30	160.1	-807	479	8,600	2,785	1,321	21.2	24.1	2,481	2,197	2,375	3,166
60	268.1	-1,402	832	8,675	3,044	1,349	22.7	31.2	1,150	840	1,838	2,298
90	454.5	-1,485.8	881	9,012	3,325	1,404	24.4	41.6	686	406	1,547	1,803
120	506.6	-1,080.8	641	8,615	4,397	1,429	31.7	49.9	877	579	1,679	2,030
150	445	-502.1	298	7,800	5,588	1,432	40.6	54.4	1,367	1,111	1,947	2,523
180	418.3	48.5	29	7,397	5,884	1,424	45	55.5	1,661	1,428	2,077	2,743
210	449.7	570.9	338	7,754	5,453	1,427	41.2	54.2	1,317	1,070	1,923	2,491
240	514.8	1,110.4	659	8,594	4,353	1,426.5	31.2	50.1	908	625	1,699	2,083
270	467.4	1,503.6	892	9,028	3,293	1,403.4	23.3	42.1	768	473	1,606	1,898
300	269.4	1,384.5	821	8,595	3,009	1,346	22.7	31.2	1,139	847	1,832	2,305
330	161.1	749.1	444	8,587	2,773	1,319.5	21.1	24.1	2,483	2,196	2,376	3,166
360	138.3	-31.9	19	8,632	2,600	1,320	19.9	21.8	3,294	3,002	2,610	3,513
	× 1,000	(μm)	(N)	(r/s)	(r/s)	(r/s)	(deg)	(deg)	(N)	(N)	(MPa)	(MPa)

WORN THERMAL, CASE "M"

AZIM.	SPIN/R	B.EXC.	CAGE F.	WX	WY	Wcage	C.NGL/O	C.NGL/I	C.F/O	C.F/I	HRTZ/O	HRTZ/I
0	133.2	0.2	0.2	8,679	2,449	1,316	18.8	20.7	3,241	2,959	2,566	3,486
30	153.4	686.6	407.2	8,641	2,622	1,318	20	22.8	2,542	2,252	2,367	3,183
60	238.4	-1,266	750.6	8,630	2,925	1,334	22.4	29.1	1,293	1,011	1,889	2,338
90	409.6	-1,273	755.3	9,022	3,196	1,410	23.5	38.8	854	545	1,645	1,984
120	439.1	-930.5	551.9	8,459	4,252	1,390	30.8	46.3	917	654	1,685	2,108
150	393.8	-534	316.6	7,828	5,338	1,418	38.7	50.7	1,341	1,140	1,912	2,537
180	400	67.6	40.1	7,686	5,473	1,423	42.2	52	1,674	1,398	2,059	2,715
210	410.5	570	338.1	7,832	5,132	1,402	39.1	50.5	1,336	1,100	1,910	2,506
240	459.8	996	590.7	8,580	4,110	1,411	30.5	46.4	956	659	1,708	2,113
270	402.5	1,269	752.7	8,789	3,204	1,378	23.6	38.8	833	558	1,632	1,999
300	238.8	1,125	667.4	8,694	2,954	1,344	22.2	29.2	1,314	1,008	1,900	2,435
330	147.7	647.6	384.1	8,629	2,690	1,324	19.9	22.8	2,546	2,254	2,368	3,184
360	133.2	0.2	0.2	8,679	2,449	1,316	18.8	20.7	3,241	2,952	2,566	3,486
	× 1,000	(μm)	(N)	(r/s)	(r/s)	(r/s)	(deg)	(deg)	(N)	(N)	(MPa)	(MPa)

Table 6. Data modeled with SHABERTH™/SINDA™.

The following data were used to compute the linear wear "*I*."
o/i = outer/inner contact

Time (min)	1	10	100
Sliding velocity (*o/i*) (m/s)	0.335/1.159	0.361/1.083	0.414/1.152
Sliding distance (*o/i*) (m)	20.1/69.54	216.6/649.8	2,484/6,913
Contact area (*o/i*) (mm^2)	1.099/0.680	1.101/0.68	0.968/0.575
Hertz pressure (*o/i*) (MPa)	1,959/2,502	1,966/2,554	1,725/2,136

Note: The values shown have been averaged for the 12 balls around the bearing.

Table 7. Wear record for flight (*F*) and development (*D*) bearings of the standard phase II HPOTP configuration for the 1987–1993 period.

HPOTP Phase II Bearing Wear (Rocketdyne Record 1987–1993)				
Unit	Configuration	Time (min)	No. 1 Wear (μm)	No. 2 Wear (μm)
6001R1	F	4.2	0	0
2029	F	4.85	5.1	6.4
2029?	F	4.9	5.1	7.6
6009R1	F	4.95	2.5	2.5
2421	F	5	2.5	2.5
6502R1	F	5.05	5.1	10.2
2221R1	F	5.05	2.5	2.5
2325R2	F	7	12.7	10.2
2028	F	7.3	0	0
4306	F	7.5	2.5	5.1
2123R2	F	8.7	2.5	2.5
4402R3	F	8.8	2.5	2.5
2205	F	8.8	0	0
2224R1	F	8.8	5.1	5.1
4402R1	F	8.8	7.6	10.2
2322	F	8.9	5.1	7.6
4011R1	F	9.1	7.6	7.6
6702	F	9.1	15.2	15.2
6602R1	F	9.1	2.5	5.1
4206	F	9.1	0	0
4007R1	F	9.1	7.6	7.6
2125R1	F	9.1	0	0
6202R1	F	9.1	0	0
4202R1	F	10.9	2.5	5.1
4005	F	12	0	0
4406R3	F	13.5	2.5	0
6102R1	F	13.6	5.1	2.5
2122R1	F	13.6	5	2.6
2422R2	F	13.8	5.1	7.6
2026R1	F	14	0	5.1
2324R5	F	14.9	2.5	5.1
2522R2	F	15.8	7.6	7.6
2223R1	F	17.4	5.1	7.6
2222R1	F	17.4	0	0
4105R1	F	17.4	0	2.5
4406R1	F	17.8	2.5	7.6
6302R1	F	17.8	2.5	5.1
4302R1	F	17.8	0	5.1
2321R2	F	18.8	10.2	5.1
2324R2	F	20.4	0	5.1
2424R5	F	20.4	2.5	2.5
2124R2	F	21.5	5.1	5.1
4106R1	F	21.8	2.5	2.5
2025R1	F	21.8	7.6	7.6
2121R1	F	21.9	5.1	5.1
4305R1	F	22.3	5.1	5.1
4008R3	F	23.6	2.5	2.5
9109R1	F	25.7	10.2	5.1
2425R2	F	26.3	5.1	7.6
2305R3	F	27.3	5.1	5.1
2225R3	F	27.8	7.6	5.1
4107R3	F	27.8	0	10.2

Table 7. Wear record for flight (*F*) and development (*D*) bearings if the standard phase II HPOTP configuration for the 1987–1993 period (continued).

HPOTP Phase II Bearing Wear (Rocketdyne Record 1987–1993)				
Unit	Configuration	Time (min)	No. 1 Wear (μm)	No. 2 Wear (μm)
4205R3	F	28.6	5.1	10.2
6003R3	F	28.7	7.6	7.6
2323R4	F	28.8	5.1	7.6
2126R4	F	29.2	7.6	5.1
4009R3	F	30.4	5.1	7.6
4502R3	F	30.9	2.5	5.1
2027R3	F	30.9	2.5	5.1
4010R4	F	31.2	5.1	10.2
2226R4	F	32.3	2.5	7.6
6402R3	F	34.1	7.6	5.1
2024	F	34.6	2.5	5.1
6002R1	F	34.6	0	5.1
2023	F	36.1	2.5	10.2
2521R2	F	45.3	5.1	17.8
2129	F	66.4	10.2	10.2
9209R3	F	71.2	5.1	17.8
4204R3	D	1.7	5.1	2.5
0507	D	5	2.5	2.5
9505	D	9.7	0	0
0607R2	D	16.8	33	0
2315	D	31.6	2.5	27.9
0810	D	34	0	2.5
4104R1	D	34.7	2.5	2.5
2215R2	BK1	39.7	7.6	55.9
0307R2	D	41.2	0	12.7
2315R1	D	49.4	5.1	86.4
4201R1	D	52.8	2.5	12.7
9808R2	D	56.4	12.7	12.7
4301R2	D	65.3	0	20.3
0607	D	67.8	66	185.4
0810R1	D	69.4	5.1	53.3
2510	D	69.8	315	78.7
2510R1	D	70.4	5.1	106.7
9311R6	D	78.1	7.6	17.8
4101	D	79.8	132.1	457.2
2317R1	D	84.1	0	40.6
2215R1	BK1	86.4	5.1	76.2
4004R1	D	89.3	17.8	53.3
9505R2	D	96	0	10.2
0307R4	D	97.2	185.4	762
4204R1	D	107.5	0	25.4
0510	D	113.8	7.6	40.6
2118R4	D	116.3	10.2	10.2
9908R2	D	118.4	10.2	221
4204R2	D	132.5	7.6	48.3
4304R3	D	133	15.2	88.9
9311R2	D	151.4	12.7	71.1
0407R5	D	161	12.7	10.2

Table 8. Wear histograms data of ball wear for the phase II HPOTP (*F*) and development (*D*) bearings for the 1987–1993 period.

Updated record on ball wear of the phase II HPOTP 45-mm bearings (1987–1993)

MARK	INTERV	Frequency			Average Wear					
		D	*F*	*F&D*	No. 1 *D*	No. 2 *D*	No. 1 *F*	No. 2 *F*	No. 1 *F&D*	No. 2 *F&D*
5	<10 min	3	23	26	2.5	1.7	4	4.8	3.83	4.44
20	10/30	1	33	34	33	0	4.1	5.1	4.95	4.95
40	30/50	6	10	16	3	32.2	3.03	6.11	3.02	15.89
60	50/70	6	1	7	66.9	60.5	10.2	10.2	58.8	53.31
80	70/90	6	1	7	28	125.3	5.1	17.8	24.73	109.94
100	90/110	3	0	3	61.8	265.9	0	0	61.8	265.9
120	110/130	3	0	3	9.3	90.6	0	0	9.3	90.6
140	>130	4	0	4	12.1	54.6	0	0	12.1	54.6

Table 9. Linear regression analysis of the 1987–1993 ball wear data with QUATTRO PRO™, 99 DOF.

Bearing No. 1 Flight		Bearing No. 2 Flight	
Regression Output:		Regression Output:	
Constant	3.256811211	Constant	2.741475141
Std. Err. of Y Est.	3.264953839	Std. Err. of Y Est.	3.362692183
R Squared	0.030114481	R Squared	0.259865045
No. of Observations	68	No. of Observations	68
Degrees of Freedom	66	Degrees of Freedom	66
X Coefficient(s)	0.043414	X Coefficient(s)	0.150359
Std. Err. of Coef.	0.030327	Std. Err. of Coef.	0.031235
Bearing No. 1 Development		Bearing No. 2 Development	
Regression Output:		Regression Output:	
Constant	20.76916456	Constant	24.91610536
Std. Err. of Y Est.	66.56687996	Std. Err. of Y Est.	151.8615966
R Squared	0.003695111	R Squared	0.043808517
No. of Observations	32	No. of Observations	32
Degrees of Freedom	30	Degrees of Freedom	30
X Coefficient(s)	0.0951066	X Coefficient(s)	0.761866
Std. Err. of Coef.	0.2848534	Std. Err. of Coef.	0.649847
Bearing No. 1 Flight and Development		Bearing No. 2 Flight and Development	
Regression Output:		Regression Output:	
Constant	2.170343408	Constant	−7.60069182
Std. Err. of Y Est.	37.47813839	Std. Err. of Y Est.	85.34034054
R Squared	0.059451386	R Squared	0.15872466
No. of Observations	100	No. of Observations	100
Degrees of Freedom	98	Degrees of Freedom	98
X Coefficient(s)	0.2582488	X Coefficient(s)	1.016182
Std. Err. of Coef.	0.1037612	Std. Err. of Coef.	0.236272

Table 10. Linear regression analysis of the 1987–1993 ball wear data with QUATTRO PRO™, 98 DOF (forced zero).

Bearing No. 1 Flight		Bearing No. 2 Flight	
Regression Output:		Regression Output:	
Constant	0	Constant	0
Std. Err. of Y Est.	3.72171779	Std. Err. of Y Est.	3.675989
R Squared	−0.27933455	R Squared	0.102125
No. of Observations	68	No. of Observations	68
Degrees of Freedom	67	Degrees of Freedom	67
X Coefficient(s)	0.1589123	X Coefficient(s)	0.247582
Std. Err. of Coef.	0.0192856	Std. Err. of Coef.	0.019049
Bearing No. 1 Development		Bearing No. 2 Development	
Regression Output:		Regression Output:	
Constant	0	Constant	0
Std. Err. of Y Est.	66.29116117	Std. Err. of Y Est.	149.9033
R Squared	−0.02100425	R Squared	0.037253
No. of Observations	32	No. of Observations	32
Degrees of Freedom	31	Degrees of Freedom	31
X Coefficient(s)	0.3093513	X Coefficient(s)	1.018996
Std. Err. of Coef.	0.1386086	Std. Err. of Coef.	0.313434
Bearing No. 1 Flight and Development		Bearing No. 2 Flight and Development	
Regression Output:		Regression Output:	
Constant	0	Constant	0
Std. Err. of Y Est.	37.31965551	Std. Err. of Y Est.	85.07662
R Squared	0.05787268	R Squared	0.155443
No. of Observations	100	No. of Observations	100
Degrees of Freedom	99	Degrees of Freedom	99
X Coefficient(s)	0.2882873	X Coefficient(s)	0.910985
Std. Err. of Coef.	0.0723631	Std. Err. of Coef.	0.164964
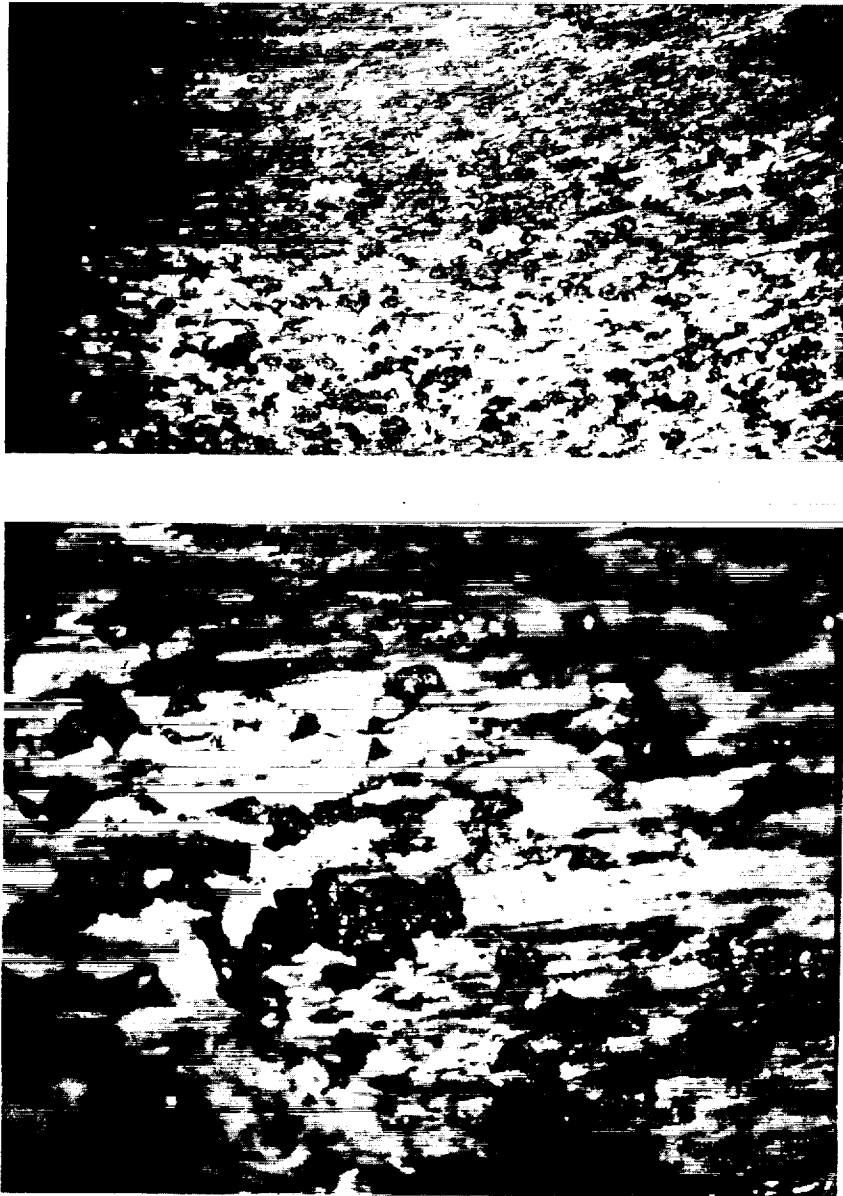
Figure 1. ASP (microfatigue) mode of wear. Ball surface of a heavily worn bearing No. 352. Note many surface cracks and wear debris. Optical microscopy (magnification: ×200 top, ×1,000 bottom).
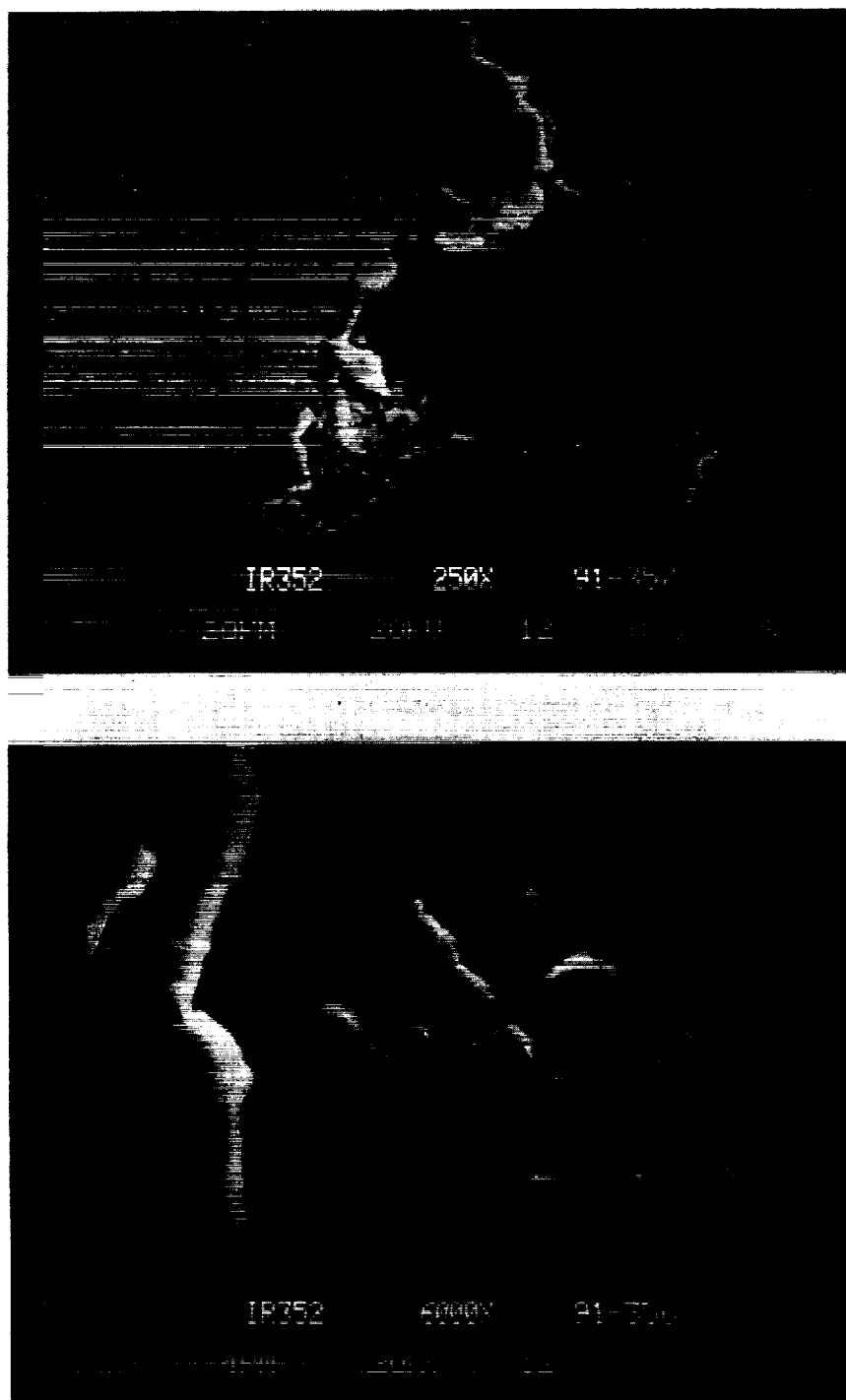
Figure 2. ASP (microfatigue) mode of wear. Wear track of a heavily worn inner ring or bearing No. 352. Scanning electron microscopy.
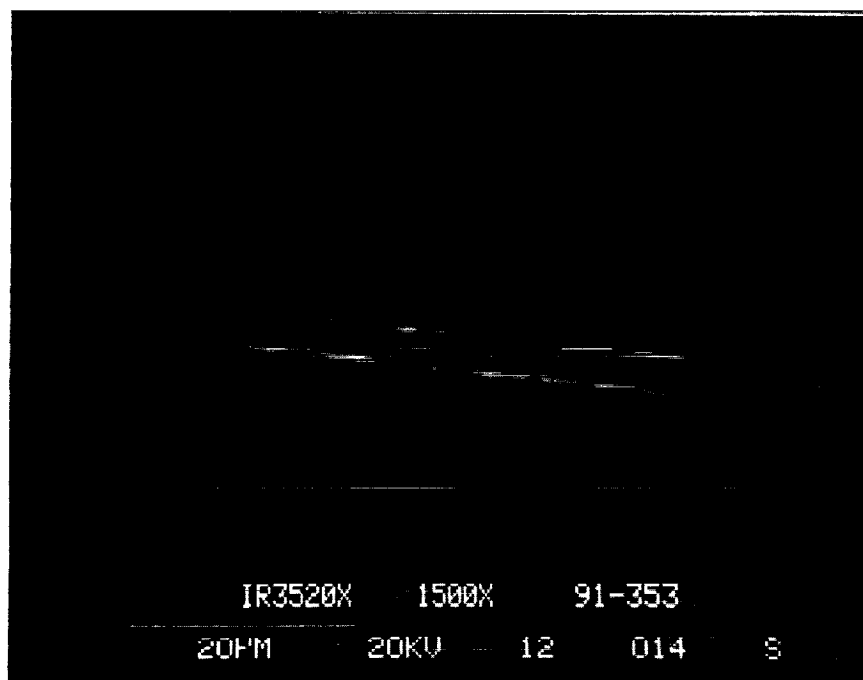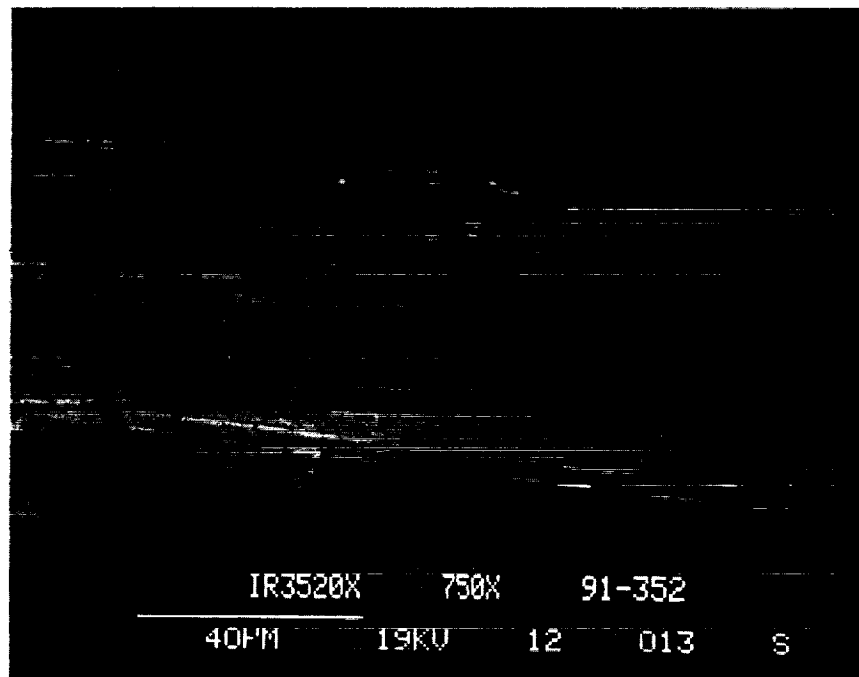
Figure 3. Abrasion mode of wear. Wear track of a heavily worn inner ring of bearing No. 352. Scanning electron microscopy.
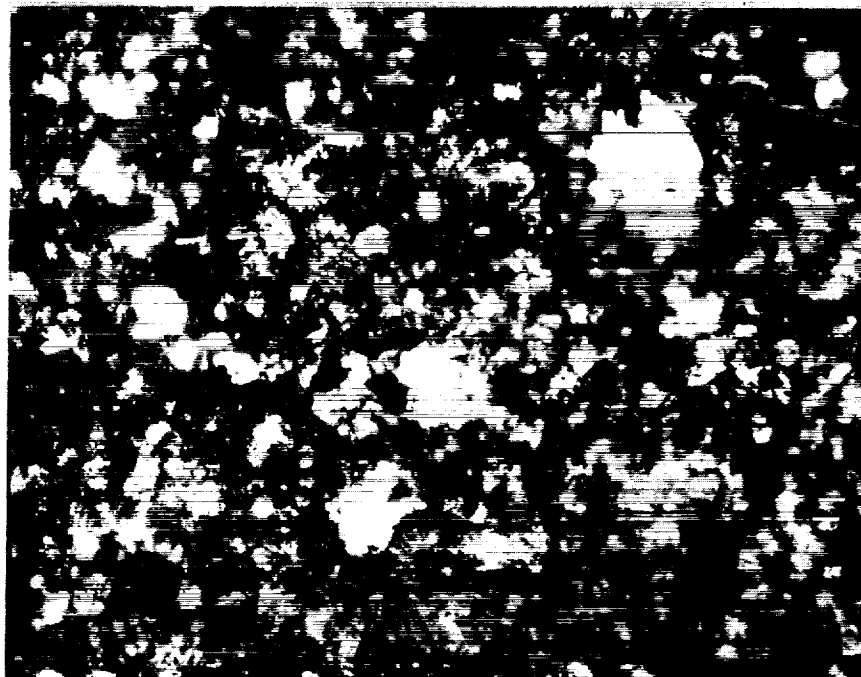
Figure 4. Wear debris collected from the NASA-MSFC's "Bearing, Seal, and Materials Tester (BSMT)." Note numerous thin flakes and broken pieces of glass fibers.
Optical microscopy (× 100).
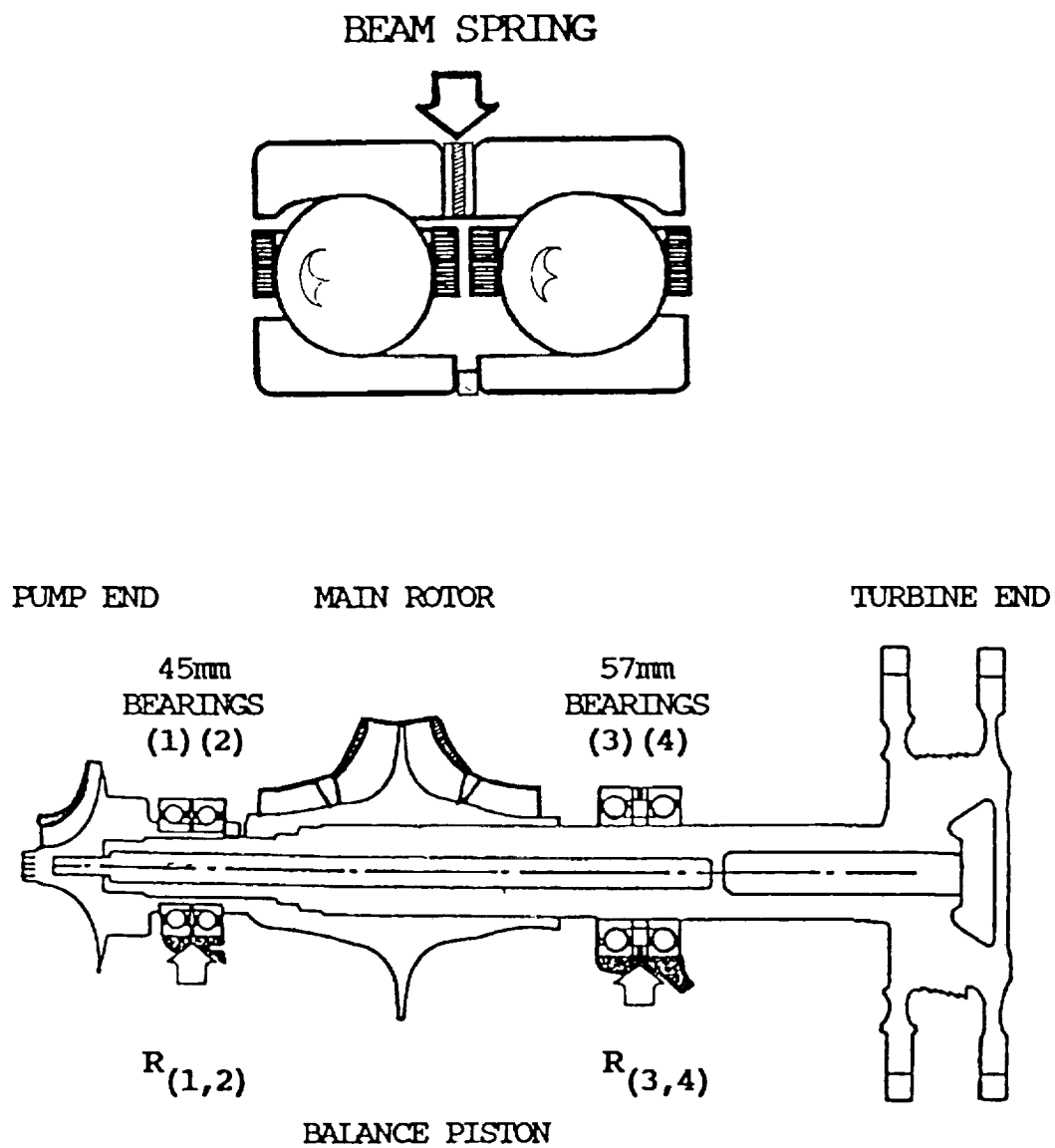
Figure 5. HPOTP shaft support configuration and bearing preload arrangement. The "balance piston" design is supposed to balance major axial loads on the shaft.

Deriving empirical variables from the NIST(Slifka) raw data on sliding friction and wear of 440C balls/440C flats in gox

Load range: 5.6 to 357[N], velocity range: 0.5 to 2[m/s], temp. range: -200 to 600 [C]
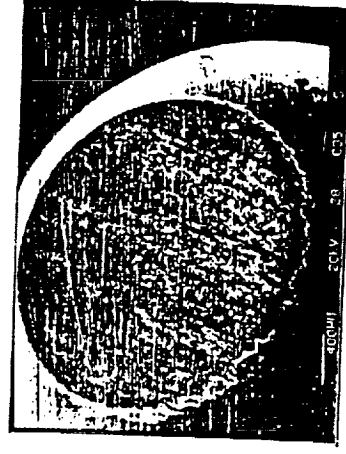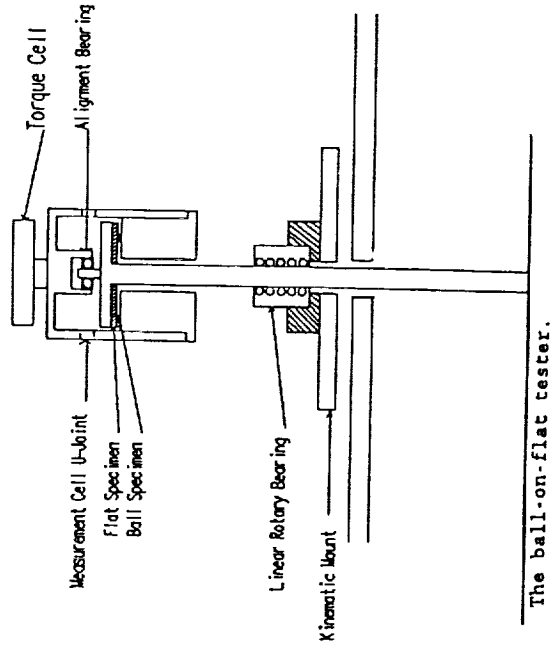
Wear scar on the ball specimen

Experimental set-up

Torque Cell

Alignment Bearing

Measurement Cell U-Joint

Flat Specimen

Ball Specimen

Linear Rotary Bearing

Kinematic Mount

The ball-on-flat tester.

Figure 6. Experimental setup, extent of study and a representative worn specimen, from the NIST report by Slifka.[11]

Kinematic relations of wear scar growth on the ball

H Wear scar area "A" and volume "V" are proportional to the max. scar depth "H"
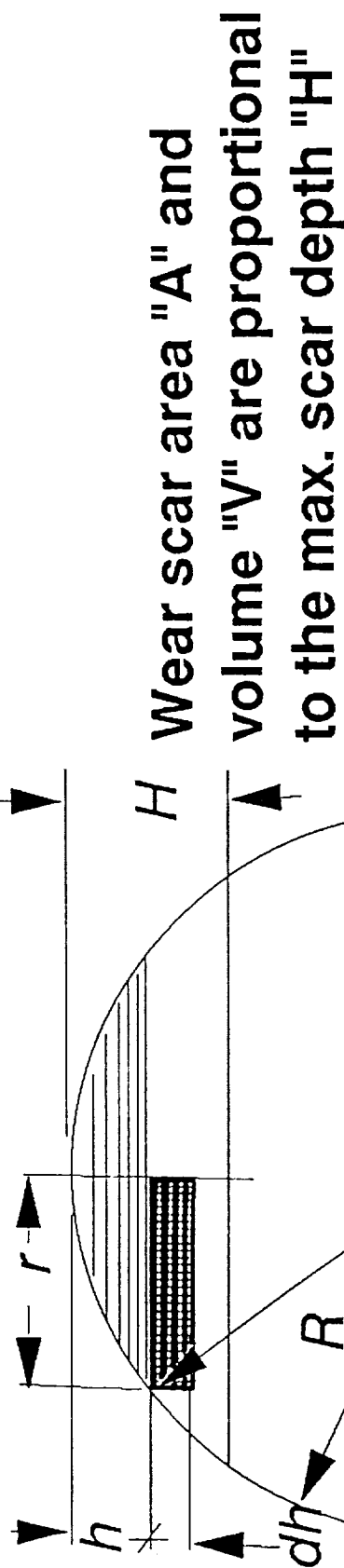
$$R^2 - 2Rh + h^2 + r^2 = R^2, ==> r^2 = h(2R-h)$$

Wear scar area $A = \pi h(2R-h) ==> 2\pi RH$, approx., (error max. 7.2%)

Wear scar vol. $V = \pi H^2(R-H/3) ==> 0.5AH$, approx., (error max. 4.7%)

Maximum error of linear approximation for wear scar A & V was carried for the wear scar depth H = 0.32 mm.

Figure 7. Kinematic relations of wear scar growth on the ball in Slifka's experiment.[11]

Molecular component of friction stress "t"

From NIST:
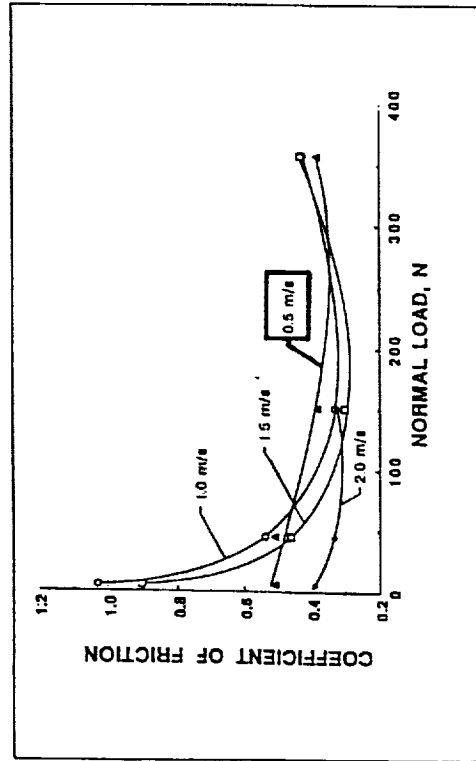
From Kragelsky:
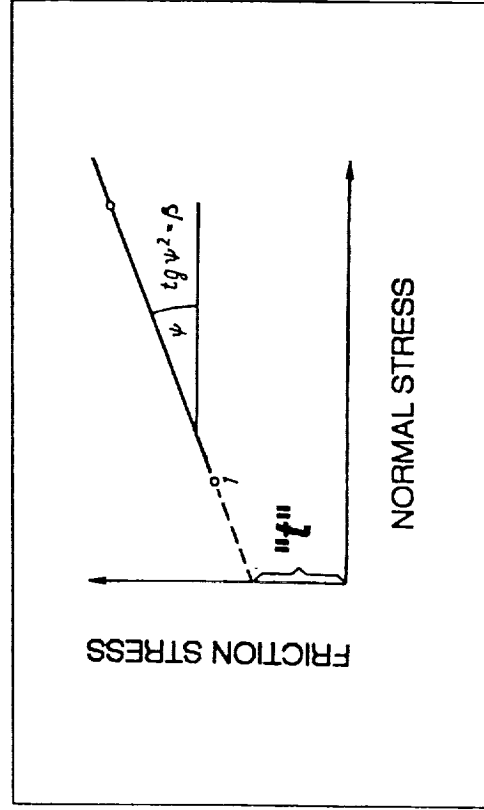
p1=94.5, p3=189.2[kG/sq.mm] $t=(f'1-f'3)/[(p1)^{\wedge}(-1)-(p3)^{\wedge}(-1)]$

f1 - f3 = 0.105 $t=(f1-f3)/[(p1)^{\wedge}(-1)-(p3)^{\wedge}(-1)]$, approx.

$$t = 19.84 \text{ [kG/sq.mm]}$$

Figure 8. Derivation of the molecular component of friction stress "t" using the Kragelsky's definition (right) and methodology in application to Slifka's[11] frictional data (left).

Conversion of "l"

Wear pattern ▬▬▬▬ assumed uniform
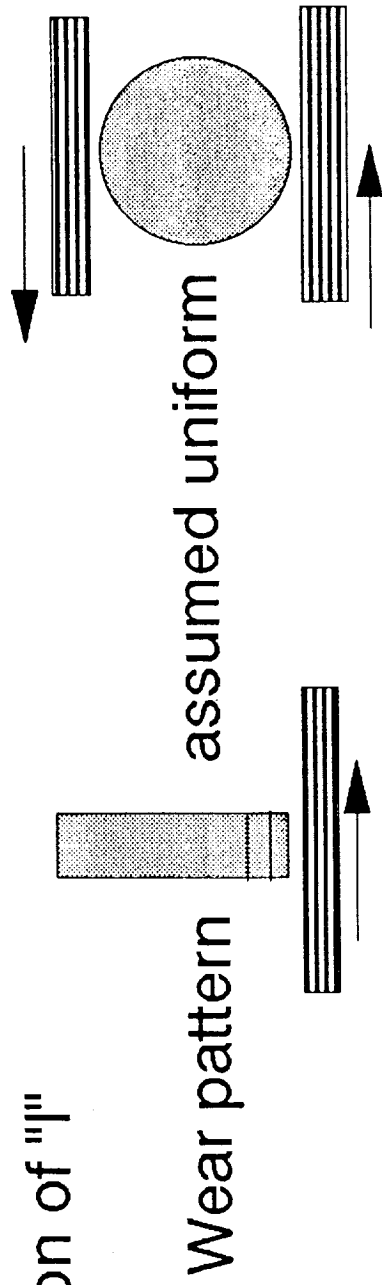
$$l(ball) ==> (A/S) \, l(pin)$$

where A=average contact area
S=ball surface area
l=linear wear rate

Conversion of "p"

Prorate ave.(p) and real (p') pressure on the same basis as it was done in the particular mode applied to the NIST experiment.

Figure 9. Adapting models of sliding wear to rolling bearings. Conversion of linear wear rate "*l*" and average pressure "*p*".
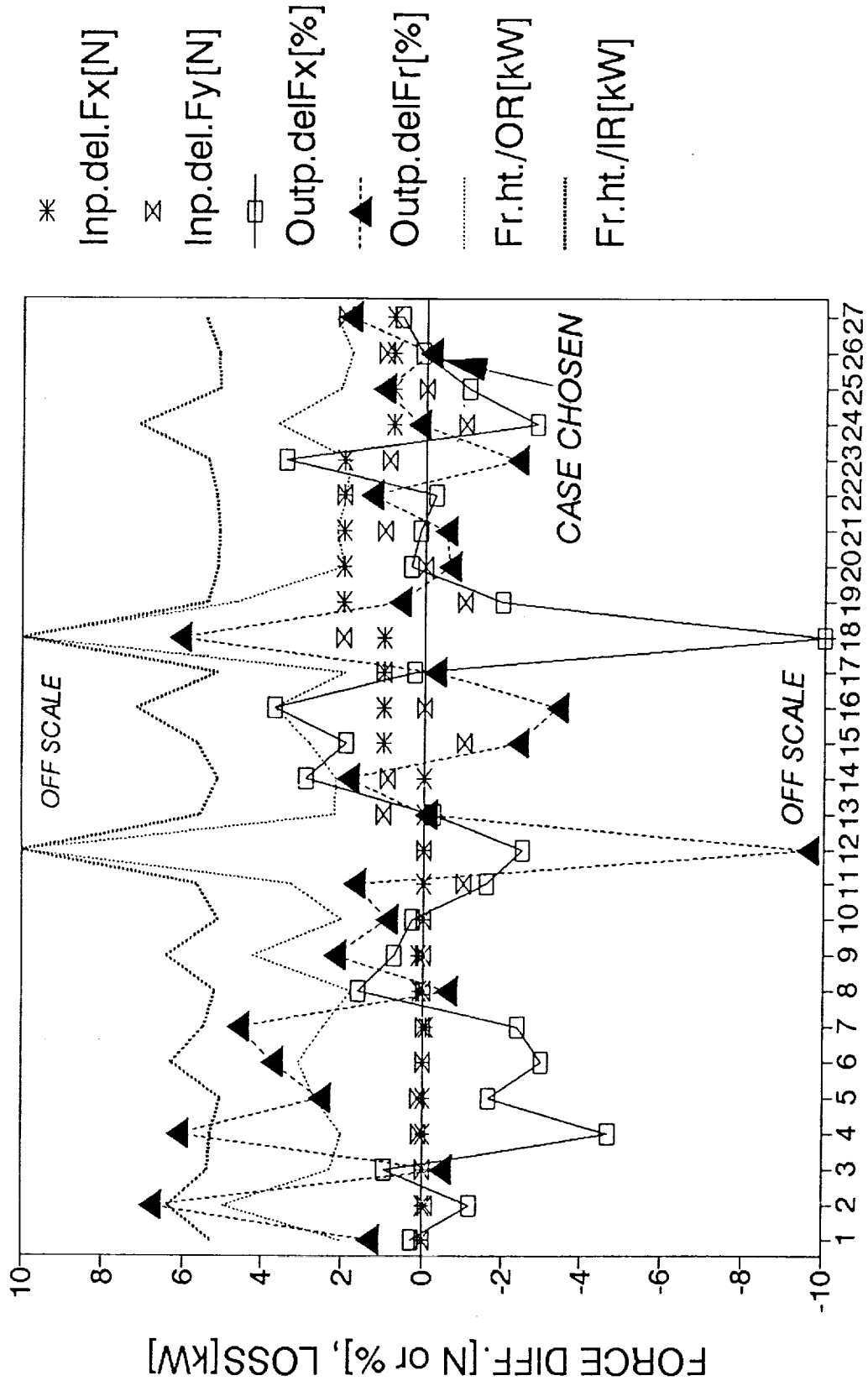
Figure 10. SHABERTH™ convergence for case "*M*," an example.
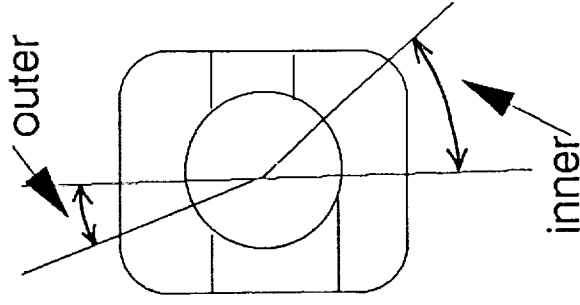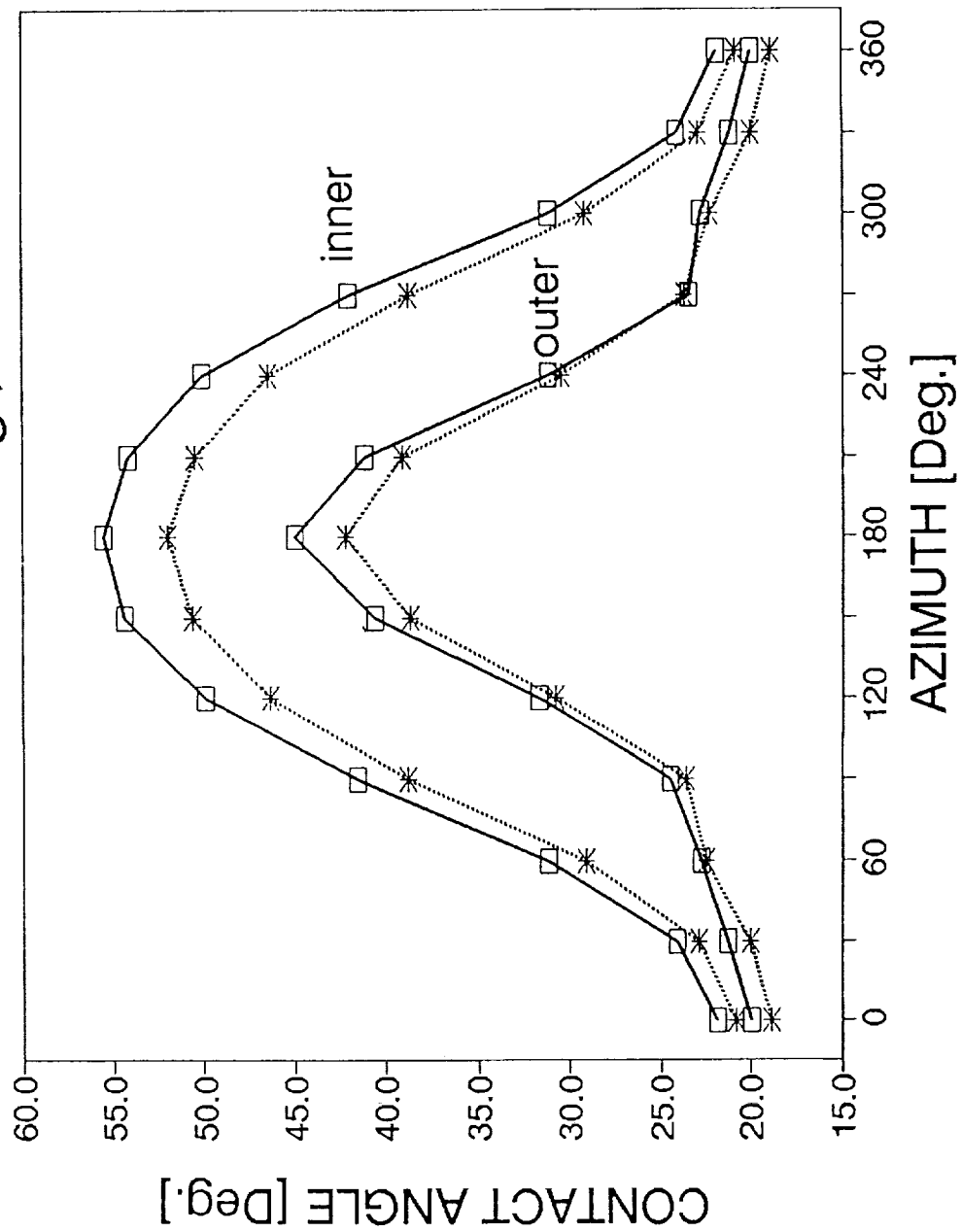
Figure 11. Variation of contact angles for inner and outer rings around the bearing.

Figure 12. Variation of ball angular velocity components with reference to the cage around the bearing.

40
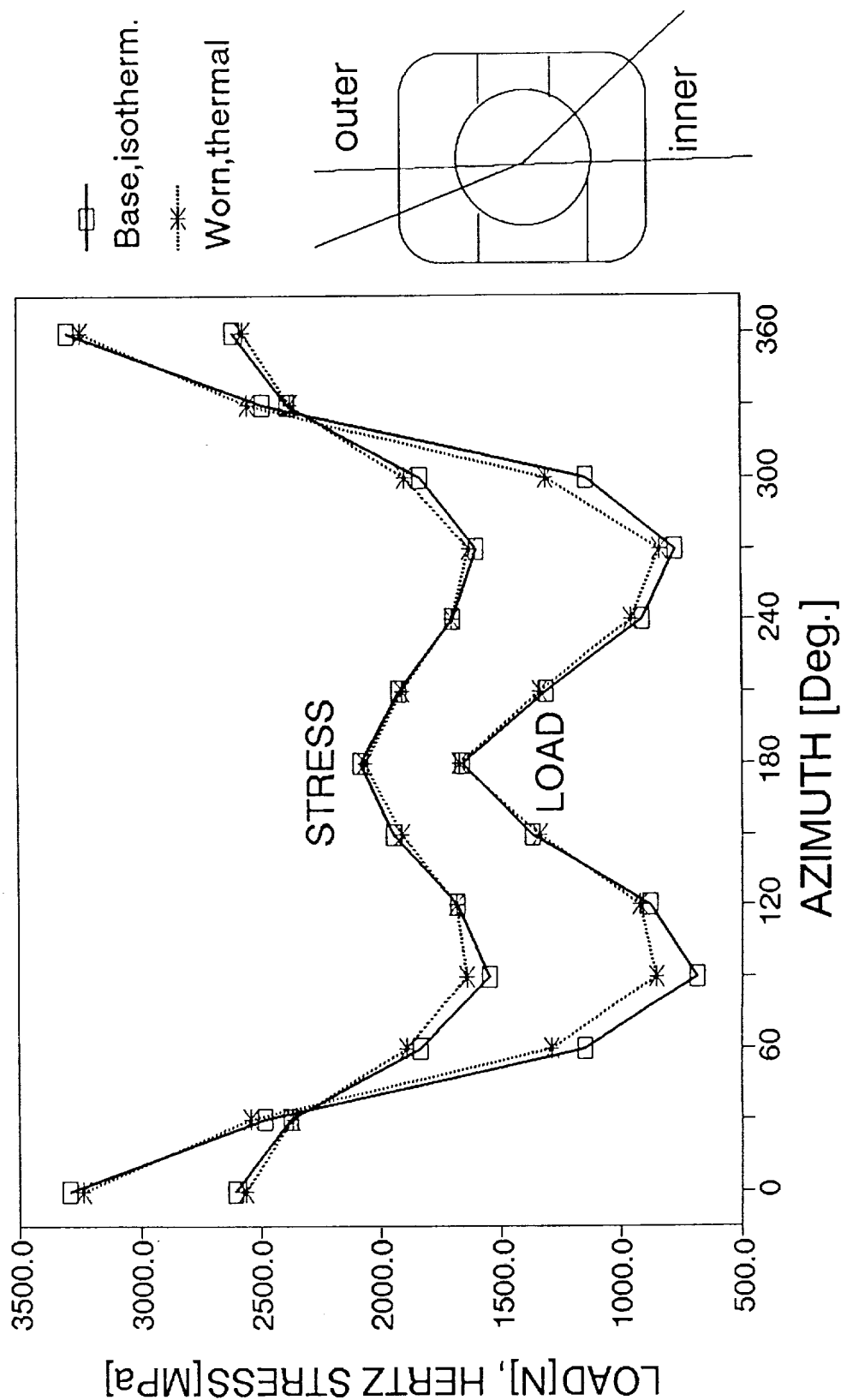
Figure 13. Variation of contact load and contact stress in the outer ring/ball contact around the bearing.

41
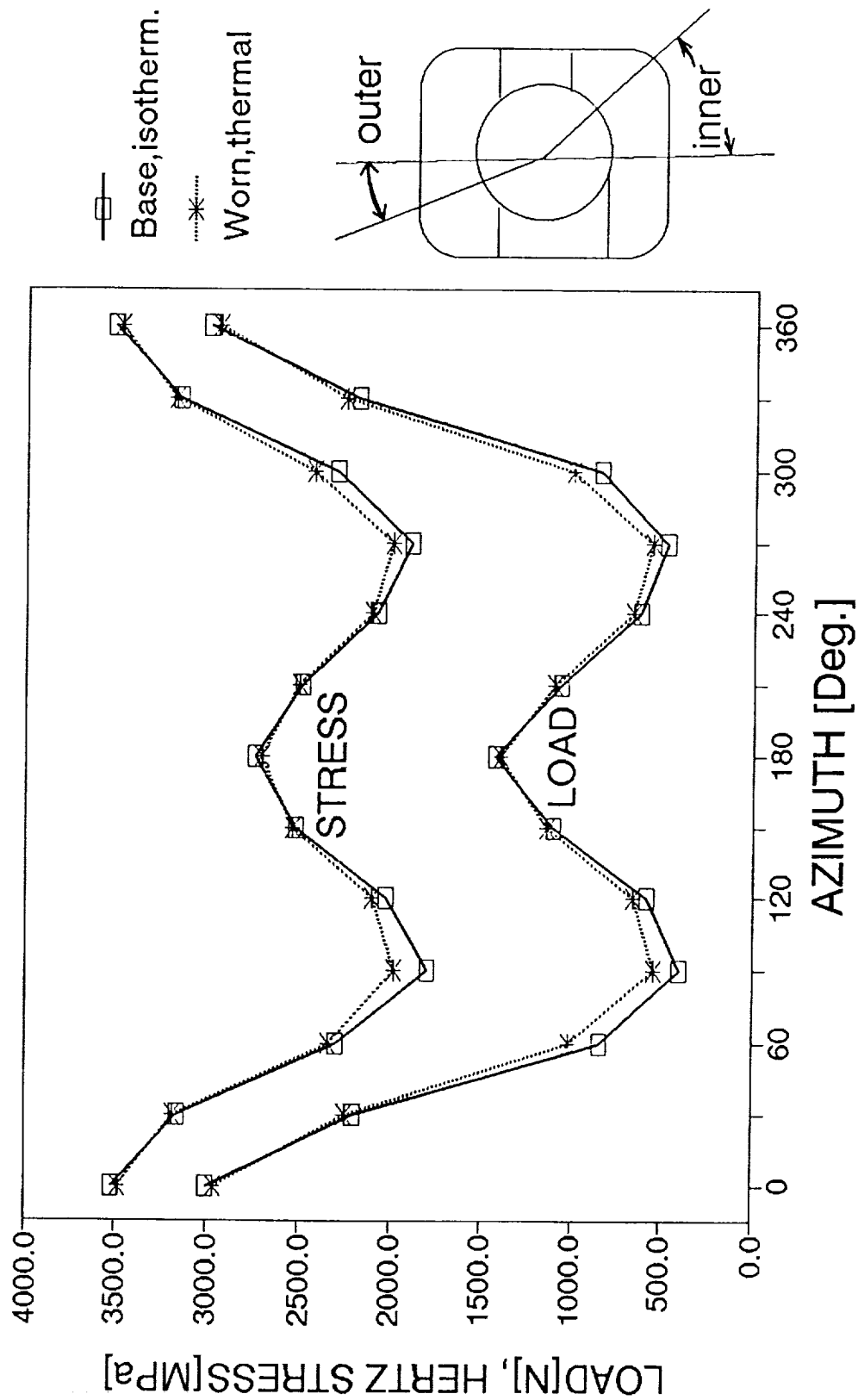
Figure 14. Variation of contact load and contact stress in the inner ring/ball contact around the bearing.

42
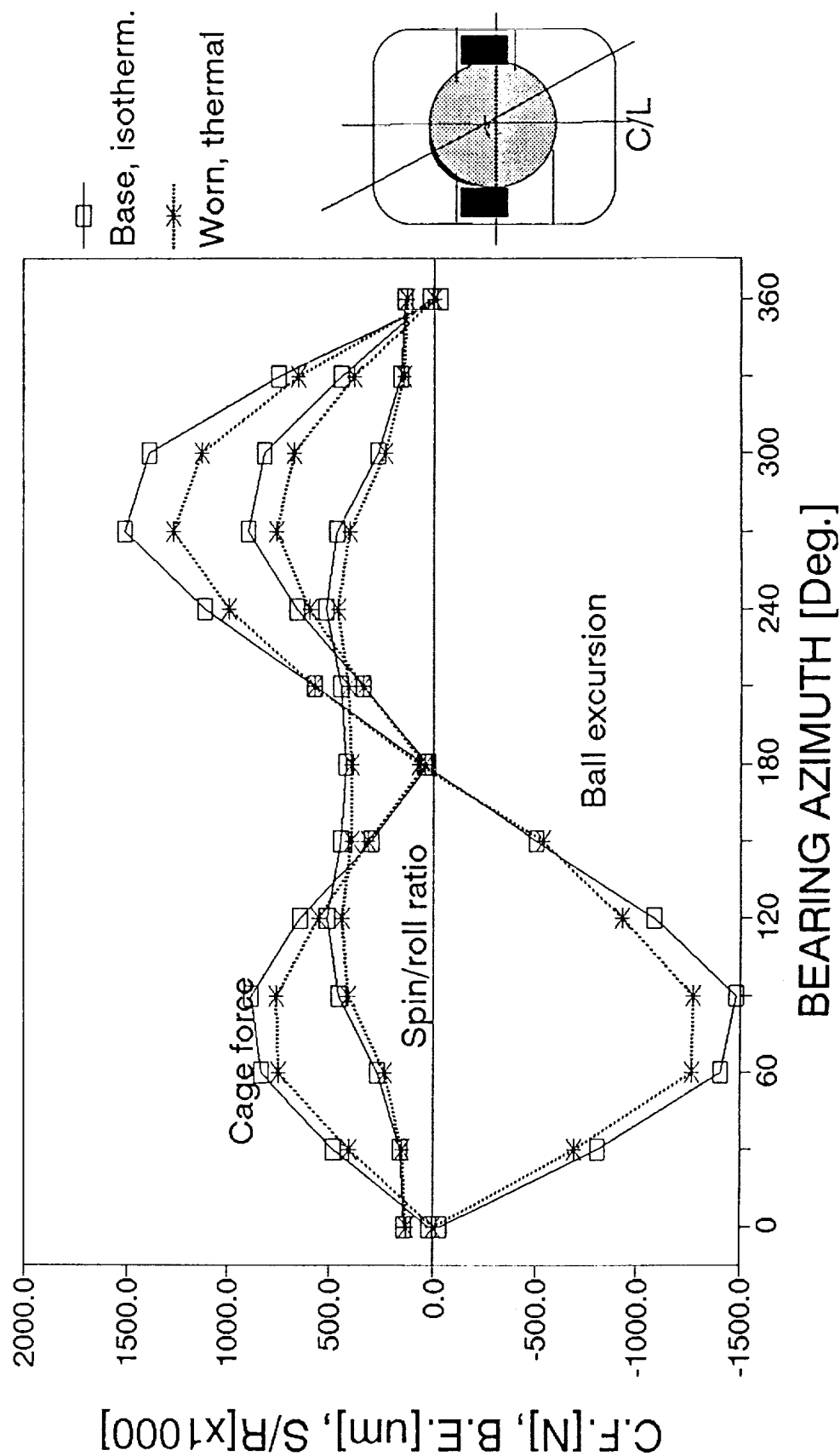
Figure 15. Variation of cage force, ball excursion, and spin-to-roll ratio around the bearing.

Figure 16. Maximum "*pV*," the pressure × sliding velocity product, along the major axis of the outer ellipse of contact.

44
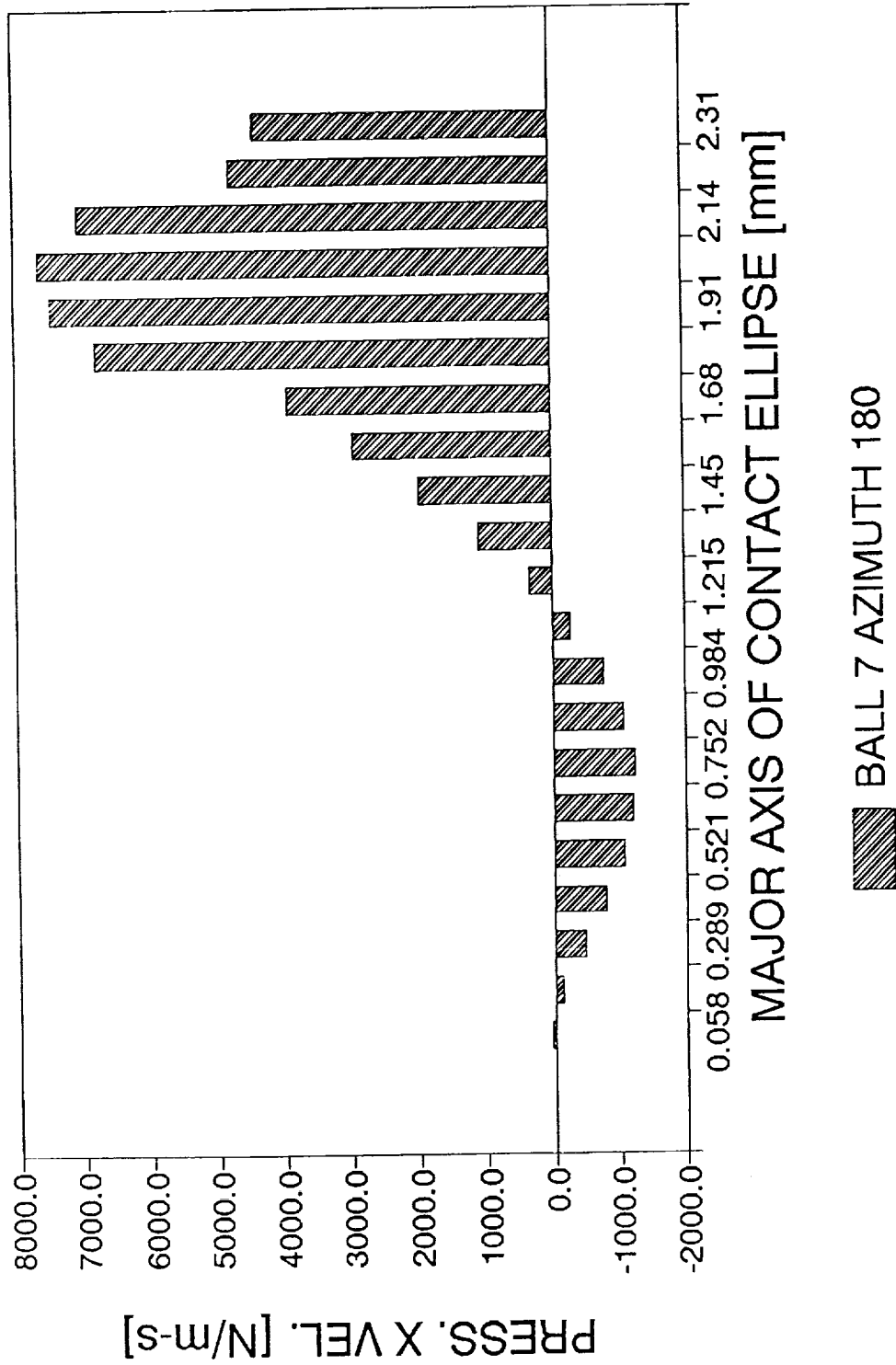
Figure 17. Maximum *"pV,"* the pressure × sliding velocity product, along the major axis of the inner ellipse of contact.

45

"pV" PROFILE IN BALL6/OUT.RING CONTACT
45mm brg., "M" load
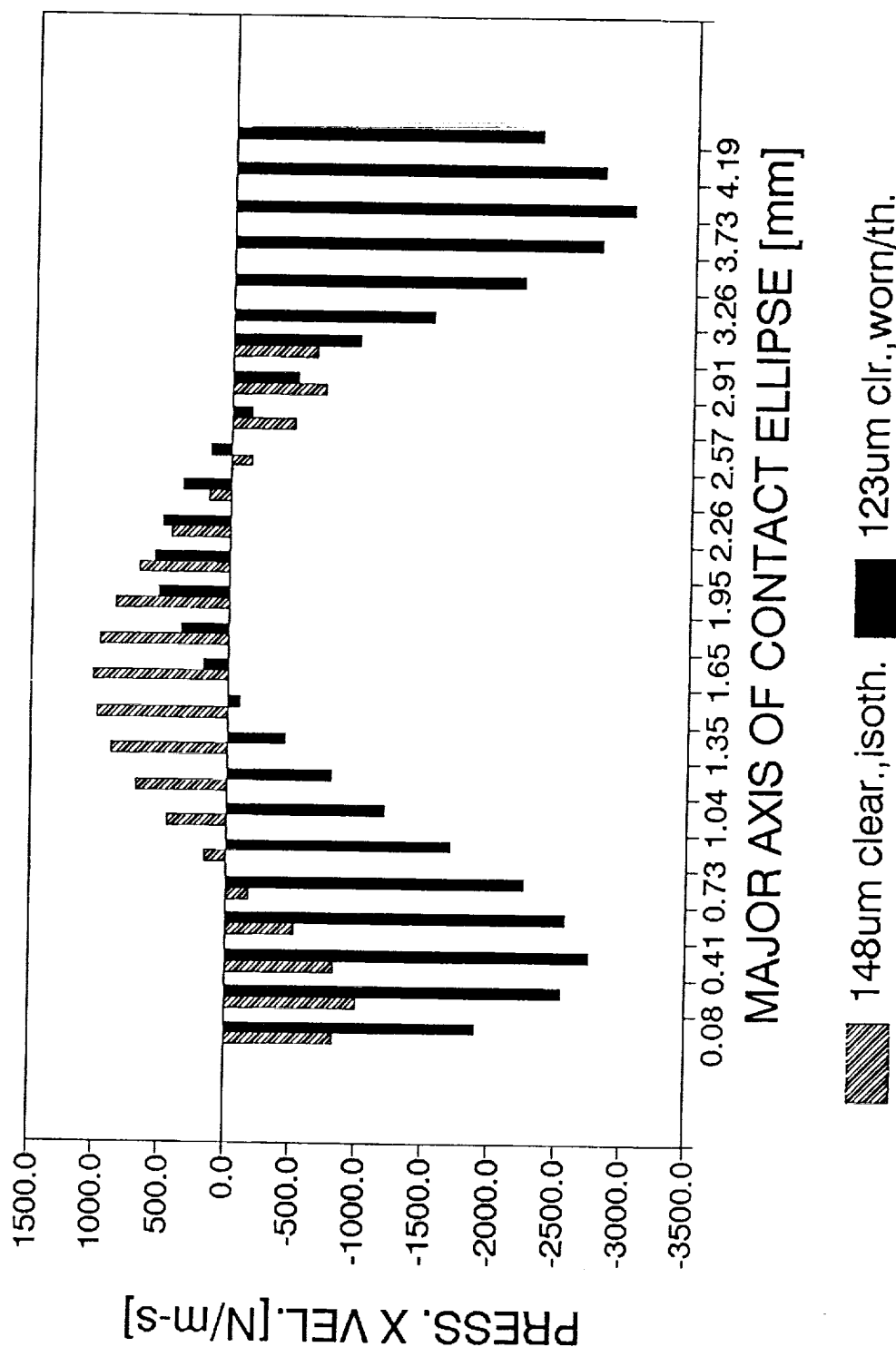
Figure 18. Profile of "pV" along the major axis of contact with the outer ring of a ball located at azimuth 150°.
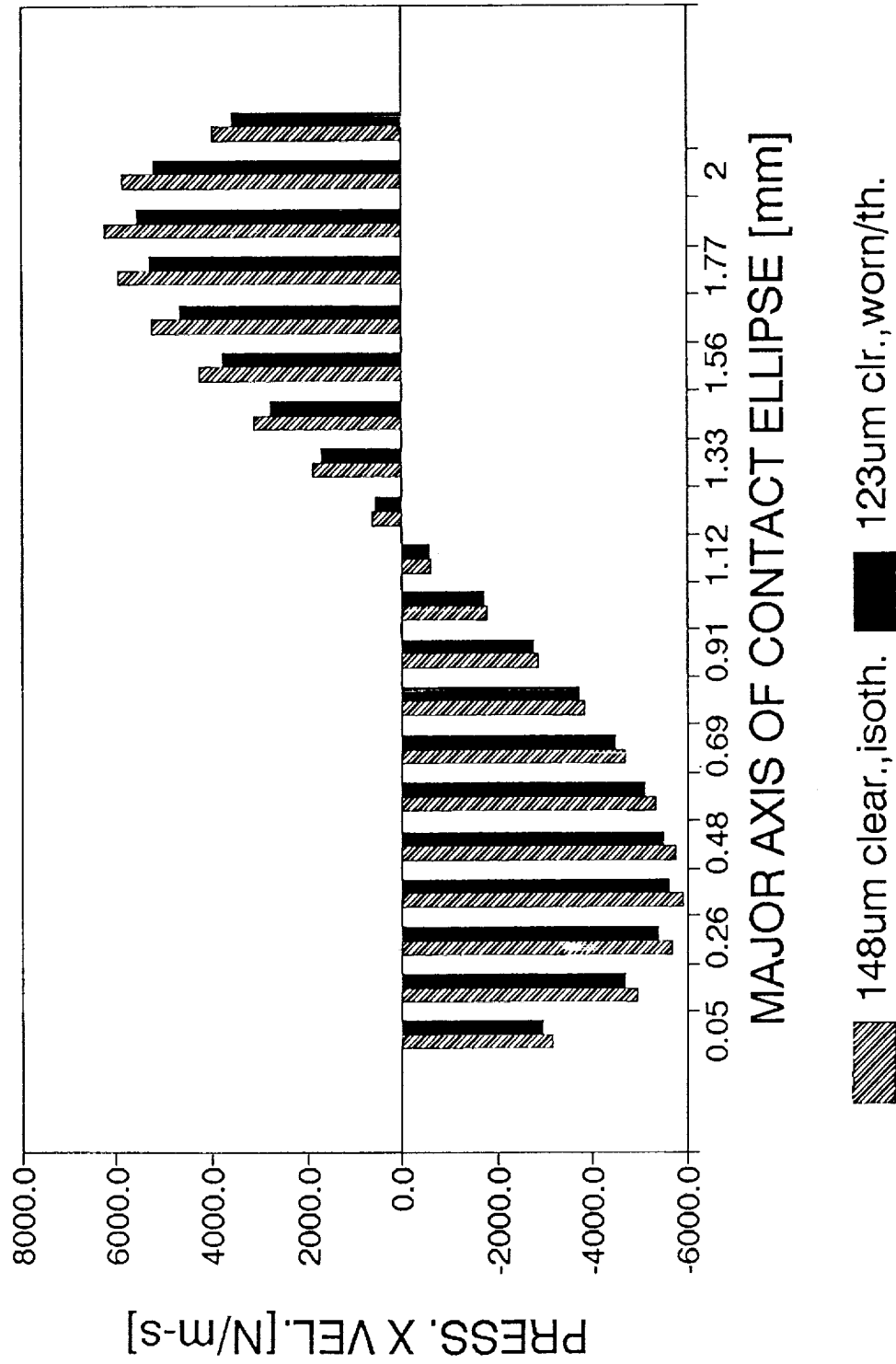
Figure 19. Profile of "*pV*" along the major axis of contact with the inner ring of a ball located at azimuth 150°.
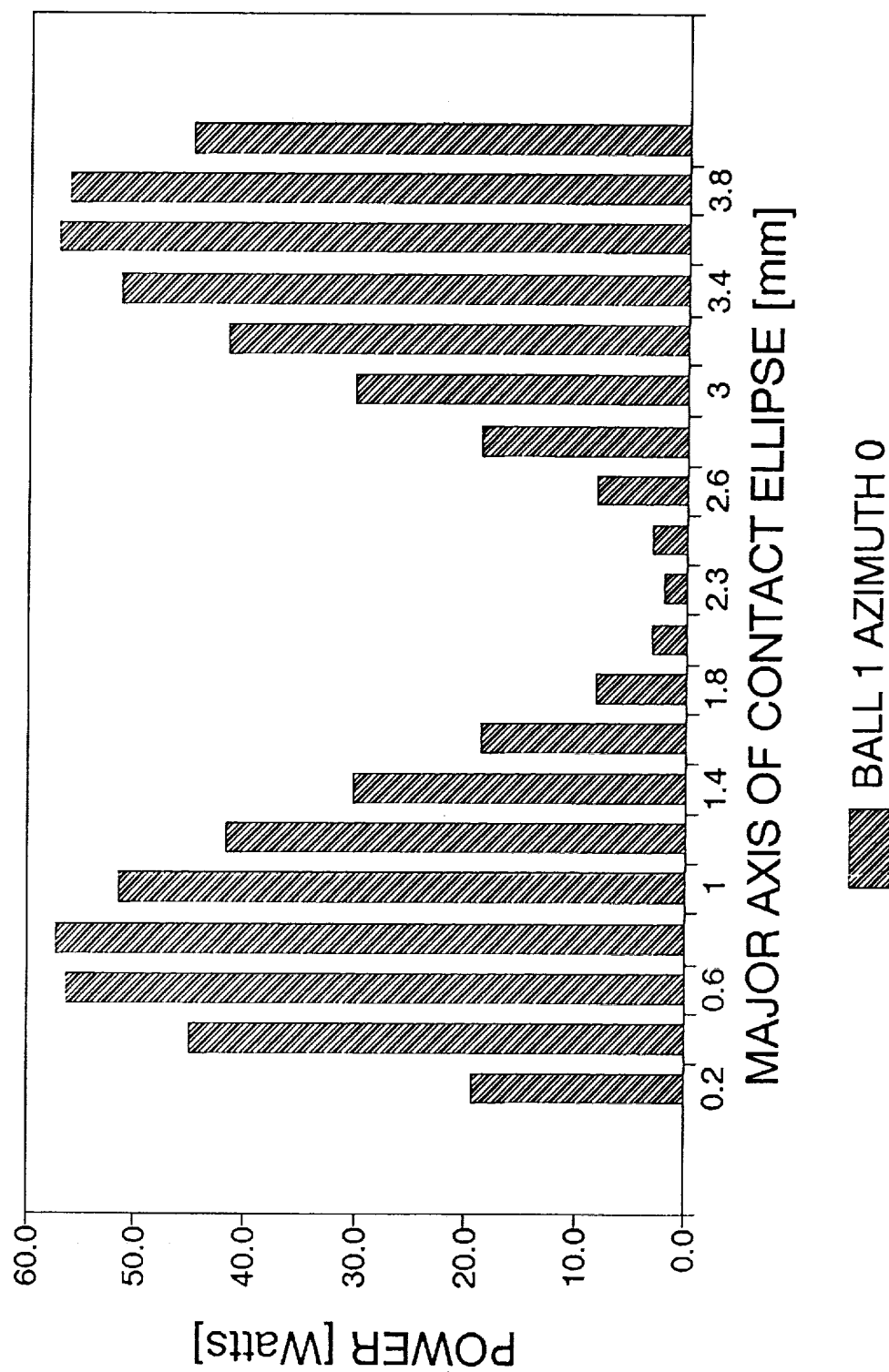
Figure 20. Frictional power loss in contact of ball No. 1 with the outer ring along the major axis of the ellipse of contact.

48
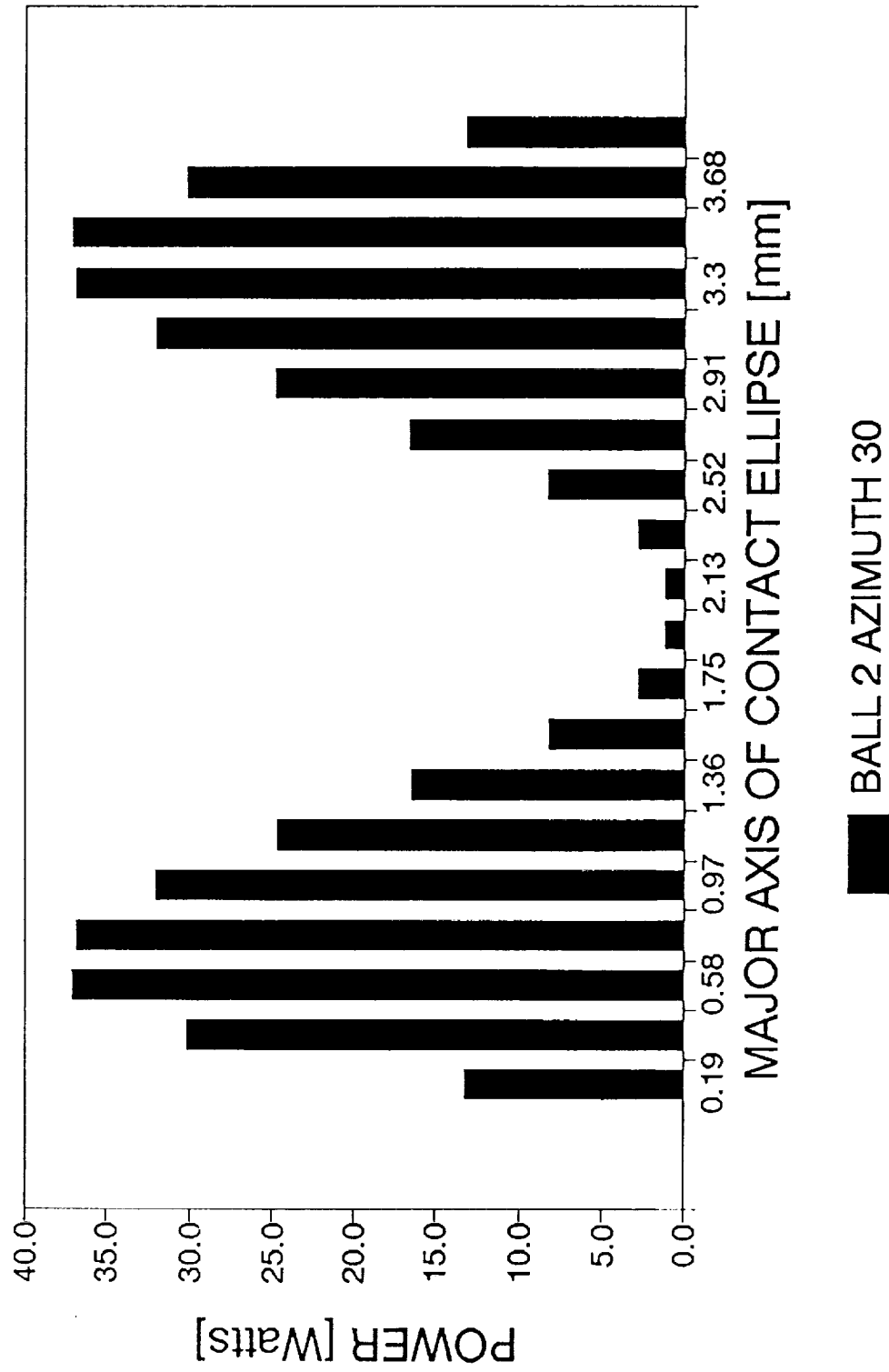
Figure 21. Frictional power loss in contact of ball No. 2 with the outer ring along the major axis of the ellipse of contact.
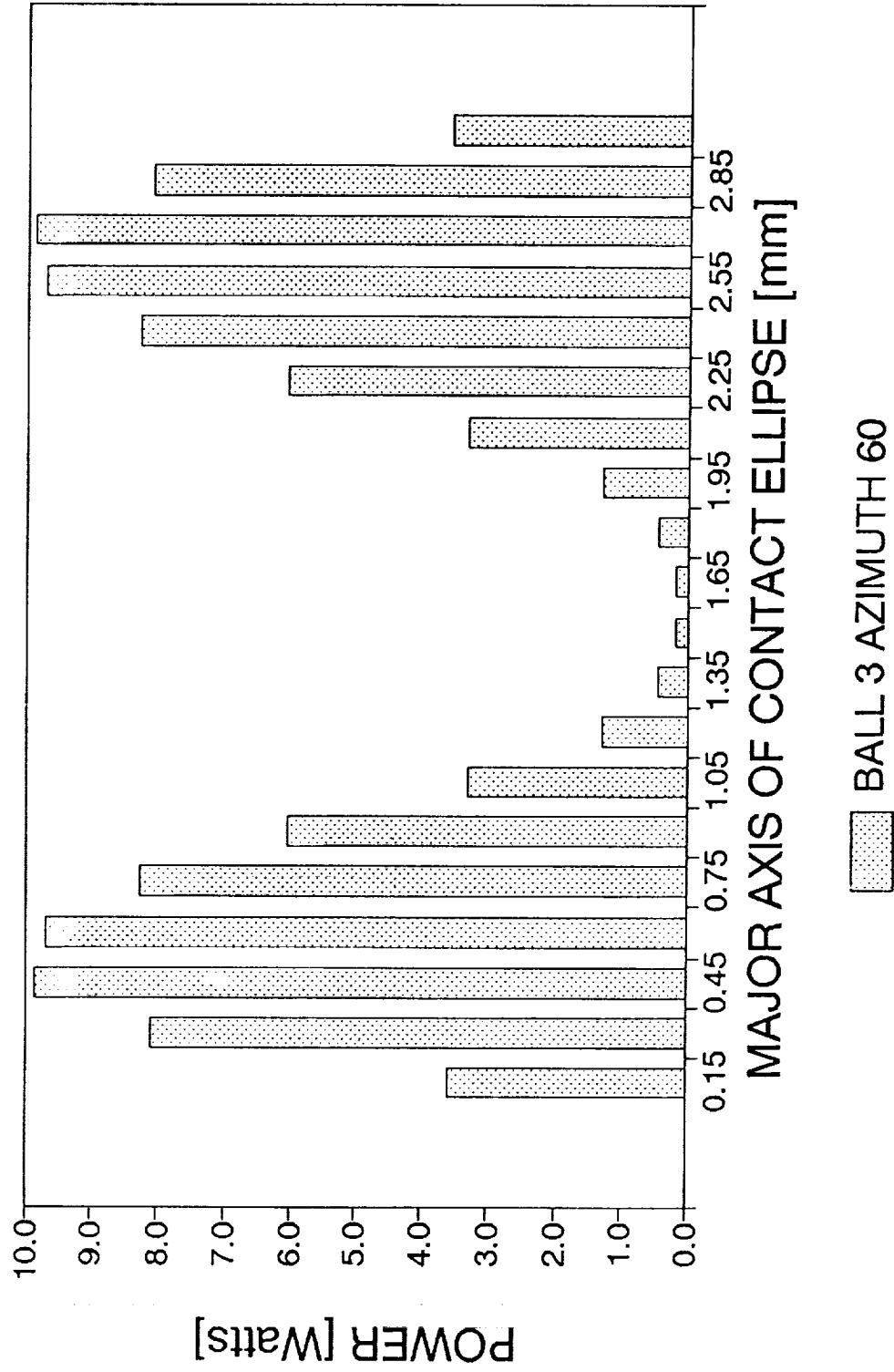
Figure 22. Frictional power loss in contact of ball No. 3 with the outer ring along the major axis of the ellipse of contact

FRICTIONAL LOSSES IN OUTER CONTACT
45mm brg.,157.5um dia.clear.,"M" load

POWER [Watts]

MAJOR AXIS OF CONTACT ELLIPSE [mm]

BALL 4 AZIMUTH 90
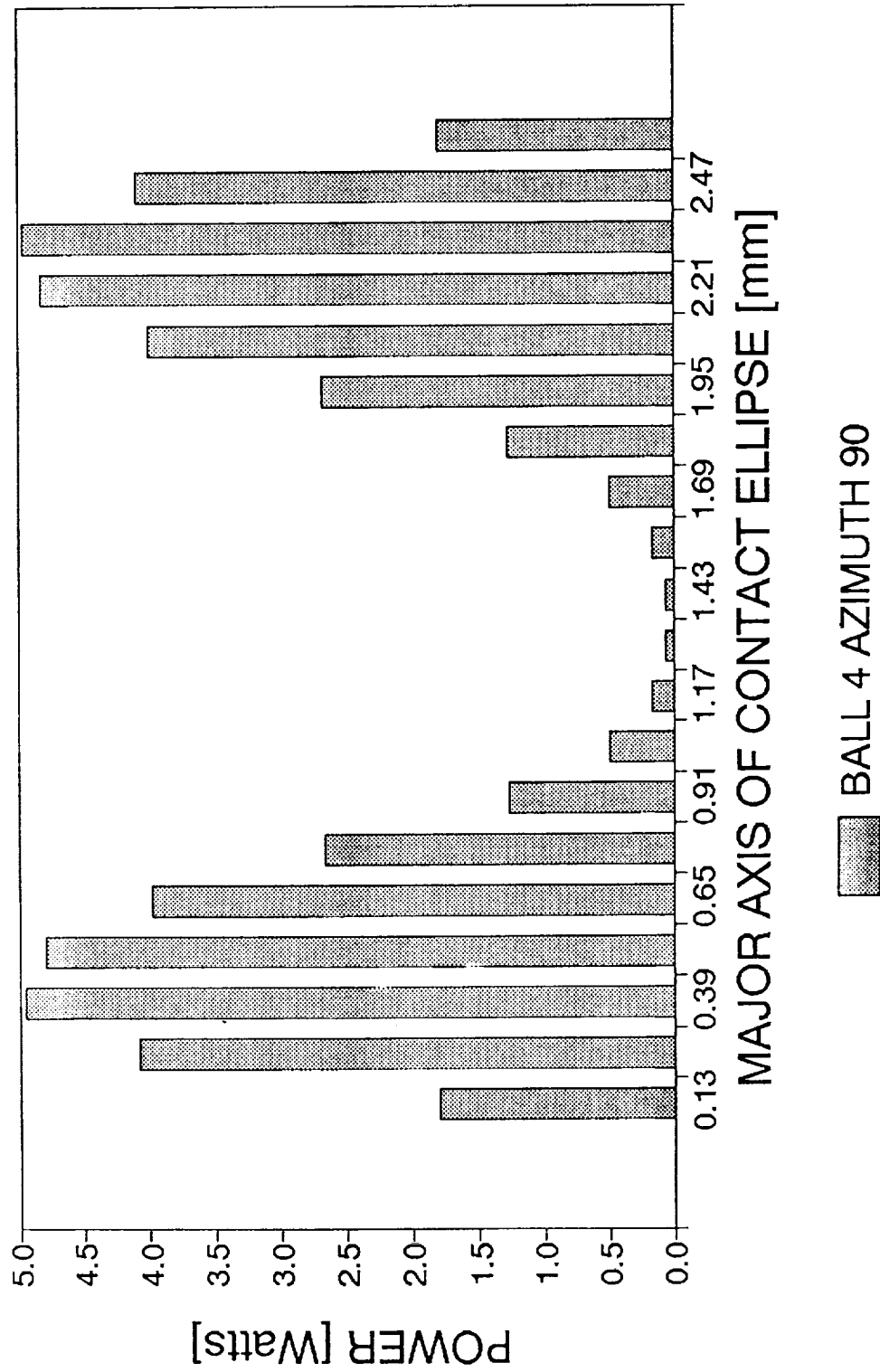
Figure 23. Frictional power loss in contact of ball No. 4 with the outer ring along the major axis of the ellipse of contact.

51

FRICTIONAL LOSSES IN OUTER CONTACT
45mm brg.,157.5um dia.clear.,"M" load
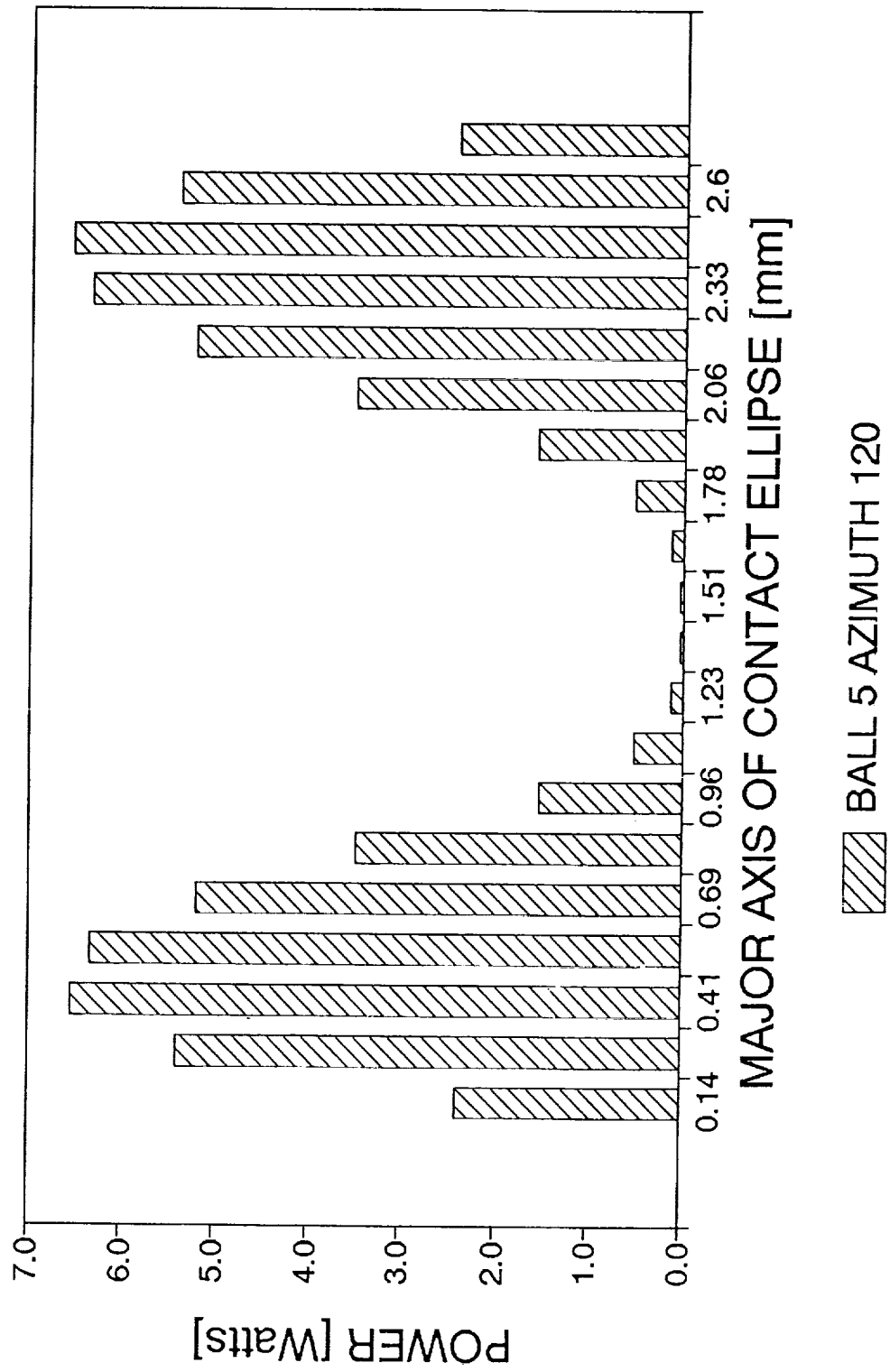
Figure 24. Frictional power loss in contact of ball No. 5 with the outer ring along the major axis of the ellipse of contact.
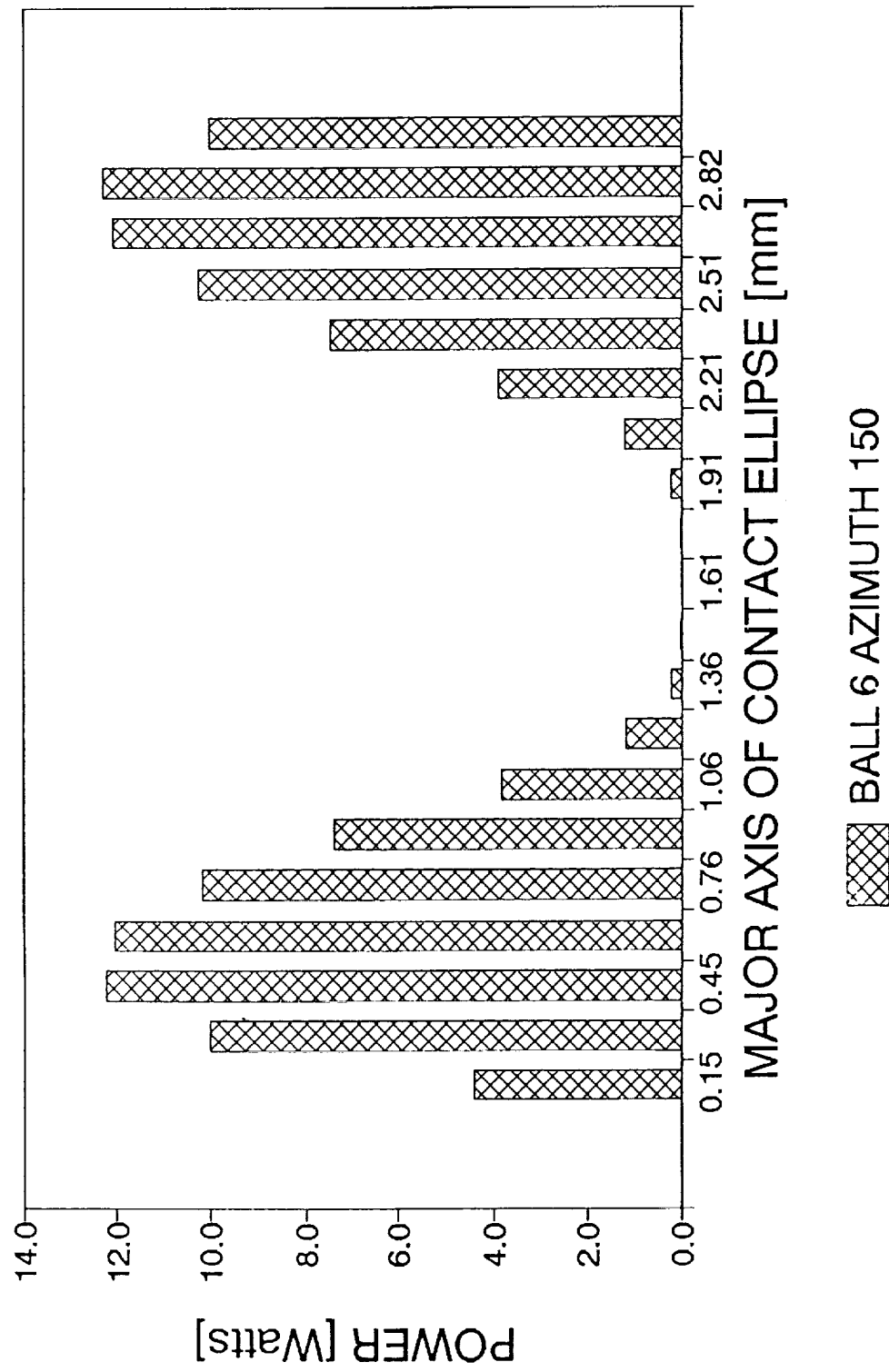
Figure 25. Frictional power loss in contact of ball No. 6 with the outer ring along the major axis of the ellipse of contact

53

FRICTIONAL LOSSES IN OUTER CONTACT
45mm brg.,157.5um dia.clear.,"M" load

Legend: BALL 7 AZIMUTH 180

Axes: POWER [Watts] (0.0 to 20.0) vs MAJOR AXIS OF CONTACT ELLIPSE [mm] (0.18, 0.53, 0.88, 1.23, 1.58, 1.97, 2.32, 2.67, 3.02, 3.38)
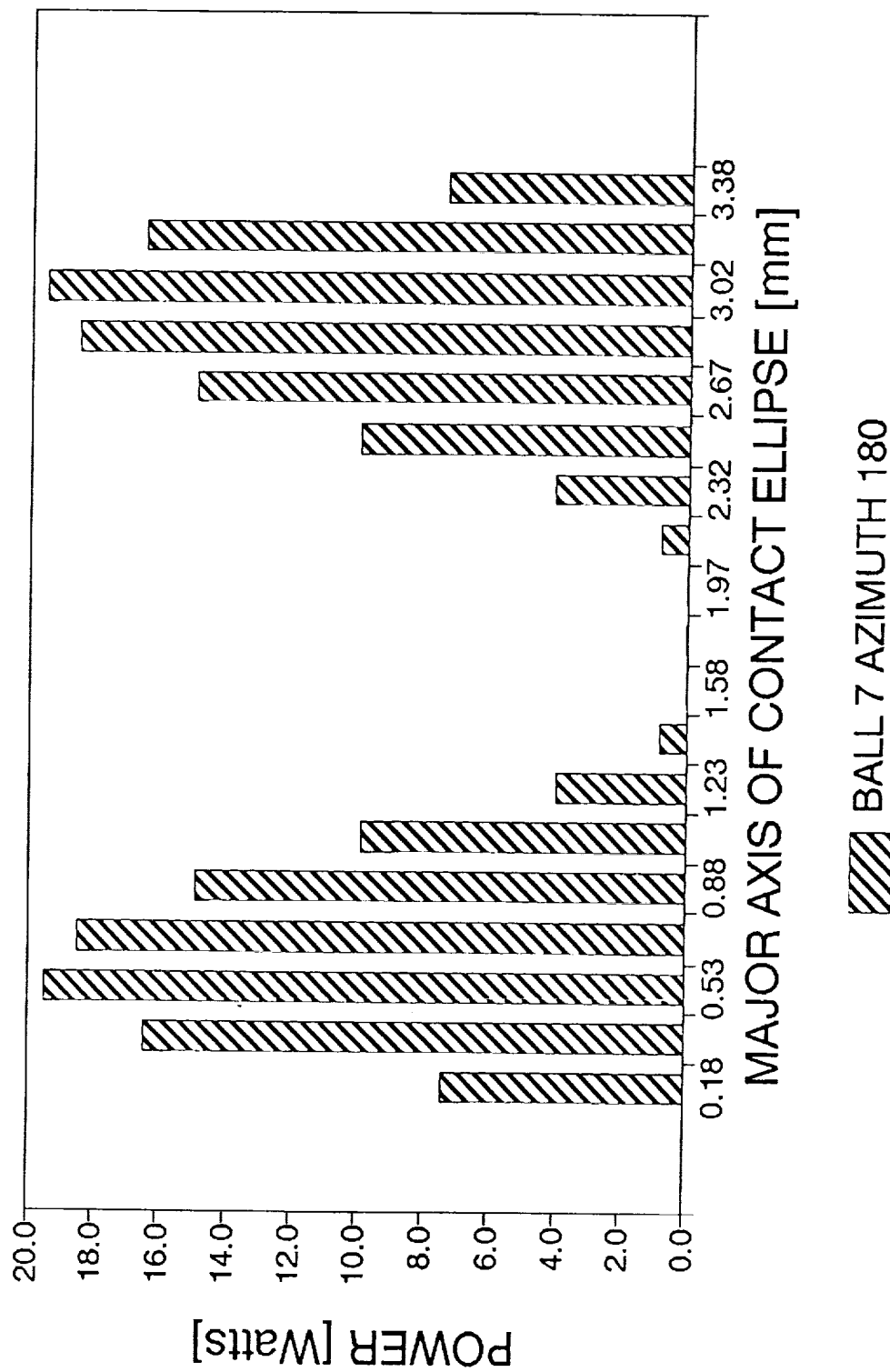
Figure 26. Frictional power loss in contact of ball No. 7 with the outer ring along the major axis of the ellipse of contact.

FRICTIONAL LOSSES IN OUTER CONTACT
45mm brg., 157um dia.clear., "M" load

Legend:
- Ball 7 at 180
- Ball 5 at 120
- Ball 4 at 90
- Ball 3 at 60
- Ball 2 at 30
- Ball 1 at 0

X-axis: MAJOR AXIS OF CONTACT ELLIPSE [mm]

X-axis values: 0.13 0.39 0.65 0.91 1.17 1.43 1.69 1.95 2.21 2.47 2.8 3.2 3.6 4

Y-axis: POWER [Watts]

Y-axis values: 0.0 10.0 20.0 30.0 40.0 50.0 60.0
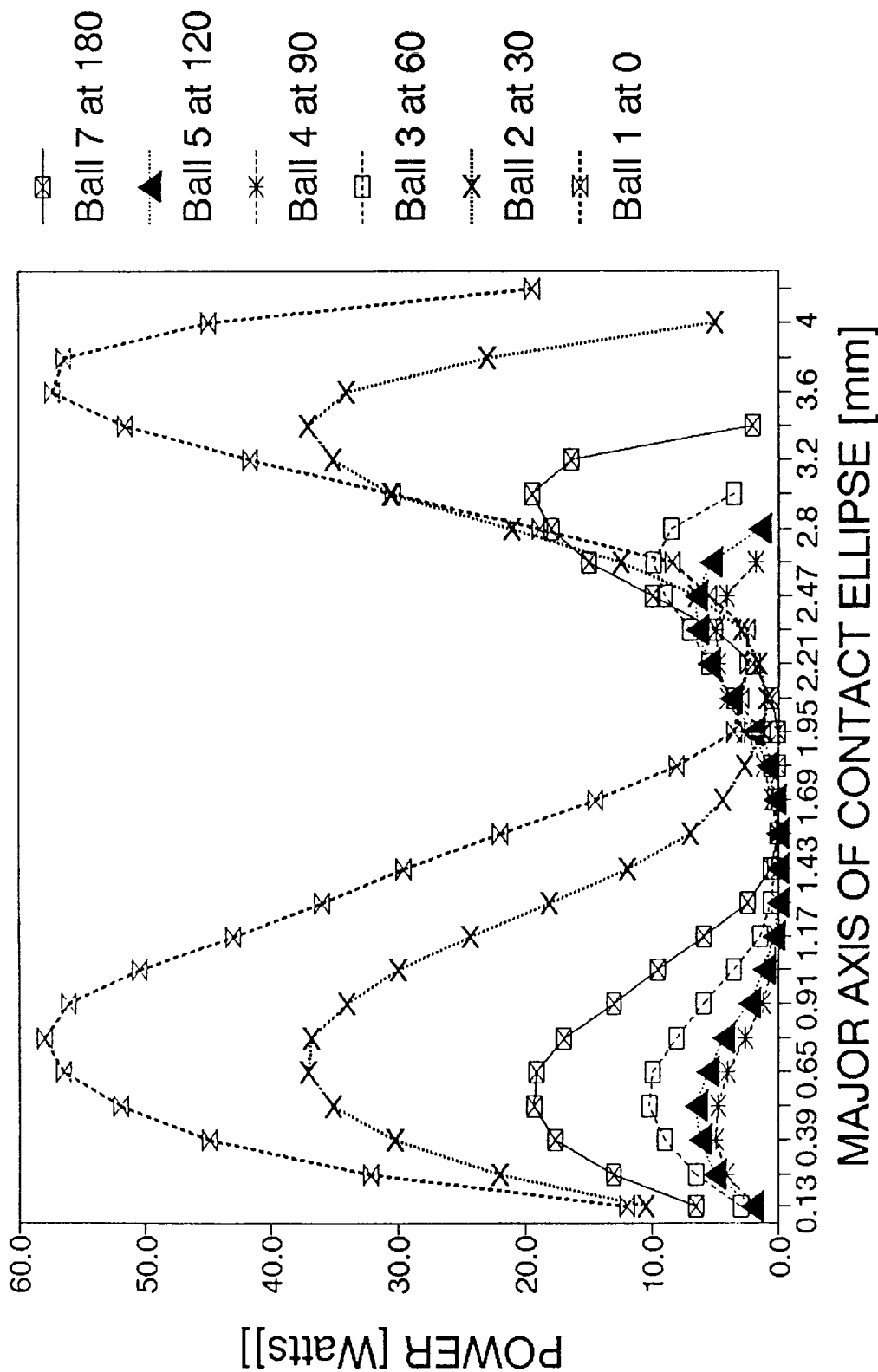
Figure 27. Frictional power loss in contact of a ball with the outer ring along the major axis of the ellipse of contact. Combined diagram (remember symmetry about the load vector).

55

FRICT. LOSS IN CONTACT BALL/OUTER RING
45mm brg.,157.5um dia.clear.,"M" load

0 (28.5%)

30 (17.4%)

60 (4.3%)

90 (2.4%)

120 (0.7%)

150 (5.3%)

180 (7.8%)

210 (5.3%)

240 (2.7%)

270 (2.1%)

300 (4.3%)

330 (17.4%)
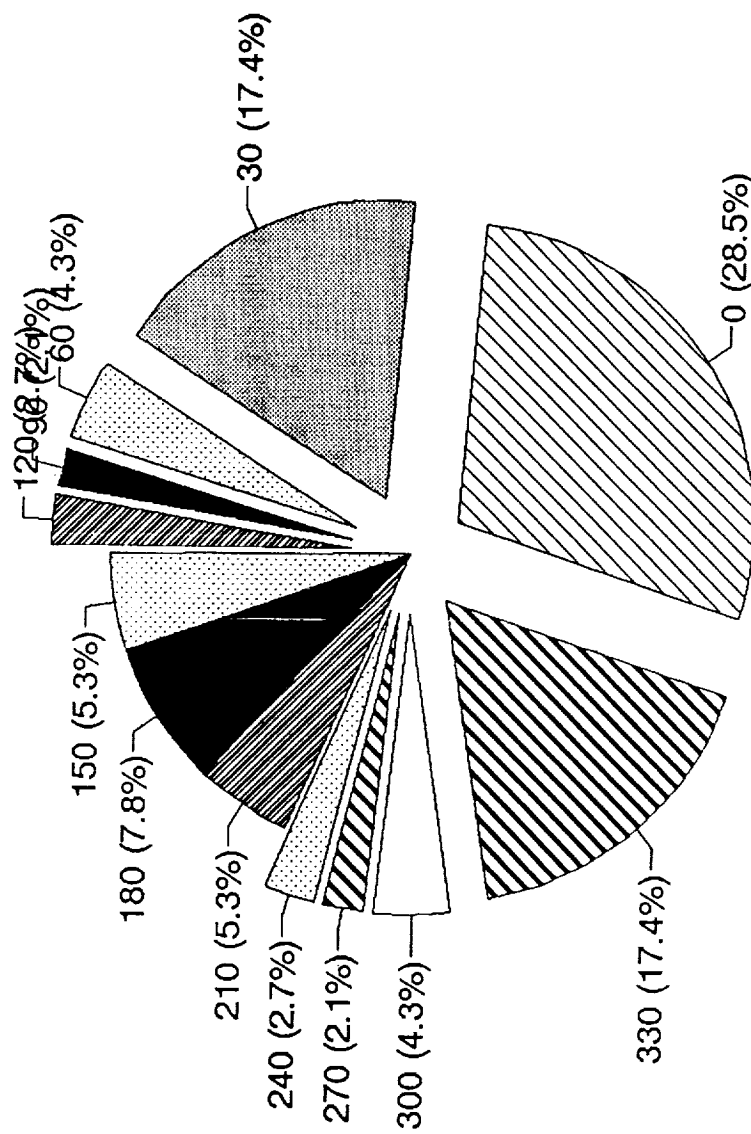
Figure 28. Comparison of power dissipation in contact with the outer ring of a ball traveling around the bearing.
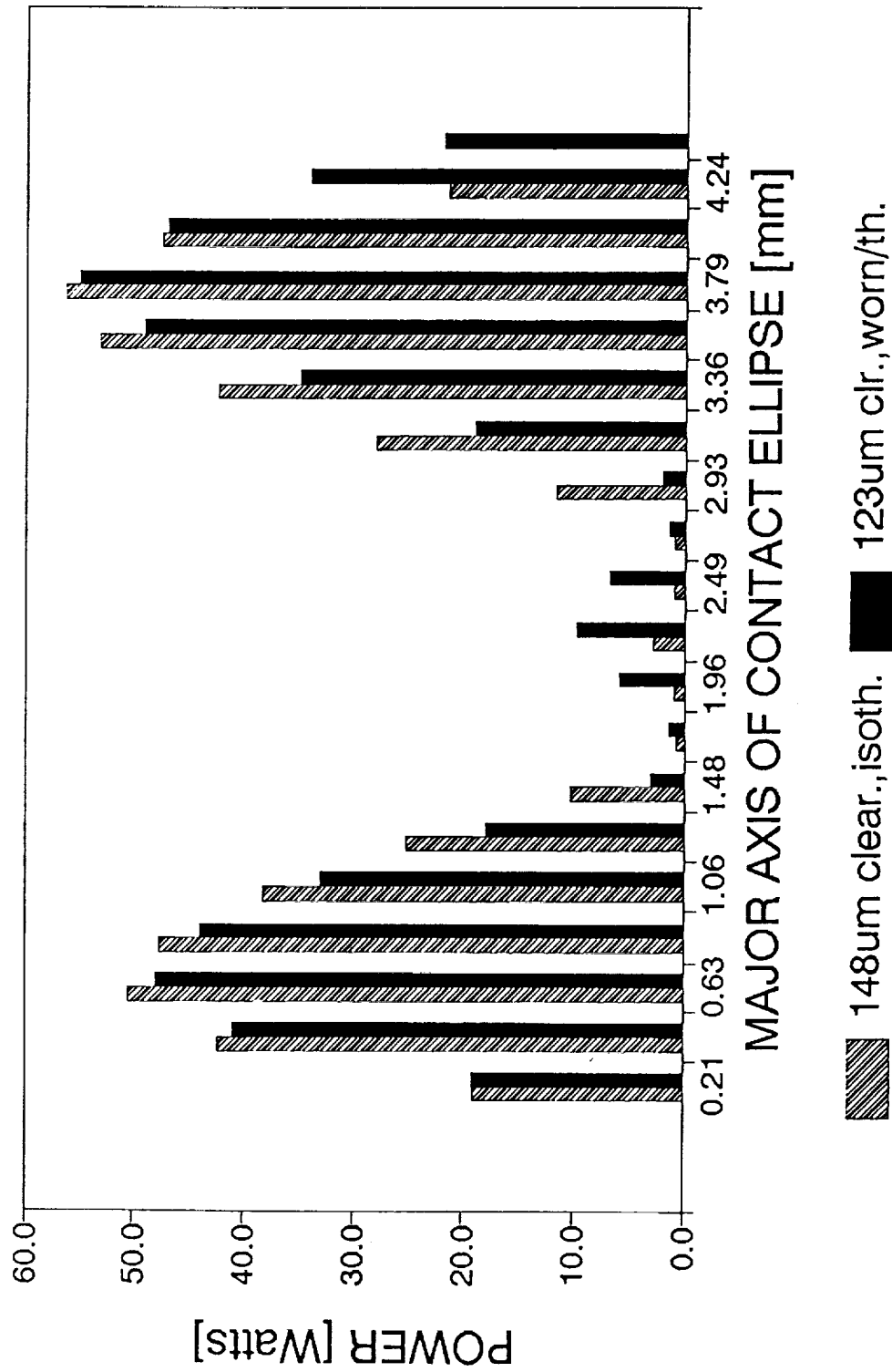
Figure 29. Effect of wear on frictional power dissipation in contact of ball No. 1 with the outer ring.

FRICTIONAL LOSSES IN INNER CONTACT
45mm brg., 157.5um dia.clear., "M" load
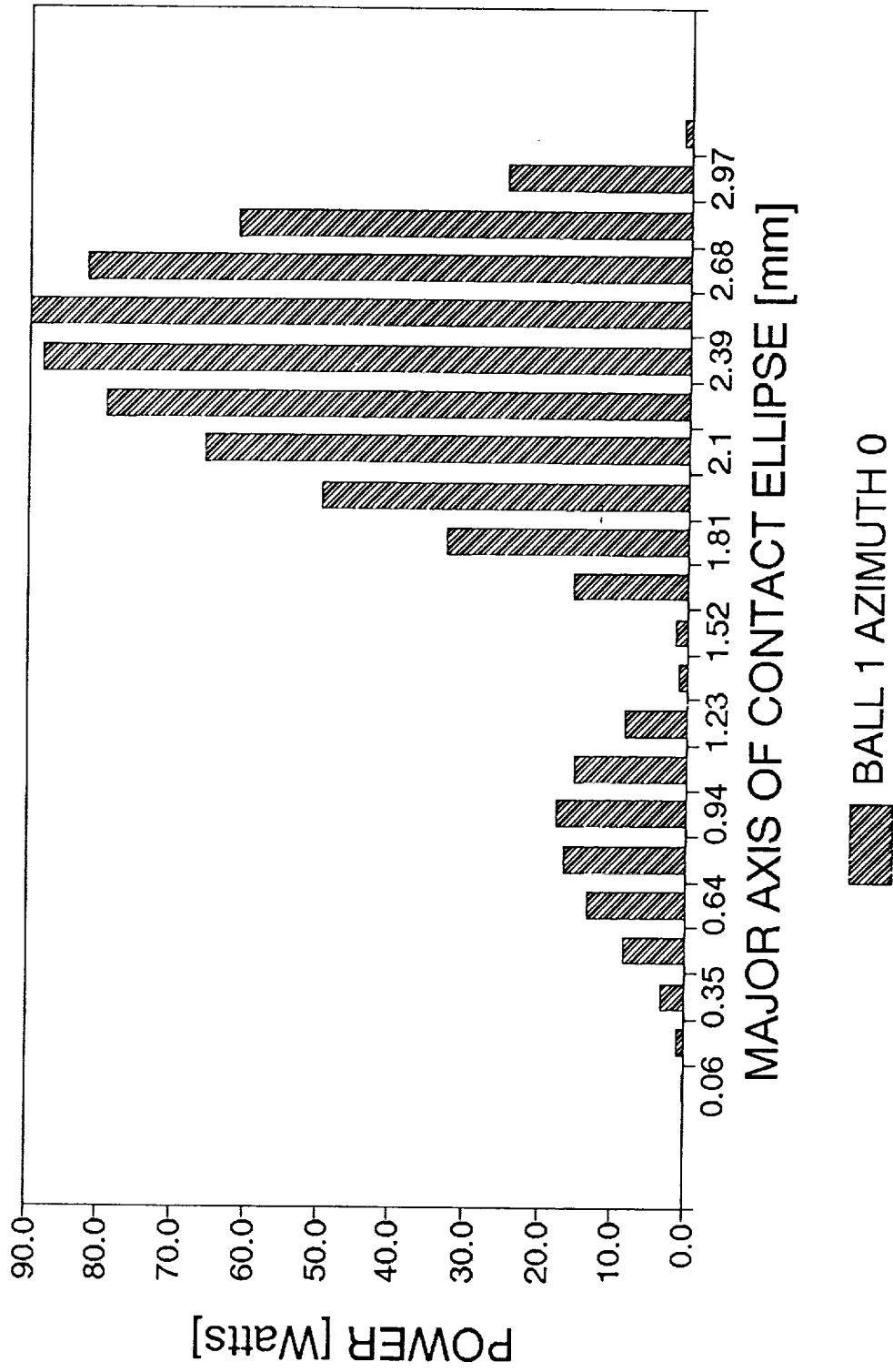
Figure 30. Frictional power loss in contact of ball No. 1 with the inner ring along the major axis of the ellipse of contact.

FRICTIONAL LOSSES IN INNER CONTACT
45mm brg.,157.5um dia.clear.,"M" load

POWER [Watts]

MAJOR AXIS OF CONTACT ELLIPSE [mm]

■ BALL 2 AZIMUTH 30
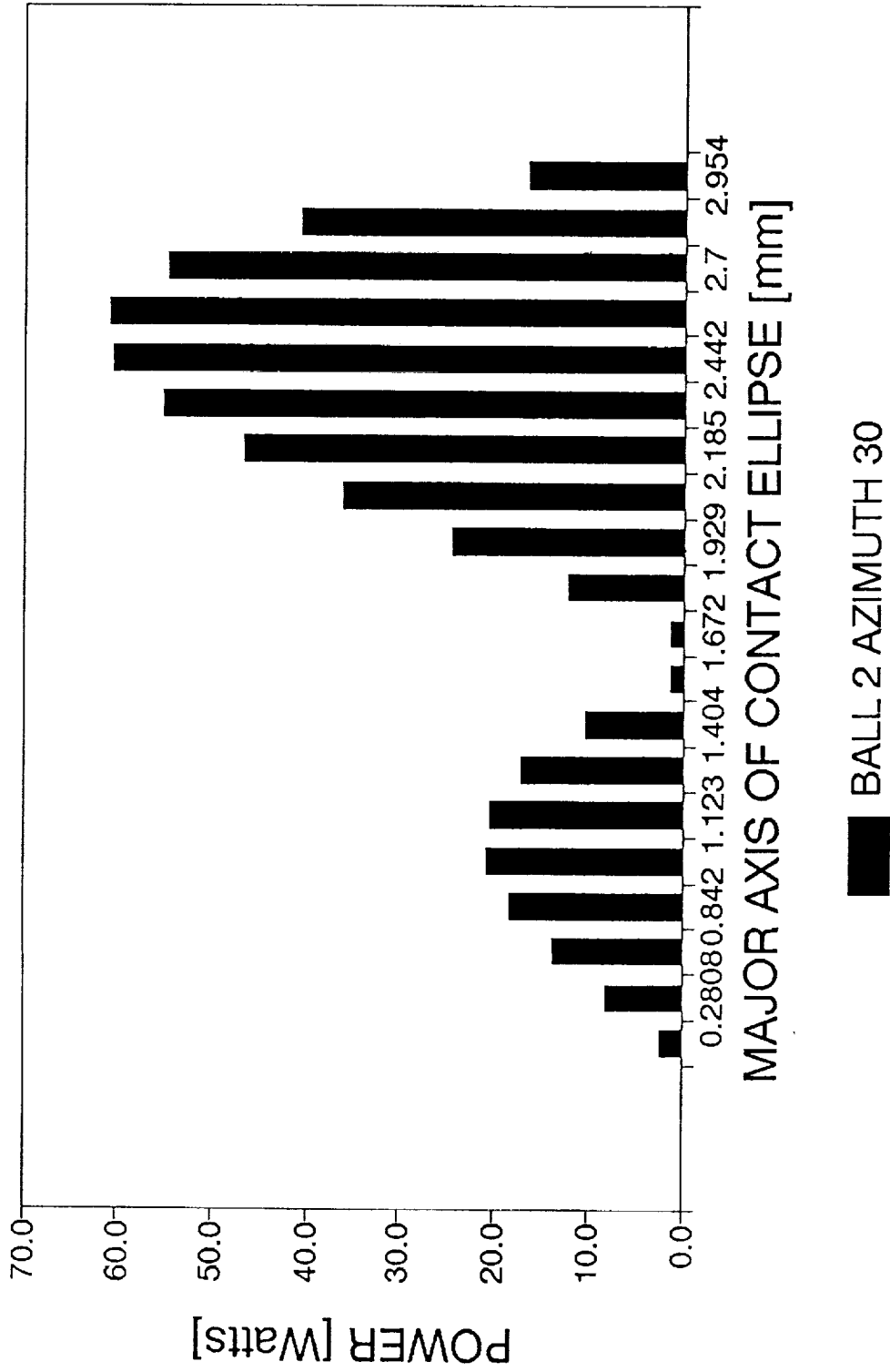
Figure 31. Frictional power loss in contact of ball No. 2 with the inner ring along the major axis of the ellipse of contact

59

FRICTIONAL LOSSES IN INNER CONTACT
45mm brg.,157.5um dia.clear.,"M" load
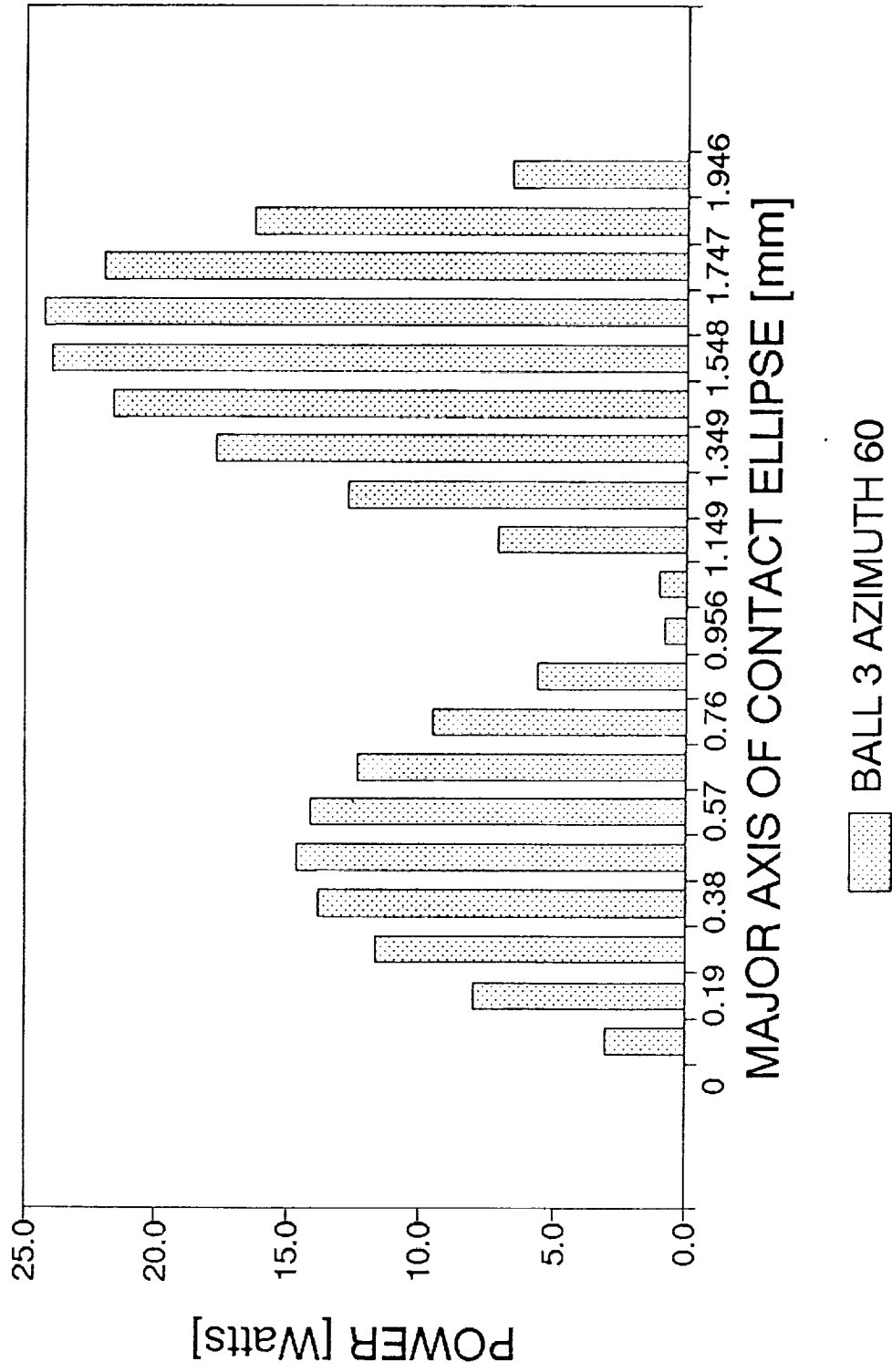
Figure 32. Frictional power loss in contact of ball No. 3 with the inner ring along the major axis of the ellipse of contact.
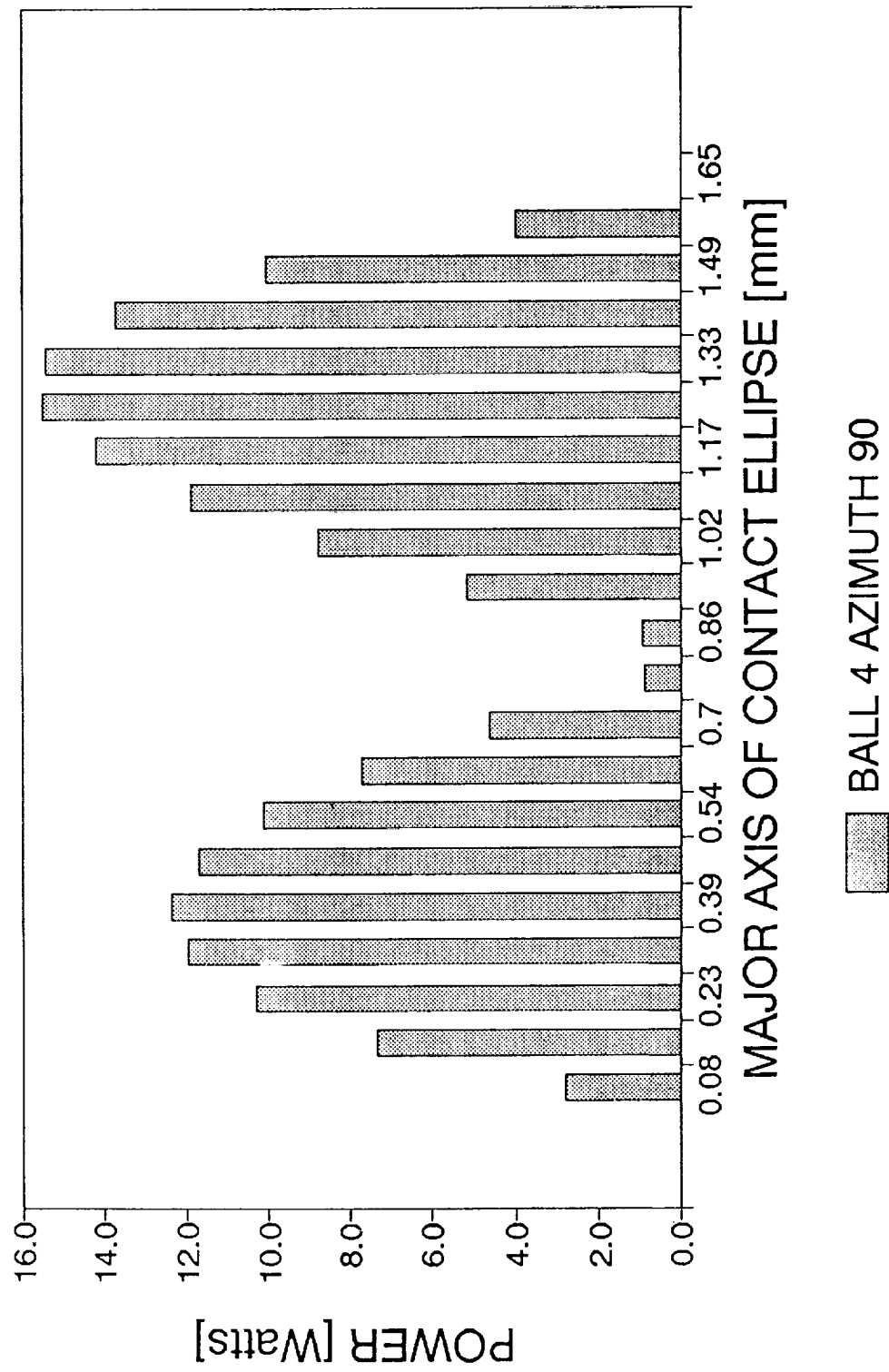
Figure 33. Frictional power loss in contact of ball No. 4 with the inner ring along the major axis of the ellipse of contact.
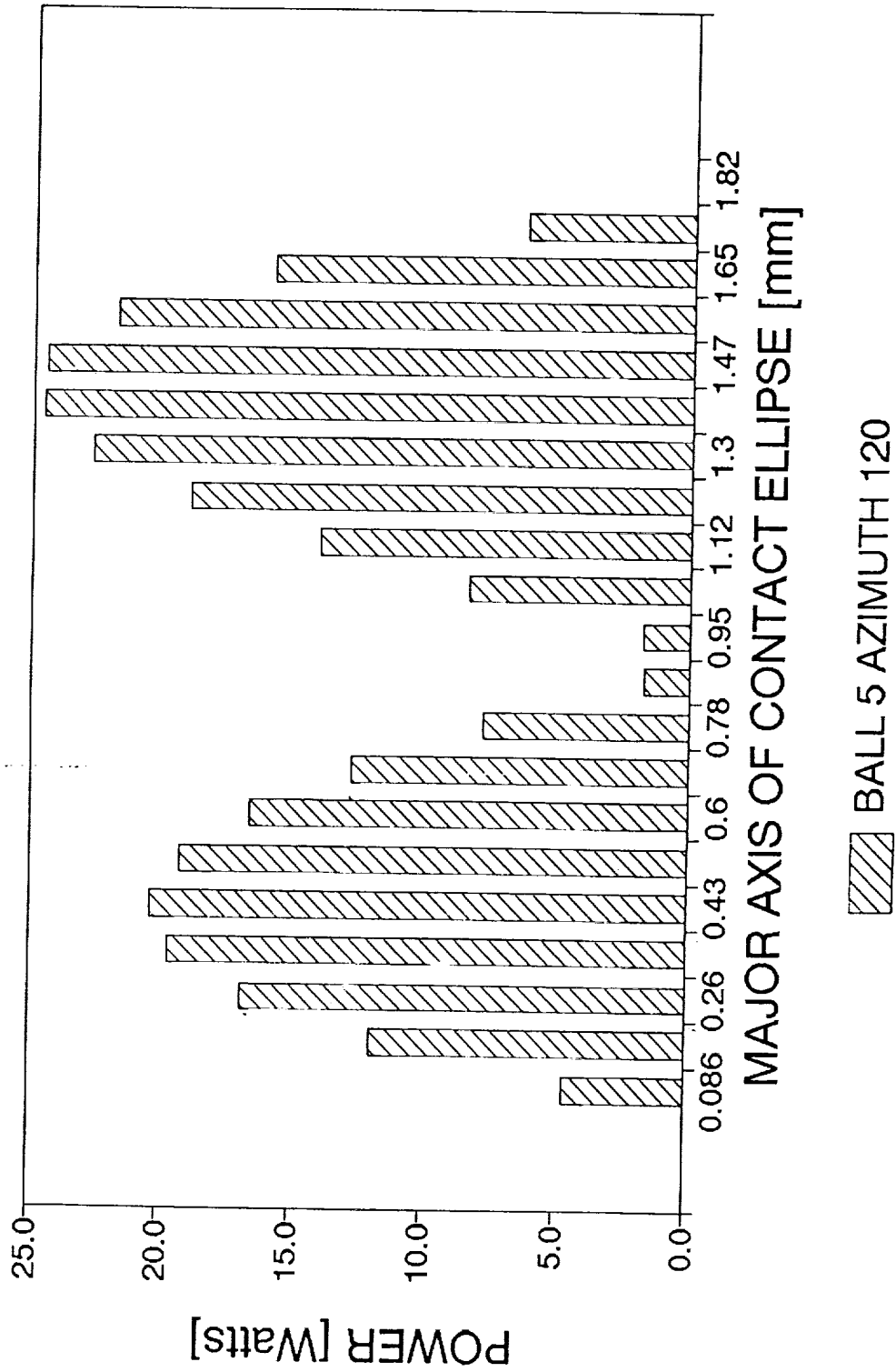
Figure 34. Frictional power loss in contact of ball No. 5 with the inner ring along the major axis of the ellipse of contact.

FRICTIONAL LOSSES IN INNER CONTACT
45mm brg., 157.5um dia.clear., "M" load

POWER [Watts]

MAJOR AXIS OF CONTACT ELLIPSE [mm]

BALL 6 AZIMUTH 150
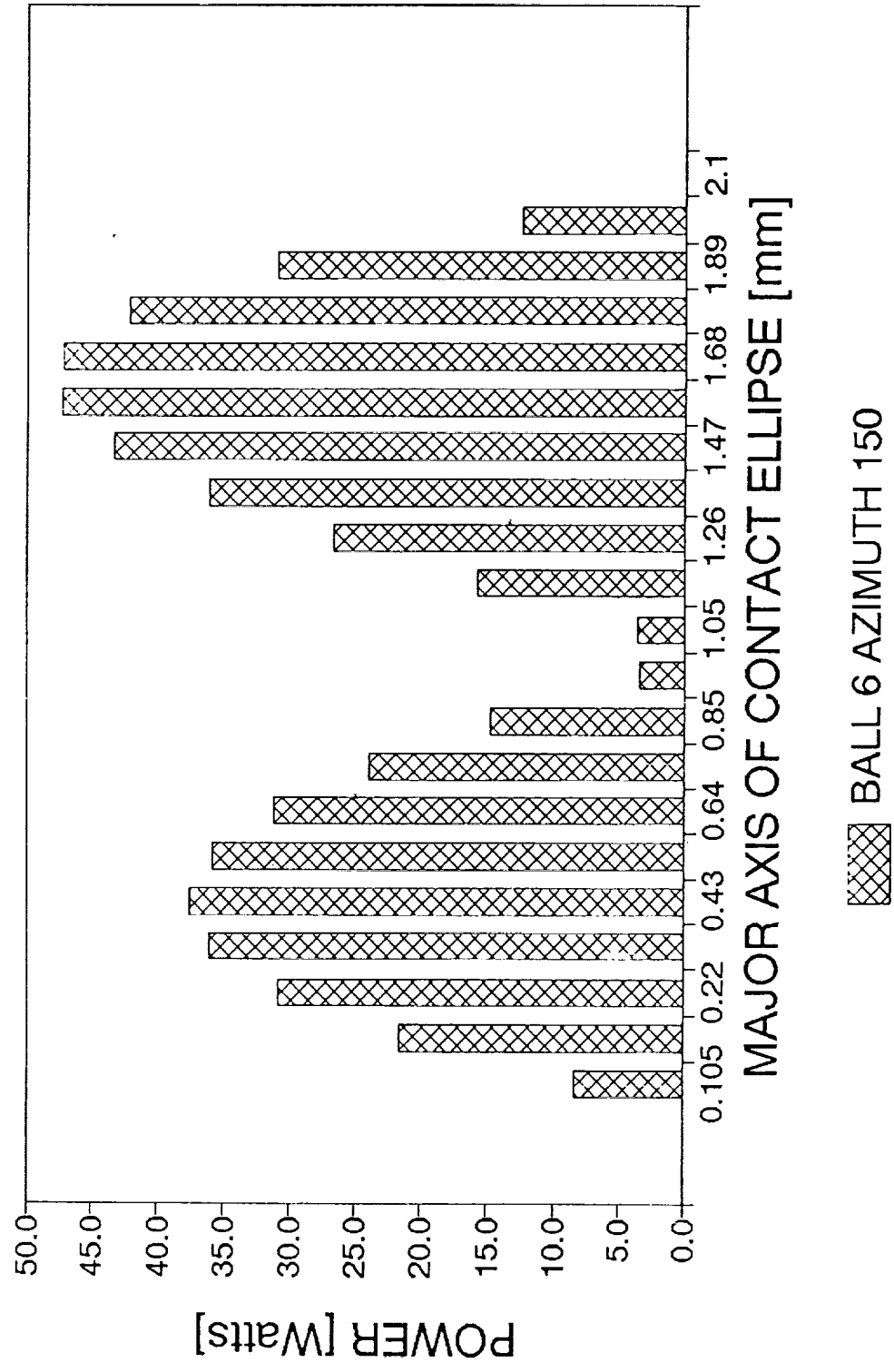
Figure 35. Frictional power loss in contact of ball No. 6 with the inner ring along the major axis of the ellipse of contact

63

FRICTIONAL LOSSES IN INNER CONTACT
45mm brg.,157.5um dia.clear.,"M" load
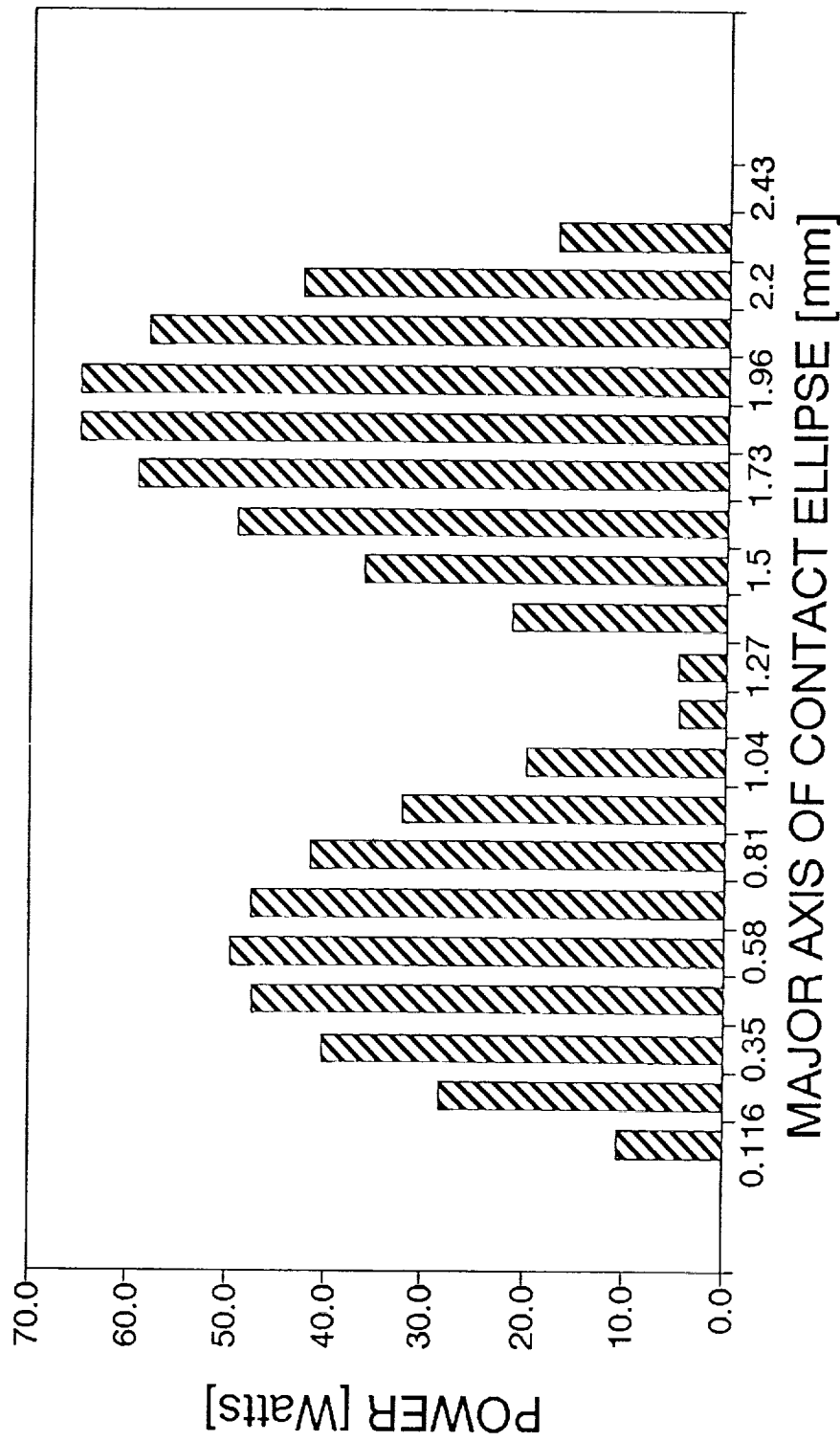
Figure 36. Frictional power loss in contact of ball No. 7 with the inner ring along the major axis of the ellipse of contact.

FRICTIONAL LOSSES IN INNER CONTACT
45mm brg., 157um dia.clear., "M" load
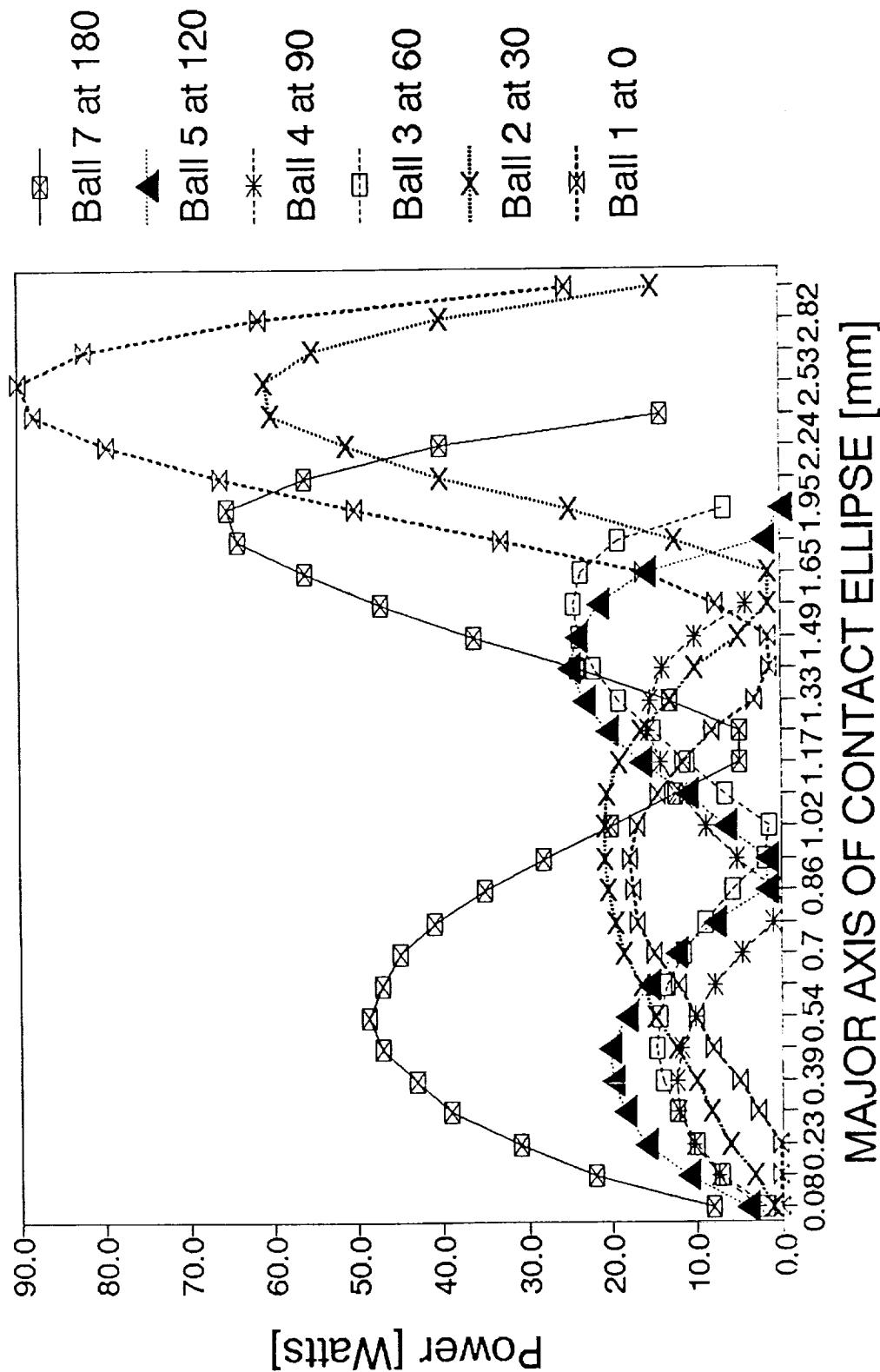
Figure 37. Frictional power loss in contact of a ball with the inner ring along the major axis of the ellipse of contact. Combined diagram (remember symmetry about the load vector).

65

FRICT. LOSS IN CONTACT BALL/INNER RING
45mm brg., 157.5um dia.clear., "M" load

0 (13.6%)
30 (10.5%)
60 (4.9%)
90 (3.6%)
120 (5.8%)
150 (11.0%)
180 (14.9%)
210 (11.0%)
240 (5.8%)
270 (3.6%)
300 (4.9%)
330 (10.5%)
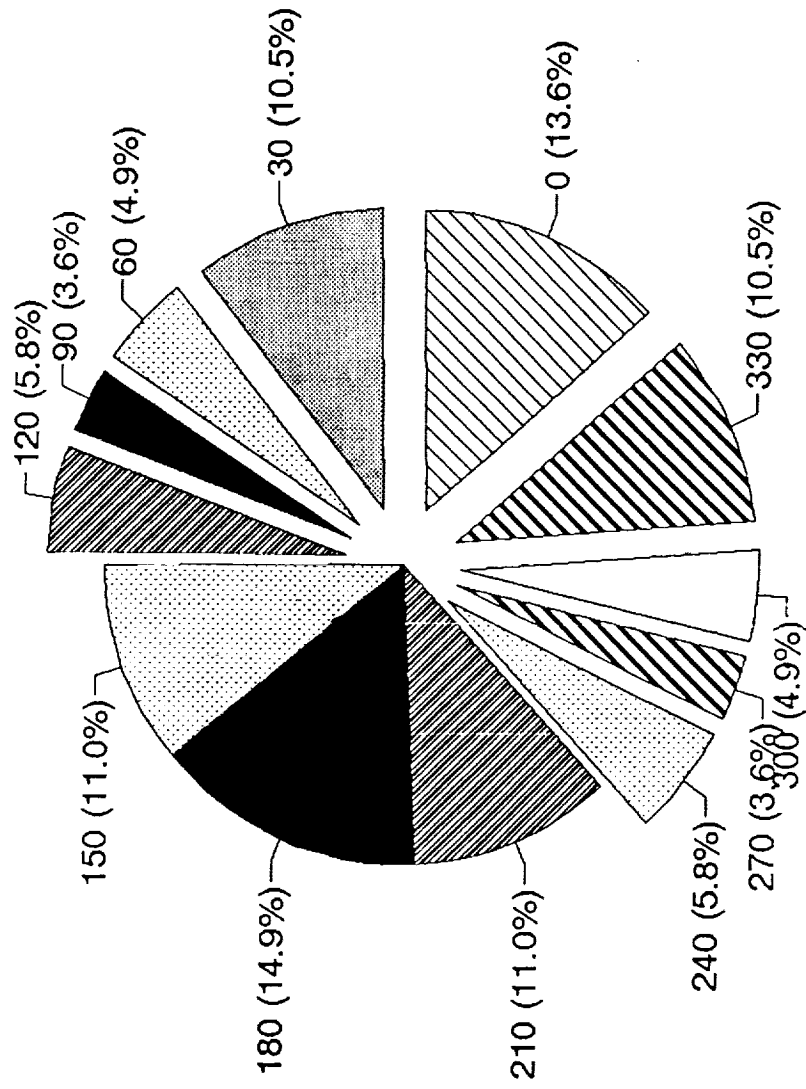
Figure 38. Comparison of power dissipation in contact with the inner ring of a ball traveling around the bearing.
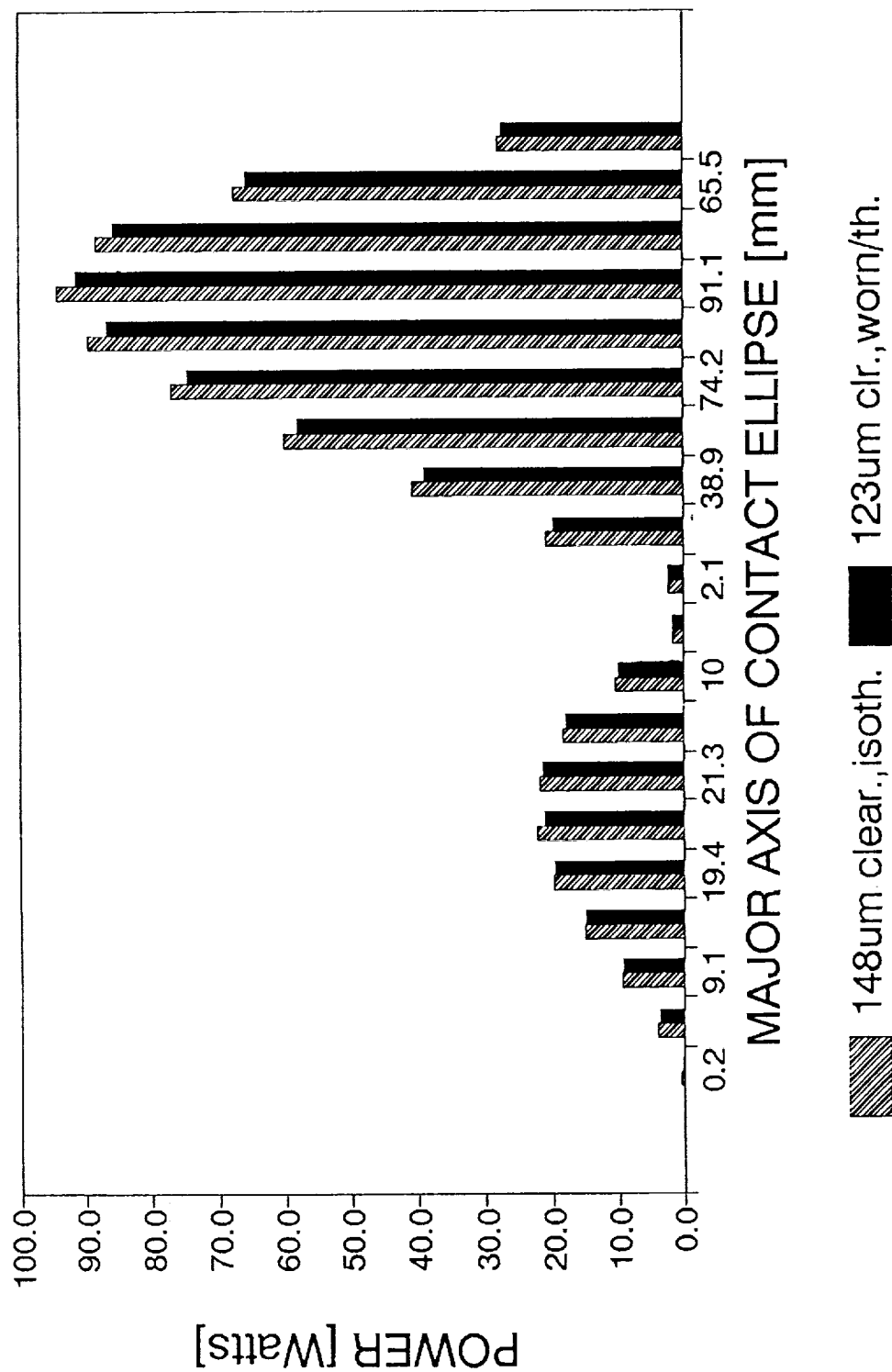
Figure 39. Effect of wear on frictional power dissipation in contact of ball No. 1 with the inner ring.

FRICTIONAL LOSS IN A BALL/RING CONTACT
45mm brg.,157.5um dia.clear., "M" load
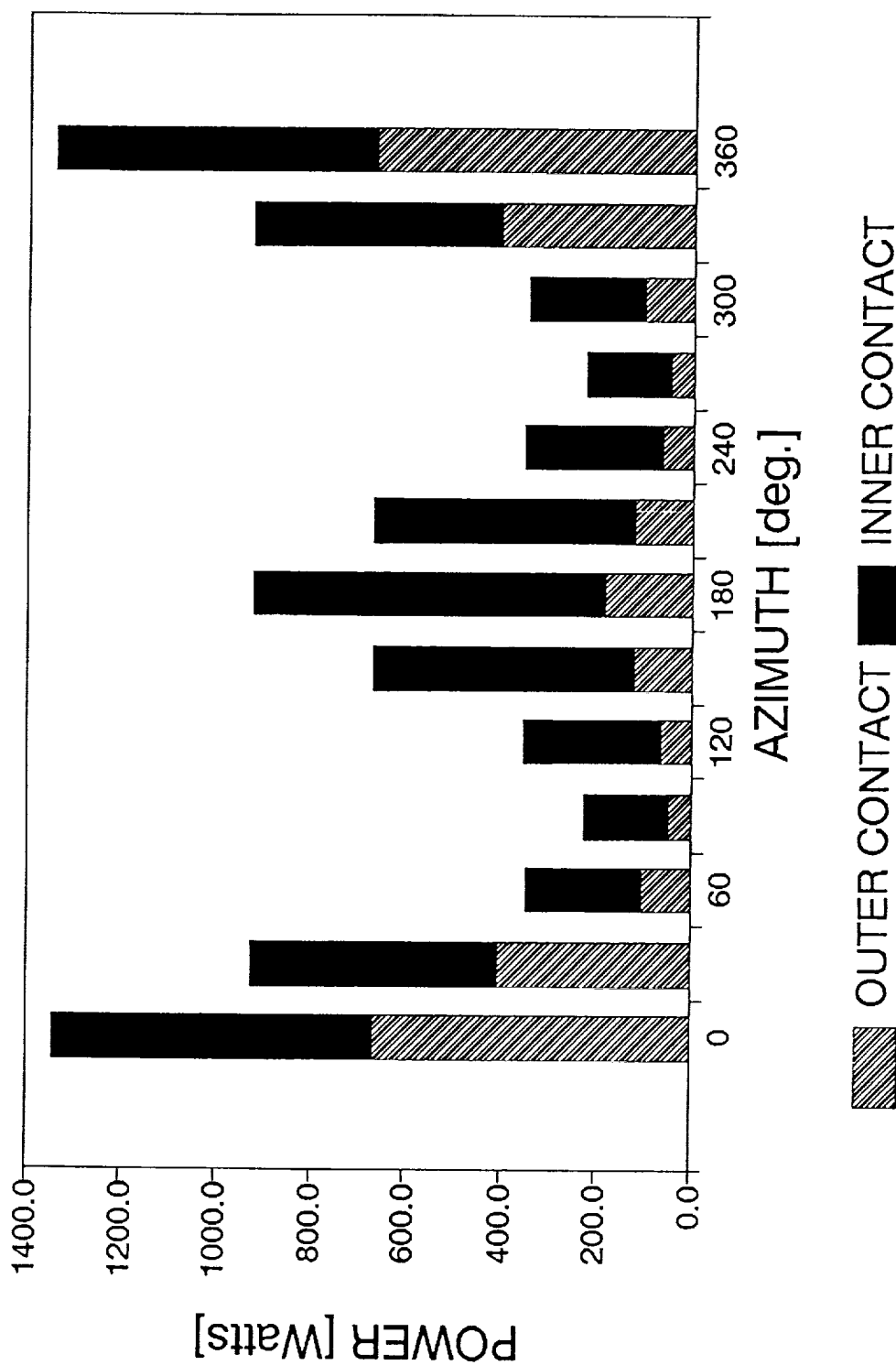
Figure 40. Frictional power dissipation in contact due to interfacial (Heathcote) slip and spin around the bearing for both contacts.

FRICTIONAL LOSSES IN OUTER CONTACT
45mm brg., 157um dia.clear., "M" load

Ball 1 at 0
Ball 2 at 30
Ball 3 at 60
Ball 4 at 90
Ball 5 at 120
Ball 7 at 180

POWER [Watts]

140.0   120.0   100.0   80.0   60.0   40.0   20.0   0.0

0.13 0.39 0.65 0.91 1.17 1.43 1.69 1.95 2.21 2.47 2.8 3.2 3.6 4

MAJOR AXIS OF CONTACT ELLIPSE [mm]

Figure 41. Combined frictional losses for all balls in contact with the outer ring on one side of the bearing, at their respective locations along the track.

FRICTIONAL LOSSES IN INNER CONTACT
45mm brg.,157um dia.clear.,"M" load

Legend:
- Ball 1 at 0
- Ball 2 at 30
- Ball 3 at 60
- Ball 4 at 90
- Ball 5 at 120
- Ball 7 at 180

POWER [Watts] axis: 0.0, 20.0, 40.0, 60.0, 80.0, 100.0, 120.0, 140.0, 160.0, 180.0

MAJOR AXIS OF CONTACT ELLIPSE [mm]: 0.08 0.23 0.39 0.54 0.7 0.86 1.02 1.17 1.33 1.49 1.65 1.95 2.24 2.53 2.82
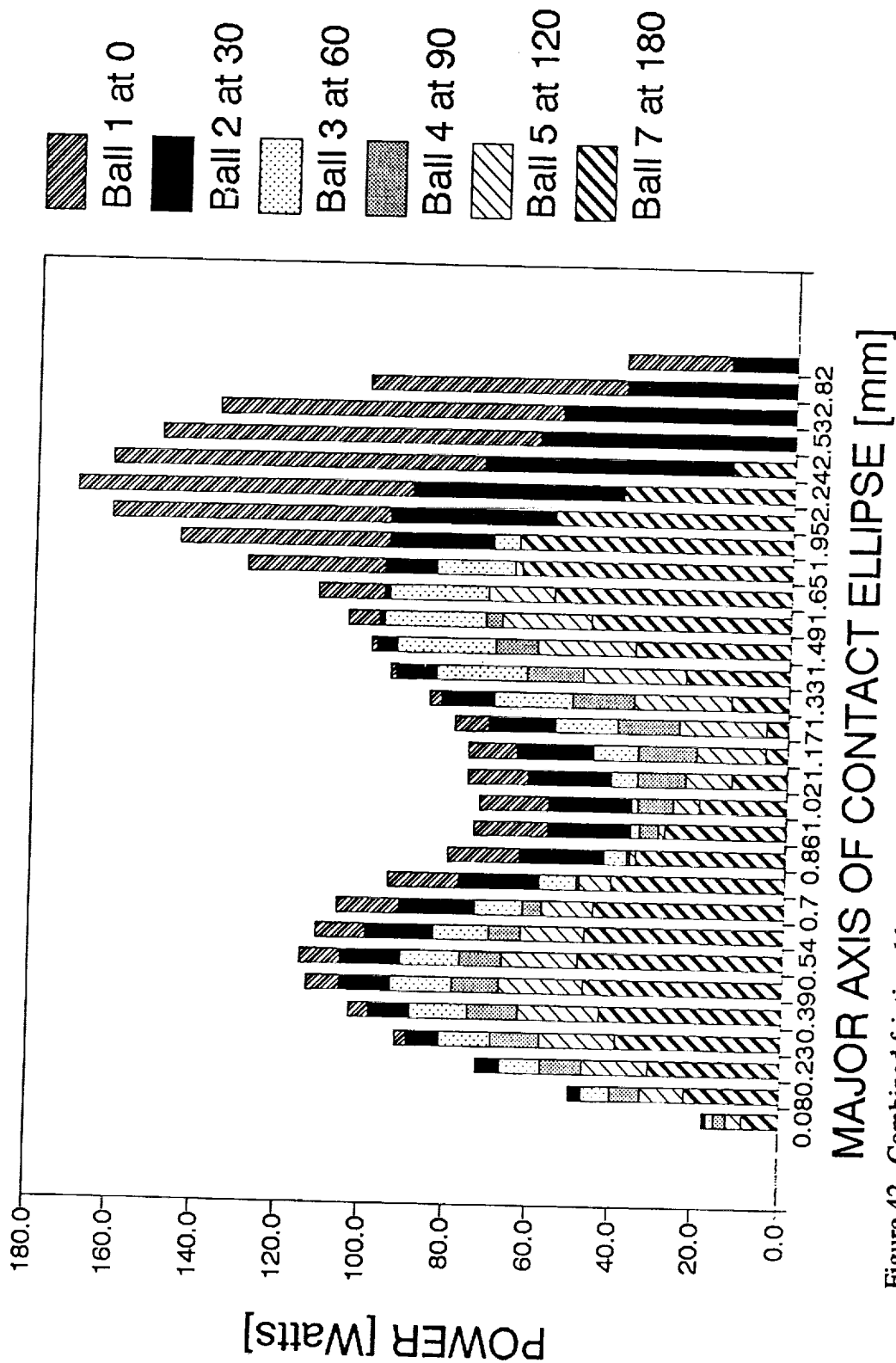
Figure 42. Combined frictional losses for all balls in contact with the inner ring on one side of the bearing, at their respective locations along the track.

COMPUTED WEAR TRACK
45mm brg., 157um dia.clear., "M" load

Outer ring

Inner ring

C/L

Bearing centerline

HIGH/LOW EDGE [mm]

BEARING AZIMUTH [Deg.]
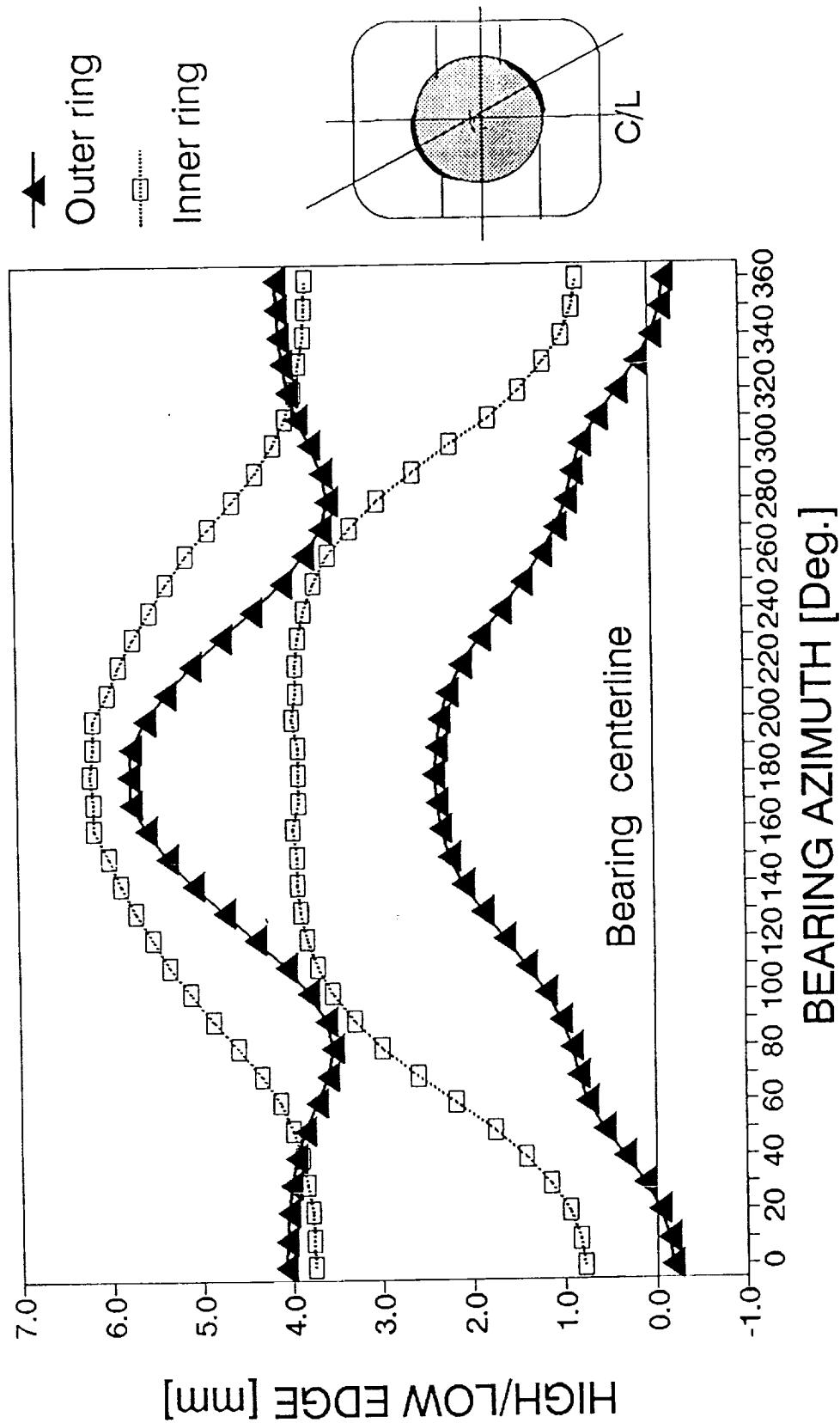
Figure 43. Computed wear track developed along the bearing circumference for both rings. Note the location of bearing center line.

BALL WEAR HPOTP 45mm FLIGHT BRGS.
(R/dyne data 87/93)
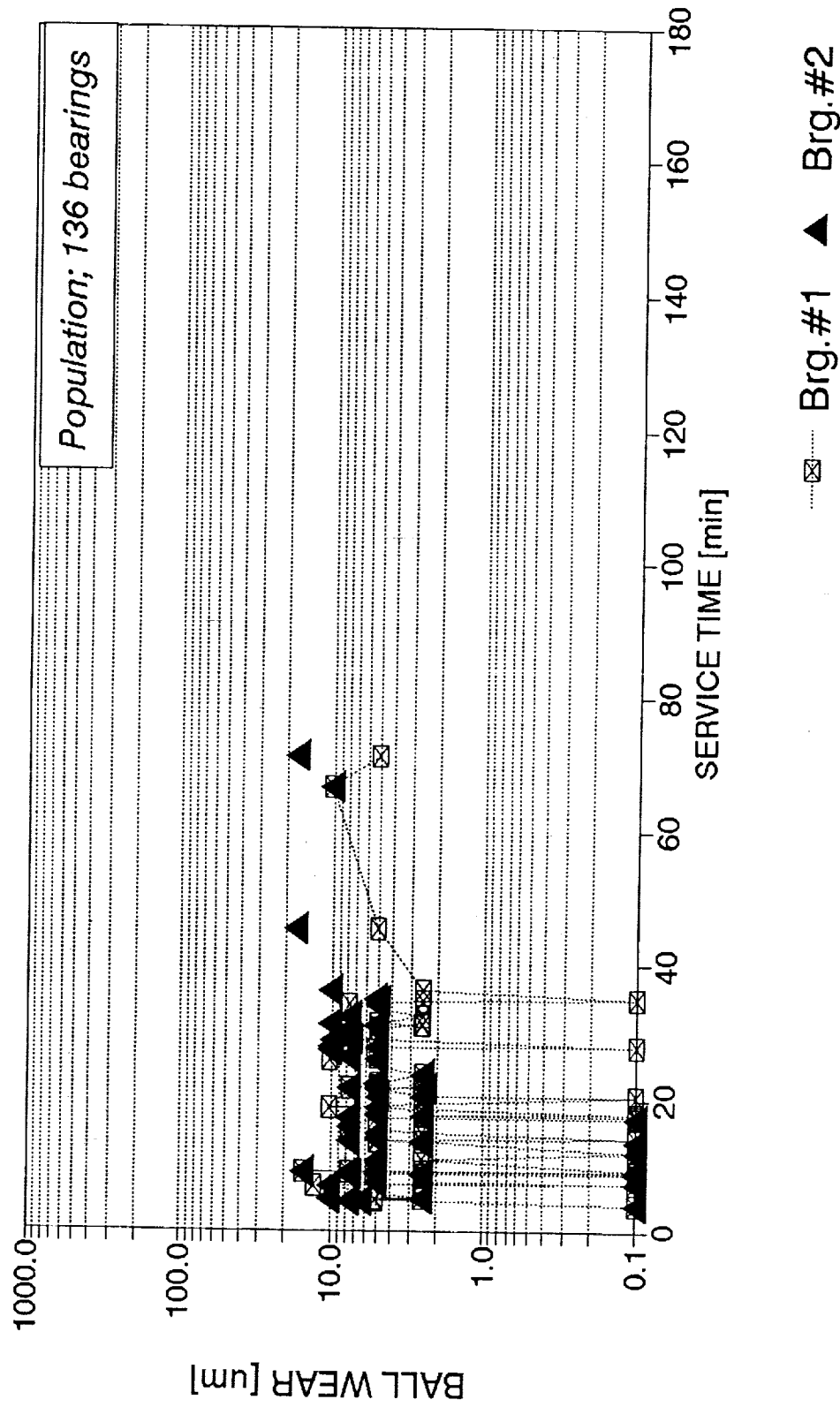
Figure 44. Ball wear record of standard phase II HPOTP flight bearings (*F*) for the 1987–1993 period, based on Rocketdyne data.

BALL WEAR HPOTP 45mm DEV. BRGS.
(R/dyne data 87/93)

Population: 64 bearings

BALL WEAR [um]

SERVICE TIME [min]

⊠ Brg.#1   ▲ Brg.#2
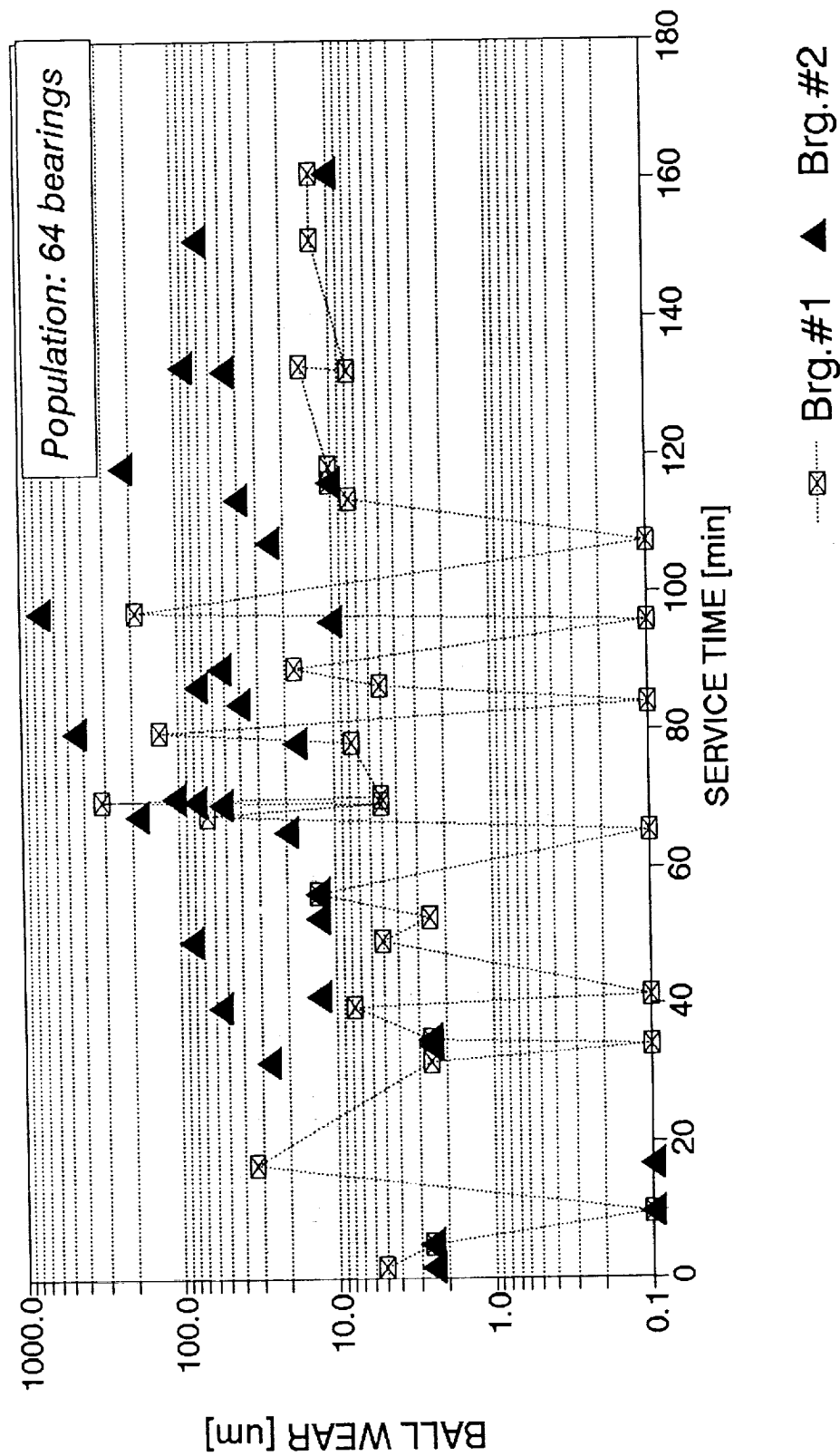
Figure 45. Ball wear record of standard configuration development bearings (*D*) for the 1987–1993 period, based on Rocketdyne data.

BALL WEAR HPOTP 45mm F&D BRGS.

(R/dyne data 87/93)

Population: 200 bearings
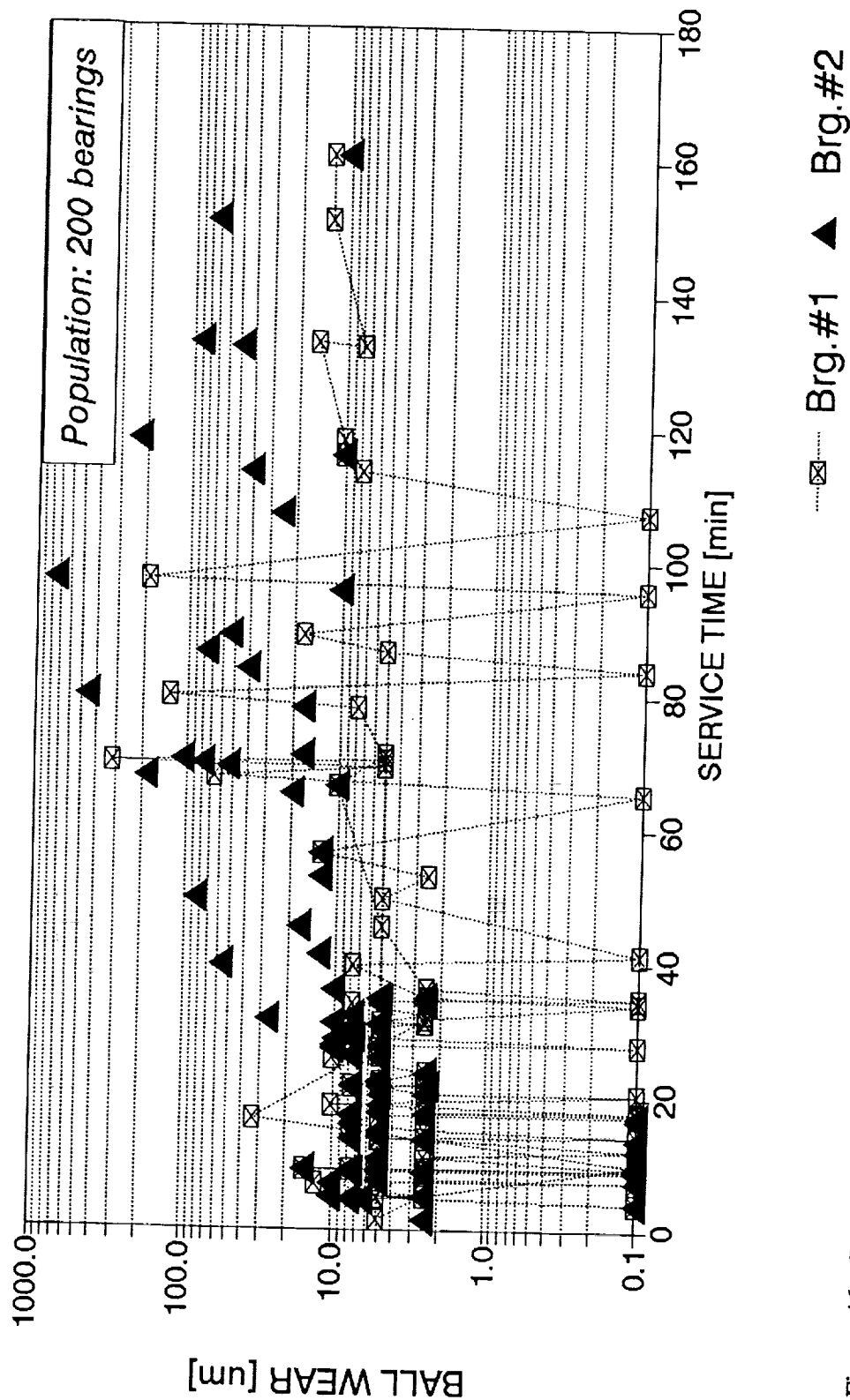
Figure 46. Combined ball wear record of standard phase II HPOTP flight bearings and standard configuration development bearings (F and D) for the 1987–1993 period, based on Rocketdyne data.

HPOTP 45mm BRG. WEAR HISTOGRAM
FLIGHT brgs.(R/dyne data 87/93)
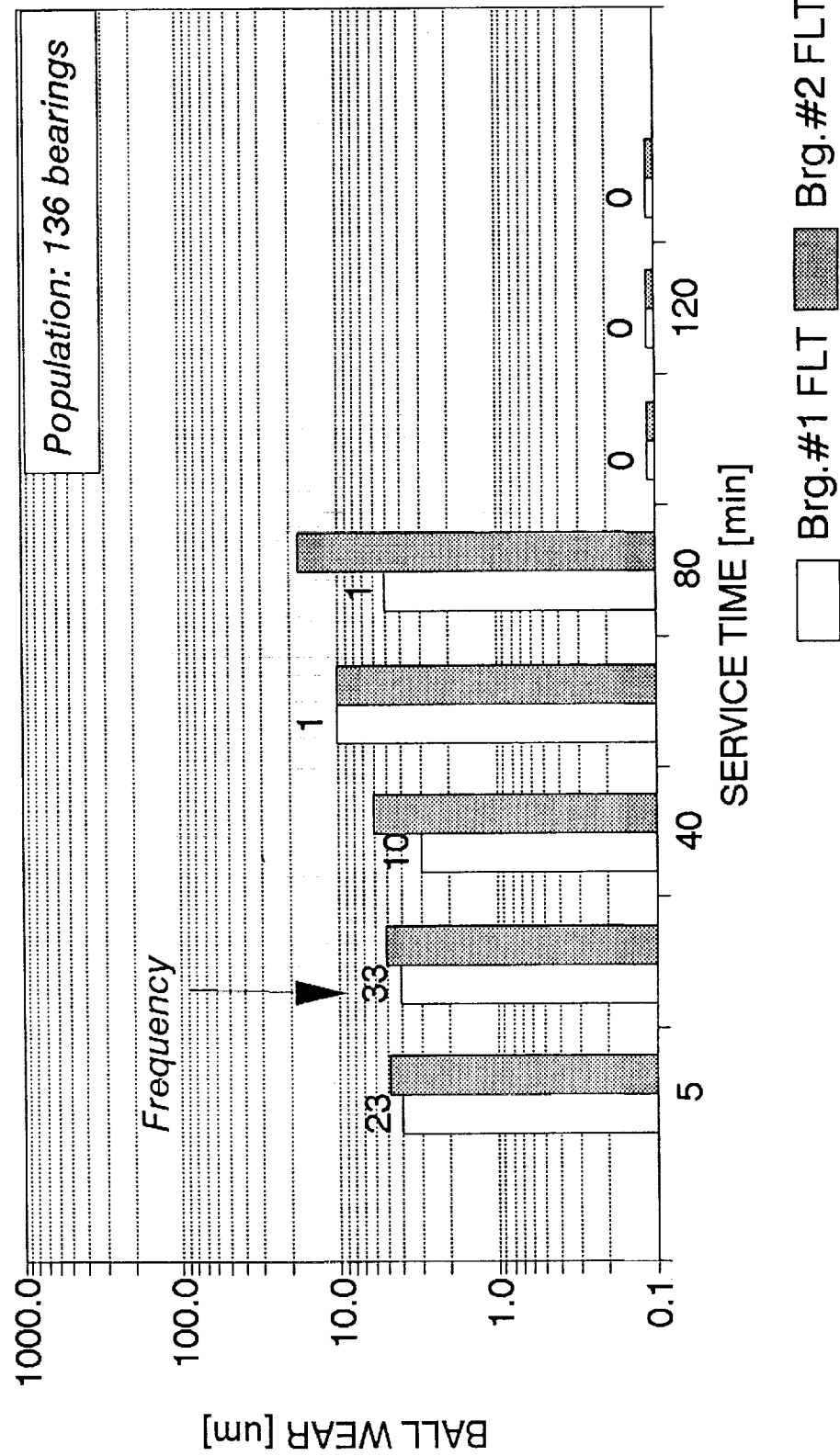
Figure 47. Histogram of ball wear for the standard phase II HPOTP flight bearings for the period of 1987–1993.

75
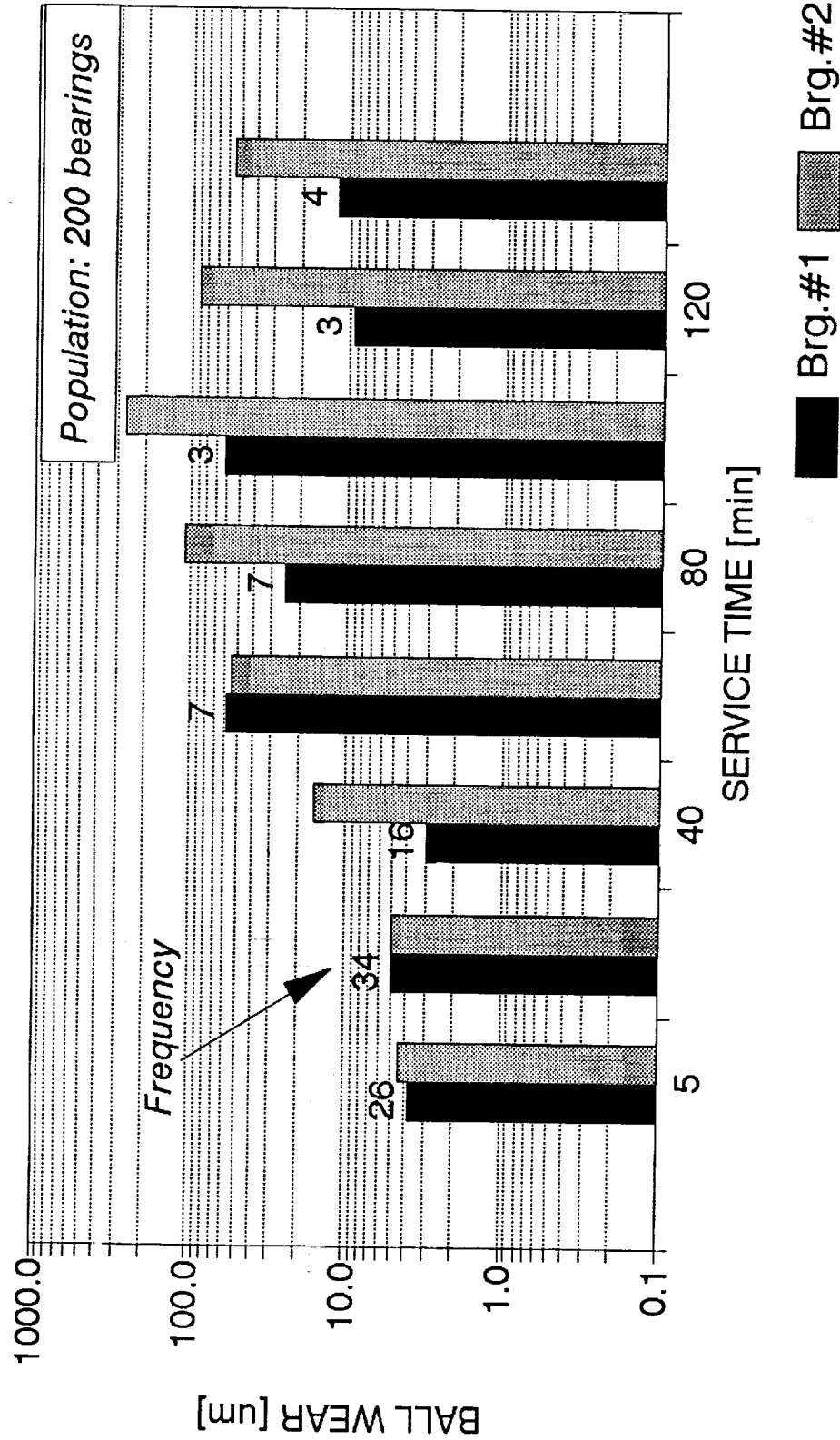
Figure 48. Histogram of ball wear for the combined (*F* and *D*) bearings for the period of 1987–1993.

Figure 49. Analysis of ball wear of bearing No. SN-477. Diameter/weight correlation for balls showing extremely low wear (0.0000 in).

Figure 50. Analysis of ball wear of bearing No. SN-500. Diameter/weight correlation for balls showing medium wear (0.0003 in).

SN 857 BALL WEAR
Diameter/Weight Correlation
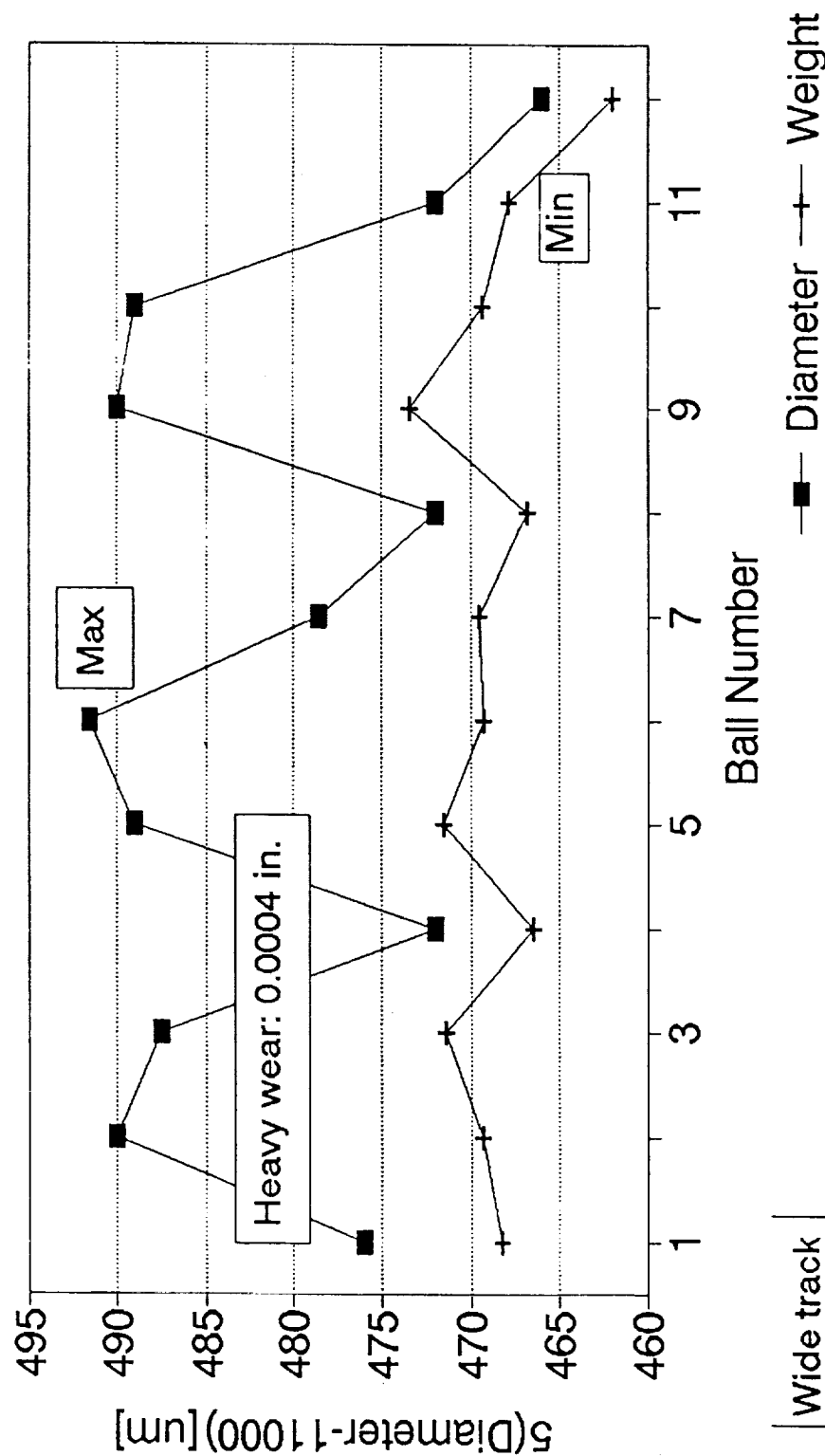
Figure 51. Analysis of ball wear of bearing No. SN-857. Diameter/weight correlation for balls showing heavy wear (0.0004 in).
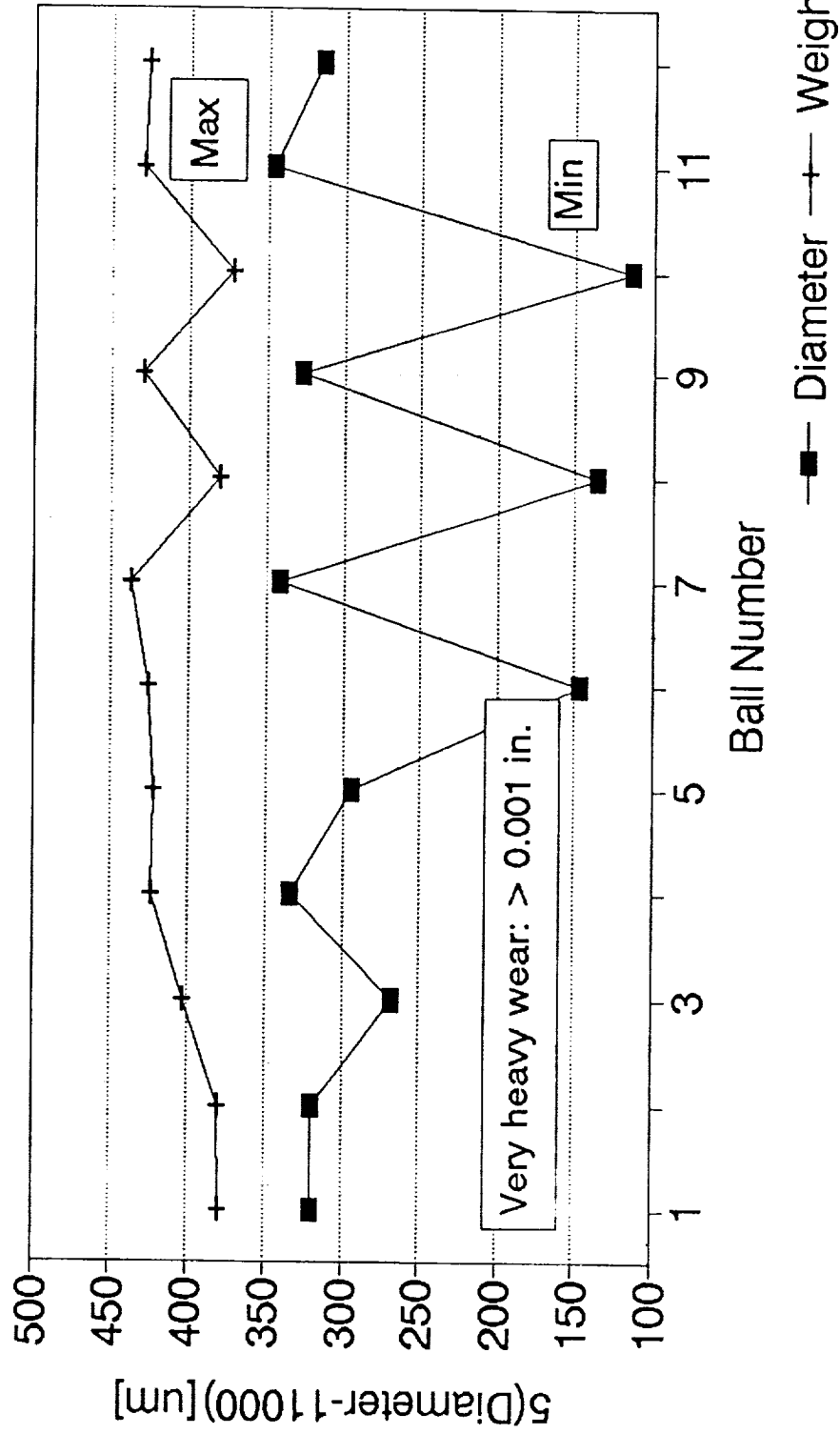
Figure 52. Analysis of ball wear of bearing No. SN-352. Diameter/weight correlation for balls showing extremely high wear (>0.001 in).

MODELING VS. STATISTICAL FIELD DATA (R/DYNE 87/93)

Ball wear HPOTP 45 mm bearings
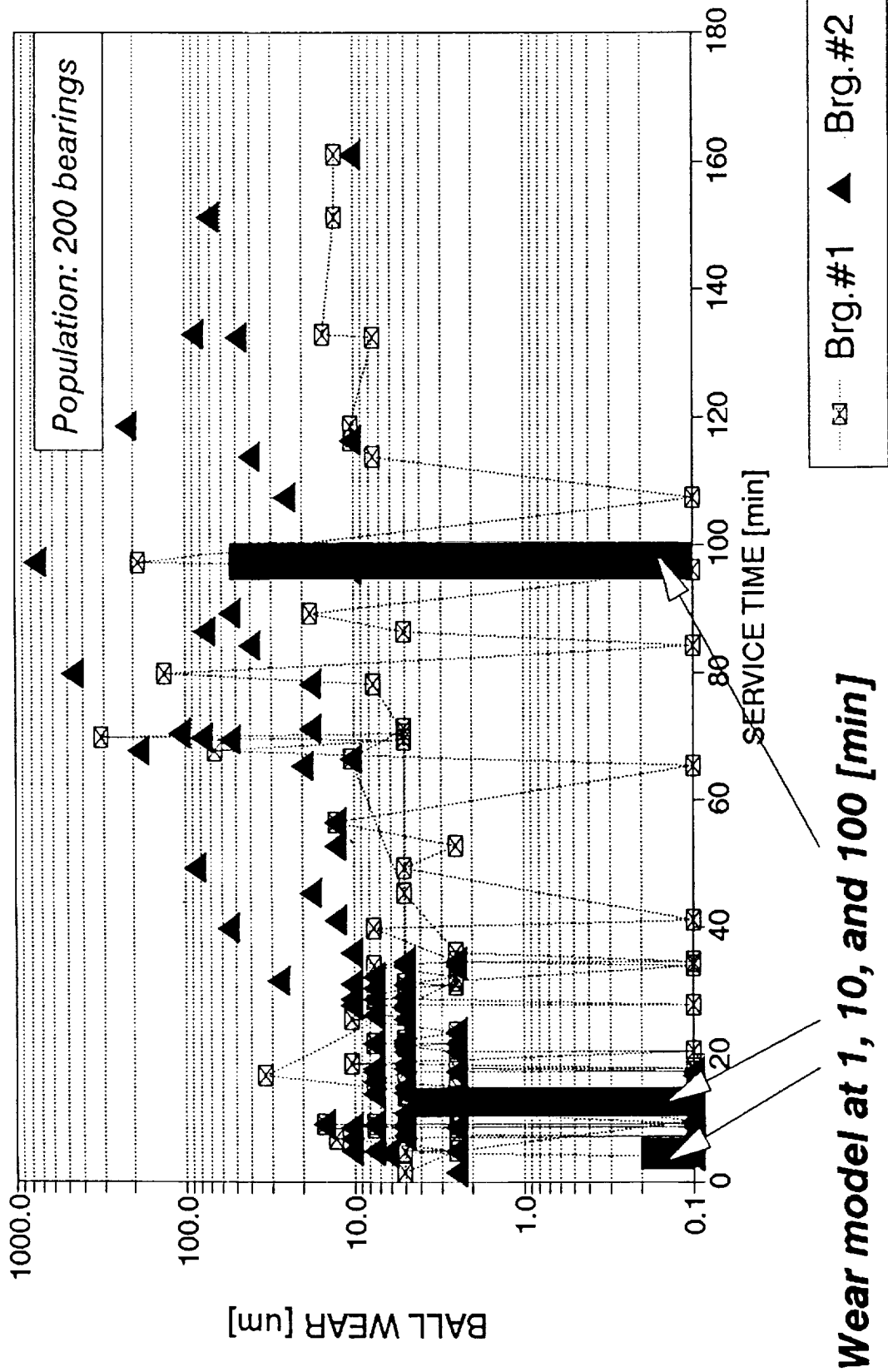
Figure 53. Wear modeling results on the background of field data for 1987–1993.

81

APPENDIX A

Molecular component of the coefficient of friction "f'(T)".

The molecular component of the coefficient of friction "f'(T)" for the range most applicable to turbopump bearings under consideration has been derived using the Kragelsky's definition and Slifka's experimental data as shown below.

From Kragelsky:

$$f = f'e^{[-b(T'-T^*)]} + f''e^{[-a(T'-T^*)]}$$
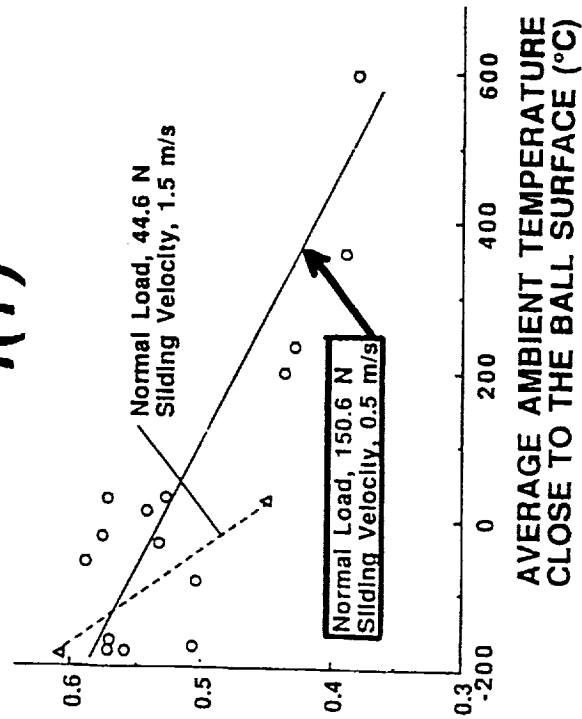
f' = molecular component, decreases with temperature
f'' = mechanical component, increases with temperature
T' = reference temperature, T* = contact temperature
a = alpha/(2v), v = asperity interaction coefficient
b = alpha-gamma, differential temperature coefficient
a, b = frictional temperature factors

Let x=f'@T*=T', y=f''@T*=T', and T=T'-T*

$$\boxed{f = xe^{(-bT)} + ye^{(-aT)}}$$

From NIST:

f(T)

Normal Load, 44.6 N
Sliding Velocity, 1.5 m/s

Normal Load, 150.6 N
Sliding Velocity, 0.5 m/s

COEFFICIENT OF FRICTION

AVERAGE AMBIENT TEMPERATURE
CLOSE TO THE BALL SURFACE (°C)

84

Molecular comp. of the coefficient of friction f'(T), cont'd

T[C]	-200	0	200	400	600
f [-]	0.57	0.50	0.45	0.41	0.37

approximate

Let T=200[deg.C]

$$f(600)=xe^{[-b(600-600)]}+ye^{[-a(600-600)]}=x \quad + \quad y = 0.37$$

$$f(400)=xe^{[-b(600-400)]}+ye^{[-a(600-400)]}=xe^{-bT}+ye^{-aT} = 0.41$$

$$f(200)============xe^{-2bT}+ye^{-2aT}=0.46$$

$$f(0)= ===========xe^{-3bT}+ye^{-3aT}=0.50$$

$$f(-200)==========xe^{-4bT}+ye^{-4aT}=0.57$$

A redundant system of 5 nonlinear eqns. with experimental coefficients. It can only be solved approximately by iterations for the 4 unknowns, i.e. x, y, a, b.

First approximation:

Since f and x are max @ -200 [C], ignore the increase of y from -200 [C] to 0[C]:

$$f(-200)-f(0)=x[e^{(-4Tb)}-e^{(-3Tb)}]+y[e^{(-4Ta)}-e^{(-3Ta)}]=xe^{(-3Tb)}[e^{(-Tb)}-1]$$

(with $y[...] \to 0$)

Molecular comp. of the coefficient of friction f'(T), cont'd

Likewise, the change of y can be ignored from 400[C] to 600[C].

$$f(400)-f(600)=x[e^{(-Tb)}-1]+y[e^{(-Tb)}-1]=x[e^{(-Tb)}-1]$$

$$0$$

Now, divide the last two eqns. side-by-side and solve for

$$bT=\ln\{[f(400)-f(600)]/[f(-200)-f(0)]\}/3=-0.1865 \qquad \text{And so on.........}$$

Iterations have shown that the system does not have a unique solution.
In fact, there are infinitely many approximate solutions.

Combine the first and the last eqn. of the original set and solve for
$x=[f(-200)-f(600)]/[e^{(-4bT)}-1]$, *approx.*

-bT	0.40	0.35	0.30	0.25	0.20	0.15
x	0.051	0.066	0.086	0.116	0.163	0.243
xe^(-4bT)	0.253	0.266	0.286	0.316	0.363	0.443
f	0.571	0.571	0.570	0.570	0.570	0.570

← f'(600)
← f'(-200)
← f(600)

After refinements and assuring compatibility with Slifka's wear data .

the molecular component of the coefficient of friction

$$f'(T) = 0.0655\ e^{\wedge}\ [\ -0.00175\ (T\text{-}600)\ ],\quad T[deg.C]$$

T	-200	0	200	400	600
f'	0.2656	0.1872	0.1319	0.0929	0.0655

$$f' = 0.12 \quad\longleftarrow \text{Average value for the range 0 to 600 [deg.C]}$$

This value coincides with empirical data Kragelsky quoted for sliding of diamond on hard steel. No other data is available.

APPENDIX B

Oxidation mode - modified Quinn's model

Original bilinear approximation for AISI 316 ss is of the form

$$w = c\,(A/V)\,e^{\wedge}(-b/T)$$

where

w[cu.m/m]= volumetric wear rate per unit sliding distance
T [deg.K]   = contact temperature at asperity level
V[m/s]   = sliding velocity
A[sq.m]   = real area of contact (at asperity level)
b,c = empirical constants dependent on T (T<350, T>350 [deg.C])

- Since the range of T is the same, the eqns. will hold.
- Draw empirical constants from the NIST experiment.

Empirical constants "b" and "c", and the wear equations

The Quinn's equations

$$w' = c(A'/V) e^{(-b/T')}$$
$$w'' = c(A''/V) e^{(-b/T'')}$$

$V = 0.5 m/s \text{ (const.)}$

Solve for constants

$$b = ln[A'V''w''/(A''V'w')] T'T''/(T''-T')$$
$$c = [A'/(w'V')]^{[T'/(T''-T')]}/[A''/(w''V'')]^{[T''/(T''-T')]}$$

Using data from Slifka's Fig.5(c)

T[deg.K]	73	473
w[cu.m/m] /multiply x 10^(-13)/	8	36
A [sq.m] /multiply x 10^(-6)/	1.20	2.54

the constants are

b=64.896
c=8.1224x10^(-7)

The modified Quinn's eqn.

w'=8.1224x10^(-7)x(A/V)xe^(-64.896/T), T<350 [deg.C]

Likewise,

w''=25.9631x10^(-6)x(A/V)xe^(-1,613.71/T), T>350 [deg.C]

C-2

91

PAGE 92 INTENTIONALLY BLANK

APPENDIX C

Abrasion mode - Holm/Archard model

The original eqn. $U/L = l = kp/y$ *can be solved for* **$k = ly/p$**

where
$U[m]$=linear wear, $L[m]$=sliding distance, $l=U/L$
$k[-]$=empirical wear coefficient, $p[MPa]$=load pressure
$y[MPa]$=yield stress

Using Slifka's data on wear (converted to l) and ave. pressure as follows

T[deg.C]	-200	0	200	400	600
p[MPa]	142.72	142.13	141.03	140.42	140.04

the following wear coefficient was obtained

T[deg.C]	-200	0	200	400	600
k [-] /multiply x 10^(-6)	0.936	1.153	2.013	3.368	5.866

$k = 3.10 \times 10^{-6}$ ⟵ Average value for $0 < T < 600$ [deg.C]

APPENDIX D

SHABERTH computer printouts.

File Ref. # singl"M" - op.clear. 148um

UNLESS OTHERWISE STATED, LINEAR DIMENSIONS ARE SPECIFIED IN MILLIMETERS, TEMPERATURES IN DEGREES CENTIGRADE, FORCES IN NEWTONS, WEIGHTS IN KILOGRAMS, PRESSURES AND ELASTIC MODULI IN NEWTONS PER SQUARE MILLIMETER, ANGLES AND SLOPES IN DEGREES, SURFACE ROUGHNESS IN MICRONS, SPEEDS IN REVOLUTIONS PER MINUTE, DENSITY IN GRAMS PER CUBIC CENTIMETER, KINEMATIC VISCOSITY IN CENTISTOKES AND THERMAL CONDUCTIVITY IN WATTS PER METER-DEGREE CENTIGRADE.

SOLUTION LEVEL = 2
THE MAXIMUM NUMBER OF FIT ITERATIONS ALLOWED IS 5 AND THE RELATIVE ACCURACY REQUIRED IS 0.00010

BEARING NUMBER	NUMBER OF ROLLING ELEMENTS	AZIMUTH ANGLE ORIENTATION	PITCH DIAMETER	DIAMETRAL CLEARANCE	CONTACT ANGLE	INNER RING SPEED	OUTER RING SPEED
1	12	0.000	65.024	0.160	25.190	30000.	0.

C A G E D A T A

BEARING NUMBER	CAGE TYPE	CAGE POCKET CLEARANCE	RAIL-LAND WIDTH	RAIL-LAND DIAMETER	RAIL-LAND CLEARANCE	WEIGHT
1	OUTER RING LAND RIDING	0.750000	2.4400	71.5518	0.229	0.020000

S T E E L D A T A

BRG.NO.	INNER RING TYPE	LIFE FACTOR	OUTER RING TYPE	LIFE FACTOR
1	440C	1.000	440C	1.000

R O L L I N G E L E M E N T D A T A
BEARING NUMBER (1)   TYPE - BALL BEARING

BALL DIAMETER	OUTER RACEWAY CURVATURE	INNER RACEWAY CURVATURE
11.1125	0.520	0.550

S U R F A C E D A T A

BEARING NUMBER	CLA ROUGHNESS OUTER	INNER	ROLL. ELM.	RMS ASPERITY SLOPE OUTER	INNER	ROLL. ELM.
1	0.01	0.01	0.01	2.000	2.000	2.000

L U B R I C A T I O N A N D F R I C T I O N D A T A
BEARING 1 IS OPERATING DRY WITH FRICTION COEFFICIENTS OF, RACE/R.E. 0.300 CAGE/R.E. AND CAGE/RING 0.100

F I T D A T A A N D M A T E R I A L P R O P E R T I E S

BEARING NUMBER	COLD FITS (MM TIGHT) SHAFT	HOUSING	EFFECTIVE WIDTHS SHAFT	INNER RING	OUTER RING	HOUSING
1	0.0356	-0.0660	33.8800	16.9200	16.9200	33.8800

BEARING NUMBER	SHAFT I.D.	BEARING BORE	EFFECTIVE DIAMETERS INNER RING AVE. O.D.	OUTER RING AVE. I.D.	BEARING O.D.	HOUSING O.D.
1	19.050	44.988	56.410	73.980	83.894	95.500

BEARING NUMBER (1)	SHAFT	INNER RING	ROLL. ELEM.	OUTER RING	HOUSING
MODULUS OF ELASTICITY	234200.0	212700.0	212700.0	212700.0	193200.0
POISSONS RATIO	0.2900	0.2900	0.2900	0.2900	0.2900
WEIGHT DENSITY	8.190	7.667	7.667	7.667	8.190
COEFF. OF THERMAL EXP.	0.00001440	0.00000929	0.00000929	0.00000929	0.00001440

GIVEN TEMPERATURES (C)

BRG	O.RACE	I.RACE	BULK OIL	FLNG.1	FLNG.2	FLNG.3	FLNG.4	CAGE	SHAFT	I.RING	ROLL.EL.	O.RING	HSG.
1	-145.00	-145.00	-145.00	-145.00	-145.00	-145.00	-145.00	-145.00	-145.00	-145.00	-145.00	-145.00	-145.00

LOADING IN THE X - Y PLANE

CONCENTRATED FORCE, FY   CONCENTRATED MOMENT ABOUT Z
*   4701.0 NEWTONS   0.0 NEWTON-MM.

LOADING IN THE X - Z PLANE

CONCENTRATED FORCE, FZ   CONCENTRATED MOMENT ABOUT Y
*   0.0 NEWTONS   0.0 NEWTON-MM.

THRUST LOAD FX =   8230.8 NEWTONS
**** ERROR MESSAGE FROM THE EQUATION SOLVING ROUTINE, AT ITERATION LOOP 23 ****
**** ERROR MESSAGE FROM THE EQUATION SOLVING ROUTINE, AT ITERATION LOOP   5 ****

B E A R I N G S Y S T E M O U T P U T

BRG.	LINEAR (MM) AND ANGULAR (RADIANS) DEFLECTIONS DX	DY	DZ	GY	GZ	REACTION FORCES (N) AND MOMENTS (MM-N) FX	FY	FZ	MY	MZ
1	0.137	0.139	3.391E-08	-6.982E-10	5.137E-03	8.238E+03	4.703E+03	698.	-2.859E+03	1.071E+03

BRG.	FATIGUE LIFE (HOURS) O. RACE	I. RACE	BEARING	H/SIGMA O. RACE	I. RACE	LUBE-LIFE FACTOR O. RACE	I. RACE	MATERIAL FACTOR O. RACE	I. RACE
1	44.9	4.96	4.60	0.000	0.000	1.00	1.00	1.00	1.00

TEMPERATURES RELEVANT TO BEARING PERFORMANCE (DEGREES CENTIGRADE)

BRG	O.RACE	I.RACE	BULK OIL	FLNG.1	FLNG.2	FLNG.3	FLNG.4	CAGE	SHAFT	I.RING	ROLL.EL.	O.RING	HSG.
1	-145.00	-145.00	-145.00	-145.00	-145.00	-145.00	-145.00	-145.00	-145.00	-145.00	-145.00	-145.00	-145.00

FRICTIONAL HEAT GENERATION RATE (WATTS) AND FRICTION TORQUE (N-MM)

BRG.	O. RACE	O. FLNGS.	I. RACE	I. FLNGS.	R.E.DRAG	R.E.-CAGE	CAGE-LAND	TOTAL	TORQUE
1	1.820E+03	0.000	5.135E+03	0.000	0.000	3.306E+04	0.298	4.002E+04	1.274E+04

EHD FILM THICKNESS, FILM REDUCTION FACTORS AND HEAT CONDUCTIVITY DATA FOR THE OUTER AND INNER RACEWAYS RESPECTIVELY

BRG.	FILM (MICRONS)		STARVATION FACTOR		THERMAL FACTOR		MENISCUS DIST. (MM)		CONDUCTIVITY (W/DEG.C)	
1	0.000	0.000	0.000	0.000	0.000	0.000	0.000	0.000	19.3	13.0

FIT PRESSURES (N/MM2)   BEARING CLEARANCES (MM)   SPEED GIVING ZERO FIT PRESSURE

BRG.	SHAFT-COLD,	OPER.	HSG.-COLD,	OPER.	ORIGINAL	CHANGE	OPERATING	SHAFT-INNER RING (RPM)
1	31.7	0.000	0.000	0.000	0.160	-1.178E-02	0.148	0.000

CAGE DATA   (CAGE HAS ONE DEGREE OF FREEDOM)

CAGE RAIL - RING LAND DATA   CAGE SPEED DATA

	TORQUE	HEAT RATE	SEP.FORCE	ECCENTRICITY	EPICYCLIC SPEED		CALCULATED SPEED		CALC/EPIC	CAGE/SHAFT
BRG.	(MM-N)	(WATTS)	(NEWTONS)	RATIO	(RAD/SEC)	(RPM)	(RAD/SEC)	(RPM)	RATIO	RATIO
1	-0.215	0.298	6.049E-02	0.100	1.388E+03	1.325E+04	1.383E+03	1.321E+04	0.997	0.440

AZIMUTH	ANGULAR SPEEDS (RADIANS/SECOND)					SPEED VECTOR ANGLES (DEGREES)		SPIN TO ROLL RATIO	
ANGLE (DEG.)	WX	WY	WZ	TOTAL	ORBITAL	TAN-1(WY/WX)	TAN-1(WZ/WX)	OUTER	INNER
0.00	-8632.202	2599.899	-0.238	9015.230	1319.887	163.24	-180.00	0.0049	0.1383
30.00	-8599.638	2785.471	-1.258	9039.503	1320.448	162.05	-179.99	0.0042	0.1601
60.00	-8674.904	3043.879	-4.043	9193.432	1349.152	160.66	-179.97	0.0032	0.2681
90.00	-9011.875	3324.964	-1.455	9605.670	1403.525	159.75	-179.99	0.0135	0.4545
120.00	-8615.381	4396.717	-33.596	9672.488	1428.572	152.96	-179.78	0.0037	0.5066
150.00	-7800.085	5587.694	-2.029	9594.981	1431.754	144.38	-179.99	-.0121	0.4450
180.00	-7397.420	5883.887	-0.004	9452.088	1424.017	141.50	-180.00	0.0065	0.4183
210.00	-7753.875	5453.086	-0.213	9479.385	1427.156	144.88	-180.00	0.0082	0.4497
240.00	-8594.141	4352.872	-0.007	9633.626	1426.810	153.14	-180.00	-.0019	0.5148
270.00	-9028.157	3293.147	-4.998	9610.020	1403.372	159.96	-179.97	-.0005	0.4674
300.00	-8594.641	3008.723	-0.304	9106.057	1343.553	160.71	-180.00	0.0037	0.2694
330.00	-8586.561	2773.264	-1.030	9023.304	1319.486	162.10	-179.99	0.0045	0.1611

AZIMUTH	NORMAL FORCES (NEWTONS)			HZ STRESS (N/MM**2)		LOAD RATIO QASP/QTOT		CONTACT ANGLES (DEG.)	
ANGLE (DEG.)	CAGE	OUTER	INNER	OUTER	INNER	OUTER	INNER	OUTER	INNER
0.00	18.946	3293.605	3001.808	2610.005	3513.446	0.0000	0.0000	19.8521	21.8420
30.00	478.649	2481.005	2196.738	2374.799	3166.152	0.0000	0.0000	21.1804	24.0594
60.00	831.541	1149.748	839.720	1837.745	2297.826	0.0000	0.0000	22.7458	31.2244
90.00	881.220	685.739	405.861	1546.929	1803.286	0.0000	0.0000	24.3782	41.6307
120.00	641.034	876.801	579.027	1679.002	2030.043	0.0000	0.0000	31.6705	49.9271
150.00	297.817	1367.291	1111.401	1947.023	2522.876	0.0000	0.0000	40.5721	54.4238
180.00	-28.775	1660.915	1428.258	2077.463	2742.887	0.0000	0.0000	44.9425	55.5436
210.00	-338.585	1317.151	1070.337	1922.927	2491.414	0.0000	0.0000	41.2271	54.1544
240.00	-658.588	907.809	625.285	1698.566	2082.723	0.0000	0.0000	31.1639	50.1308
270.00	-891.785	767.984	472.945	1606.454	1897.620	0.0000	0.0000	23.3299	42.0575
300.00	-821.111	1138.951	847.390	1831.974	2304.801	0.0000	0.0000	22.7457	31.2234
330.00	-444.271	2483.331	2196.037	2375.540	3165.816	0.0000	0.0000	21.1483	24.0729

F R I C T I O N A L   H E A T   G E N E R A T I O N   I N   C O N T A C T   E L L I P S E

R O L L I N G   E L E M E N T   N U M B E R   1

	INNER RACE				OUTER RACE		
# LAMINA	CONTACT AREA (MM**2)	SEMI-MAJOR AXIS (MM)	SEMI-MINOR AXIS (MM)	# LAMINA	CONTACT AREA (MM**2)	SEMI-MAJOR AXIS (MM)	SEMI-MINOR AXIS (MM)
20	1.282	1.480	0.2756	19	1.893	2.119	0.2843

WIDTH OF LAMINUM (MM)	HEAT GEN. PER LAM. (WATTS)	WIDTH OF LAMINUM (MM)	HEAT GEN. PER LAM. (WATTS)
0.1420076000	0.353	0.2120541000	19.113
0.1420076000	3.861	0.2120541000	42.428
0.1420076000	9.374	0.2120541000	50.360
0.1420076000	15.047	0.2120541000	47.616
0.1420076000	19.629	0.2120541000	38.162
0.1420076000	22.134	0.2120541000	25.175
0.1420076000	21.831	0.2120541000	10.151
0.1420076000	18.179	0.2120541000	0.785
0.1420076000	10.311	0.2636262000	0.850
0.1420076000	1.453	0.2636262000	2.804
0.1539963000	2.278	0.2636262000	0.858
0.1539963000	20.747	0.2189394000	0.887
0.1539963000	40.703	0.2189394000	11.678
0.1539963000	59.985	0.2189394000	27.976
0.1539963000	76.960	0.2189394000	42.415
0.1539963000	89.250	0.2189394000	53.059
0.1539963000	94.007	0.2189394000	56.272

0.1539963000	87.951	0.2189394000	4.01	47.535
0.1539963000	67.365	0.2189394000	4.23	21.466
0.1539963000	28.082	0.0000000000		0.000

M A X I M U M   S T R E S S * V E L O C I T Y   I N   C O N T A C T   E L L I P S E

BEARING NUMBER	ELEMENT NUMBER	STRESS VELOCITY (N/MM-S)	ELEMENT NUMBER	STRESS VELOCITY (N/MM-S)
		INNER RACE		OUTER RACE
1	6	2.51198E+09	6	7.56120E+09

S T R E S S   V E L O C I T Y   P R O F I L E   I N   C O N T A C T   E L L I P S E
R O L L I N G   E L E M E N T   N U M B E R   6
LAMINA POSITION FROM LOWER CONTACT ANGLE EDGE OF CONTACT ELLIPSE

	I N N E R R A C E		O U T E R R A C E
LAMINA POSITION (MM)	STRESS VELOCITY (N/MM-S)	LAMINA POSITION (MM)	STRESS VELOCITY (N/MM-S)
5.22861E-02	-3.15725E+06	8.14977E-02	-8.30584E+05
1.56858E-01	-4.94227E+06	2.44493E-01	-1.01133E+06
2.61431E-01	-5.69051E+06	4.07489E-01	-8.37530E+05
3.66003E-01	-5.90875E+06	5.70484E-01	-5.30001E+05
4.70575E-01	-5.76138E+06	7.33479E-01	-1.76990E+05
5.75147E-01	-5.33385E+06	8.90774E-01	1.59373E+05
6.79720E-01	-4.68207E+06	1.04237E+00	4.51482E+05
7.84292E-01	-3.84843E+06	1.19396E+00	6.93652E+05
8.88864E-01	-2.86894E+06	1.34555E+00	8.73399E+05
9.93436E-01	-1.77694E+06	1.49715E+00	9.82598E+05
1.09801E+00	-6.05185E+05	1.64874E+00	1.01682E+06
1.20447E+00	6.34306E+05	1.80034E+00	9.75095E+05
1.31283E+00	1.90358E+06	1.95193E+00	8.59710E+05
1.42118E+00	3.13354E+06	2.10352E+00	6.76554E+05
1.52954E+00	4.26739E+06	2.25512E+00	4.35508E+05
1.63790E+00	5.23332E+06	2.40671E+00	1.51567E+05
1.74625E+00	5.93364E+06	2.56746E+00	-1.71812E+05
1.85461E+00	6.22037E+06	2.73735E+00	-4.94960E+05
1.96296E+00	5.82364E+06	2.90725E+00	-7.19327E+05
2.07132E+00	3.98455E+06	3.07715E+00	-6.49424E+05

B A L L   E X C U R S I O N   F R O M   B A L L   P O C K E T   C E N T E R
POSITIVE FOR BALL LEADING THE CAGE

BALL NUMBER	BALL EXCURSION (MM)
1	-0.0319
2	-0.8070
3	-1.4020
4	-1.4858
5	-1.0808
6	-0.5021
7	0.0485
8	0.5709
9	1.1104
10	1.5036
11	1.3845
12	0.7491

```
1ingl001
    30000.0    1    0   -5    00.000000000.000000000.00000000              102
B1        440C              0440C              0     1.00    1.00    0.00 0 BD1
   65.0240            12   0.16000    25.19              0.000
   11.1125
    0.52000    0.55000
    0.0140     0.0140     0.0140     2.00     2.00     2.00
     -1    71.5518    2.4400    0.2290    0.7500    0.0200         1
  0.0356000 -0.066000  33.88000  16.92000  16.92000  33.88000
   19.05000  44.98850  56.41000  73.98000  83.89370  95.50000
0.2342E+060.2127E+060.2127E+060.2127E+060.1932E+06
0.290000000.290000000.290000000.290000000.29000000
    8.19030    7.66700    7.66700    7.66700    8.19030
0.1440E-040.9290E-050.9290E-050.9290E-050.1440E-04
    0.0000     0.0000        0.0000.300000000.100000000.000000000.000000000.00000000
                    1                                        TD2
-145.-145.-145.-145.-145.-145.-145.-145.-145.-145.-145.-145.-145.   0.   0.
 4701.0000     0.0000     0.0000     0.0000 8230.8000                LD1
```

T. J. Chase

PC/SHABERTH BASED MECHANICAL MODEL

File Ref. # singl"M"-op.clear.123um,ball wear 2.5um,thermal

UNLESS OTHERWISE STATED, LINEAR DIMENSIONS ARE SPECIFIED IN MILLIMETERS, TEMPERATURES IN DEGREES CENTIGRADE, FORCES IN NEWTONS, WEIGHTS IN KILOGRAMS, PRESSURES AND ELASTIC MODULI IN NEWTONS PER SQUARE MILLIMETER, ANGLES AND SLOPES IN DEGREES, SURFACE ROUGHNESS IN MICRONS, SPEEDS IN REVOLUTIONS PER MINUTE, DENSITY IN GRAMS PER CUBIC CENTIMETER, KINEMATIC VISCOSITY IN CENTISTOKES AND THERMAL CONDUCTIVITY IN WATTS PER METER-DEGREE CENTIGRADE.

SOLUTION LEVEL = 2
THE MAXIMUM NUMBER OF FIT ITERATIONS ALLOWED IS 5 AND THE RELATIVE ACCURACY REQUIRED IS 0.00010

BEARING NUMBER	NUMBER OF ROLLING ELEMENTS	AZIMUTH ANGLE ORIENTATION	PITCH DIAMETER	DIAMETRAL CLEARANCE	CONTACT ANGLE	INNER RING SPEED	OUTER RING SPEED
1	12	0.000	65.024	0.163	23.310	30000.	0.

C A G E   D A T A

BEARING NUMBER	CAGE TYPE	CAGE POCKET CLEARANCE	RAIL-LAND WIDTH	RAIL-LAND DIAMETER	RAIL-LAND CLEARANCE	WEIGHT
1	OUTER RING LAND RIDING	0.750000	2.4400	71.5518	0.229	0.020000

S T E E L   D A T A

BRG.NO.	INNER RING TYPE	LIFE FACTOR	OUTER RING TYPE	LIFE FACTOR
1	440C	1.000	440C	1.000

R O L L I N G   E L E M E N T   D A T A
BEARING NUMBER (1)   TYPE - BALL BEARING

BALL DIAMETER	OUTER RACEWAY CURVATURE	INNER RACEWAY CURVATURE
11.1100	0.519	0.549

S U R F A C E   D A T A

BEARING NUMBER	CLA ROUGHNESS OUTER	INNER	ROLL. ELM.	RMS ASPERITY SLOPE OUTER	INNER	ROLL. ELM.
1	0.01	0.01	0.01	2.000	2.000	2.000

L U B R I C A T I O N   A N D   F R I C T I O N   D A T A
BEARING 1 IS OPERATING DRY WITH FRICTION COEFFICIENTS OF, RACE/R.E. 0.300 CAGE/R.E. AND CAGE/RING 0.100

F I T   D A T A   A N D   M A T E R I A L   P R O P E R T I E S

BEARING NUMBER	COLD FITS (MM TIGHT) SHAFT	HOUSING	EFFECTIVE WIDTHS SHAFT	INNER RING	OUTER RING	HOUSING
1	0.0356	-0.0660	33.8800	16.9200	16.9200	33.8800

EFFECTIVE DIAMETERS

BEARING NUMBER	SHAFT I.D.	BEARING BORE	INNER RING AVE. O.D.	OUTER RING AVE. I.D.	BEARING O.D.	HOUSING O.D.
1	19.050	44.988	56.410	73.980	83.894	95.500

BEARING NUMBER (1)	SHAFT	INNER RING	ROLL. ELEM.	OUTER RING	HOUSING
MODULUS OF ELASTICITY	234200.0	212700.0	212700.0	212700.0	193200.0
POISSONS RATIO	0.2900	0.2900	0.2900	0.2900	0.2900
WEIGHT DENSITY	8.190	7.667	7.667	7.667	8.190
COEFF. OF THERMAL EXP.	0.00001440	0.00000929	0.00000929	0.00000929	0.00001440

GIVEN TEMPERATURES (C)

BRG	O.RACE	I.RACE	BULK OIL	FLNG.1	FLNG.2	FLNG.3	FLNG.4	CAGE	SHAFT	I.RING	ROLL.EL.	O.RING	HSG.
1	-133.00	-113.00	-145.00	-145.00	-145.00	-145.00	-145.00	-120.00	-120.00	-113.00	-65.00	-133.00	-145.00

LOADING IN THE X - Y PLANE

	CONCENTRATED FORCE, FY	CONCENTRATED MOMENT ABOUT Z	
*	4699.0 NEWTONS		0.0 NEWTON-MM.

LOADING IN THE X - Z PLANE

	CONCENTRATED FORCE, FZ	CONCENTRATED MOMENT ABOUT Y	
*	0.0 NEWTONS		0.0 NEWTON-MM.

THRUST LOAD FX =   8232.0 NEWTONS
**** ERROR MESSAGE FROM THE EQUATION SOLVING ROUTINE, AT ITERATION LOOP   6 **** $F_R = 4755$
**** ERROR MESSAGE FROM THE EQUATION SOLVING ROUTINE, AT ITERATION LOOP   5 ****

B E A R I N G   S Y S T E M   O U T P U T

LINEAR (MM) AND ANGULAR (RADIANS) DEFLECTIONS   REACTION FORCES (N) AND MOMENTS (MM-N)

BRG.	DX	DY	DZ	GY	GZ	FX	FY	FZ	MY	MZ
1	0.135	0.121	4.837E-08	-1.227E-09	4.790E-03	8.225E+03	4.689E+03	787.	-713.	37.0

FATIGUE LIFE (HOURS)   H/SIGMA   LUBE-LIFE FACTOR   MATERIAL FACTOR

BRG.	O. RACE	I. RACE	BEARING	O. RACE	I. RACE	O. RACE	I. RACE	O. RACE	I. RACE
1	47.1	4.86	4.53	0.000	0.000	1.00	1.00	1.00	1.00

TEMPERATURES RELEVANT TO BEARING PERFORMANCE (DEGREES CENTIGRADE)

```
BRG  O.RACE   I.RACE BULK OIL FLNG.1  FLNG.2  FLNG.3 FLNG.4   CAGE     SHAFT    I.RING ROLL.EL.  O.RING   HSG.
 1  -133.00  -113.00 -145.00  -145.00 -145.00 -145.00 -145.00 -120.00  -120.00  -113.00  -65.00  -133.00 -145.00
        FRICTIONAL HEAT GENERATION RATE (WATTS) AND FRICTION TORQUE (N-MM)
BRG.   O. RACE   O. FLNGS. I. RACE   I. FLNGS. R.E.DRAG R.E.-CAGE  CAGE-LAND  TOTAL    TORQUE
 1    2.032E+03  0.000    5.040E+03  0.000    0.000    2.920E+04  0.295     3.628E+04 1.155E+04
EHD FILM THICKNESS, FILM REDUCTION FACTORS AND HEAT CONDUCTIVITY DATA FOR THE OUTER AND INNER RACEWAYS RESPECTIVELY
BRG.  FILM (MICRONS)     STARVATION FACTOR    THERMAL FACTOR    MENISCUS DIST. (MM)  CONDUCTIVITY (W/DEG.C)
 1   0.000     0.000    0.000    0.000     0.000    0.000    0.000     0.000     20.0      13.6
       FIT PRESSURES (N/MM2)                    BEARING CLEARANCES (MM)    SPEED GIVING ZERO FIT PRESSURE
BRG. SHAFT-COLD, OPER.   HSG.-COLD, OPER.   ORIGINAL  CHANGE    OPERATING SHAFT-INNER RING (RPM)
 1   31.7    0.000      0.000    3.98      0.163    -3.955E-02 0.123     1.891E+04
C A G E   D A T A
(CAGE HAS ONE DEGREE OF FREEDOM)
      CAGE RAIL - RING LAND DATA              CAGE SPEED DATA
      TORQUE   HEAT RATE  SEP.FORCE ECCENTRICITY  EPICYCLIC SPEED    CALCULATED SPEED      CALC/EPIC  CAGE/SHAFT
BRG.  (MM-N)   (WATTS)   (NEWTONS)   RATIO     (RAD/SEC)  (RPM)    (RAD/SEC)   (RPM)      RATIO      RATIO
 1   -0.215    0.295    6.049E-02   0.100     1.374E+03 1.312E+04  1.373E+03 1.311E+04   0.999      0.437
R O L L I N G   E L E M E N T   O U T P U T   FOR BEARING NUMBER 1
      AZIMUTH         ANGULAR SPEEDS (RADIANS/SECOND)                  SPEED VECTOR ANGLES (DEGREES)   SPIN TO ROLL RATIO
      ANGLE (DEG.)   WX        WY        WZ       TOTAL      ORBITAL  TAN-1(WY/WX)    TAN-1(WZ/WX)  OUTER    INNER
        0.00      -8668.667  2463.823  -0.247   9012.004   1317.374    164.13         -180.00     0.0046   0.1316
       30.00      -8626.444  2658.358  -0.391   9026.761   1320.550    162.87         -180.00     0.0013   0.1493
       60.00      -8592.034  2966.567  -2.456   9089.751   1338.856    160.95         -179.98     0.0002   0.2344
       90.00      -8887.136  3250.179  -2.787   9462.814   1390.403    159.91         -179.98     0.0063   0.3986
      120.00      -8547.602  4199.339  -0.712   9523.441   1409.614    153.84         -180.00     0.0040   0.4482
      150.00      -7856.861  5278.752  -1.943   9465.490   1421.355    146.10         -179.99     0.0035   0.3936
      180.00      -7580.184  5518.724  -1.007   9376.327   1413.709    143.94         -179.99     0.0075   0.3903
      210.00      -7863.542  5169.855  -0.037   9410.775   1408.188    146.68         -180.00     0.0044   0.4099
      240.00      -8542.487  4172.008  -0.019   9506.826   1411.549    153.97         -180.00     0.0035   0.4520
      270.00      -8784.269  3231.990  -0.032   9359.975   1379.887    159.80         -180.00     0.0038   0.3976
      300.00      -8600.408  2937.726  -0.184   9088.303   1338.246    161.14         -180.00     0.0043   0.2372
      330.00      -8616.725  2627.273  -0.076   9008.357   1322.079    163.04         -180.00     0.0043   0.1520
      AZIMUTH          NORMAL FORCES (NEWTONS)         HZ STRESS (N/MM**2)  LOAD RATIO QASP/QTOT   CONTACT ANGLES (DEG.)
      ANGLE (DEG.)   CAGE      OUTER     INNER       OUTER     INNER      OUTER     INNER       OUTER      INNER
        0.00       6.552    3246.598  2954.212    2567.747  3484.260    0.0000    0.0000      18.7921    20.7086
       30.00     401.454    2541.786  2250.867    2366.587  3182.340    0.0000    0.0000      20.0717    22.7649
       60.00     717.350    1302.656  1012.278    1893.881  2438.165    0.0000    0.0000      22.2564    29.1200
       90.00     776.351     830.580   535.879    1630.059  1972.357    0.0000    0.0000      23.8015    38.7212
      120.00     575.125     934.755   656.434    1695.543  2110.378    0.0000    0.0000      30.6984    46.3625
      150.00     260.069    1257.401  1119.073    1871.690  2521.057    0.0000    0.0000      39.5627    50.3474
      180.00     -70.049    1654.214  1409.527    2050.879  2722.624    0.0000    0.0000      42.2563    51.9830
      210.00    -351.744    1357.507  1104.602    1920.099  2510.143    0.0000    0.0000      38.9443    50.6015
      240.00    -625.493     947.718   666.098    1703.344  2120.684    0.0000    0.0000      30.5323    46.4286
      270.00    -795.160     829.768   536.463    1629.528  1973.073    0.0000    0.0000      23.8009    38.7213
      300.00    -695.242    1301.609  1012.249    1893.374  2438.142    0.0000    0.0000      22.2701    29.1145
      330.00    -382.722    2542.398  2250.980    2366.777  3182.393    0.0000    0.0000      20.0521    22.7729
       F R I C T I O N A L   H E A T   G E N E R A T I O N   I N   C O N T A C T   E L L I P S E
                     R O L L I N G   E L E M E N T   N U M B E R   1
            I N N E R   R A C E                           O U T E R   R A C E
# LAMINA   CONTACT AREA   SEMI-MAJOR   SEMI-MINOR     # LAMINA    CONTACT AREA   SEMI-MAJOR   SEMI-MINOR
           (MM**2)        AXIS (MM)    AXIS (MM)                  (MM**2)        AXIS (MM)    AXIS (MM)
  20        1.272          1.484        0.2728          20         1.897          2.154        0.2803
      WIDTH OF LAMINUM        HEAT GEN. PER LAM.        WIDTH OF LAMINUM        HEAT GEN. PER LAM.
           (MM)                  (WATTS)                    (MM)                  (WATTS)
        0.0350268400            0.001                  0.2074940000            17.949
        0.1547233000            0.259                  0.2074940000            40.192
        0.1547233000            4.022                  0.2074940000            48.206
        0.1547233000           10.370                  0.2074940000            46.176
        0.1547233000           16.389                  0.2074940000            37.651
        0.1547233000           20.570                  0.2074940000            25.518
        0.1547233000           21.725                  0.2074940000            11.389
        0.1547233000           18.978                  0.2074940000             0.947
        0.1547233000           11.265                  0.2339875000             0.882
        0.1547233000            1.650                  0.2339875000             4.151
        0.1540679000            2.043                  0.2339875000             4.169
        0.1540679000           19.279                  0.2339875000             0.893
        0.1540679000           38.325                  0.2139724000             1.067
        0.1540679000           56.756                  0.2139724000            12.849
        0.1540679000           73.055                  0.2139724000            28.182
        0.1540679000           84.937                  0.2139724000            41.616
```

100

0.1540679000	89.654	0.2139724000	51.170
0.1540679000	84.032	0.2139724000	53.564
0.1540679000	64.466	0.2139724000	44.774
0.1540679000	26.912	0.2139724000	20.043

```
         M A X I M U M   S T R E S S * V E L O C I T Y   I N   C O N T A C T   E L L I P S E
    BEARING NUMBER   ELEMENT NUMBER   STRESS VELOCITY (N/MM-S)   ELEMENT NUMBER   STRESS VELOCITY (N/MM-S)
                                          INNER RACE                                 OUTER RACE
          1                8            -1.00304E+09                    6            2.30774E+09
            S T R E S S   V E L O C I T Y   P R O F I L E   I N   C O N T A C T   E L L I P S E
                          R O L L I N G   E L E M E N T   N U M B E R    8
              LAMINA POSITION FROM LOWER CONTACT ANGLE EDGE OF CONTACT ELLIPSE
```

INNER RACE		OUTER RACE	
LAMINA POSITION (MM)	STRESS VELOCITY (N/MM-S)	LAMINA POSITION (MM)	STRESS VELOCITY (N/MM-S)
5.49967E-02	-2.36192E+06	8.30503E-02	-9.46567E+05
1.64990E-01	-3.62085E+06	2.49151E-01	-1.24100E+06
2.74984E-01	-4.05333E+06	4.15251E-01	-1.16853E+06
3.84977E-01	-4.04934E+06	5.81352E-01	-9.59135E+05
4.94970E-01	-3.73790E+06	7.47452E-01	-7.02065E+05
6.04964E-01	-3.18827E+06	9.13553E-01	-4.47138E+05
7.14957E-01	-2.44769E+06	1.07965E+00	-2.25892E+05
8.24951E-01	-1.55393E+06	1.24575E+00	-5.88608E+04
9.34944E-01	-5.40935E+05	1.43942E+00	5.03953E+04
1.04214E+00	5.29538E+05	1.66064E+00	5.04629E+04
1.14655E+00	1.62045E+06	1.84729E+00	-5.34597E+04
1.25095E+00	2.72691E+06	1.99937E+00	-2.02892E+05
1.35535E+00	3.81283E+06	2.15145E+00	-4.01076E+05
1.45975E+00	4.83584E+06	2.30353E+00	-6.34237E+05
1.56416E+00	5.74408E+06	2.45561E+00	-8.82060E+05
1.66856E+00	6.47051E+06	2.60769E+00	-1.11455E+06
1.77296E+00	6.92240E+06	2.75977E+00	-1.28485E+06
1.87737E+00	6.95664E+06	2.91185E+00	-1.30896E+06
1.98177E+00	6.30707E+06	3.06393E+00	-9.66340E+05
2.08617E+00	4.20779E+06	3.21790E+00	-9.78820E+05

```
            B A L L   E X C U R S I O N   F R O M   B A L L   P O C K E T   C E N T E R
                          POSITIVE FOR BALL LEADING THE CAGE
```

BALL NUMBER	BALL EXCURSION (MM)
1	-0.0110
2	-0.6769
3	-1.2095
4	-1.3090
5	-0.9697
6	-0.4385
7	0.1181
8	0.5931
9	1.0546
10	1.3407
11	1.1722
12	0.6453

```
1ingl001
    30000.0    1    0   -5   `00.000000000.000000000.00000000                    102
B1       440C            0440C            0        1.00    1.00    0.00 0  BD1
    65.0240        12   0.16300    23.31            0.000
    11.1100
    0.51900    0.54900
    0.0140     0.0140     0.0140     2.00      2.00      2.00
      -1      71.5518    2.4400    0.2290    0.7500    0.0200        1
0.0356000 -0.066000 33.88000  16.92000  16.92000  33.88000
 19.05000  44.98850  56.41000  73.98000  83.89370  95.50000
0.2342E+060.2127E+060.2127E+060.2127E+060.1932E+06
0.290000000.290000000.290000000.290000000.29000000
   8.19030   7.66700   7.66700   7.66700   8.19030
0.1440E-040.9290E-050.9290E-050.9290E-050.1440E-04
    0.0000    0.0000     0.0000.300000000.100000000.000000000.000000000.00000000
            1                                                        TD2
-133.-113.-145.-145.-145.-145.-145.-120.-120.-113. -65.-133.-145.  0.  0.
 4699.0000    0.0000    0.0000    0.0000 8232.0000                  LD1
```

T. J. Chase

PC/SHABERTH BASED MECHANICAL MODEL

File Ref. # singl"M'", heavily worn, thermal

UNLESS OTHERWISE STATED, LINEAR DIMENSIONS ARE SPECIFIED IN MILLIMETERS, TEMPERATURES IN DEGREES CENTIGRADE, FORCES IN NEWTONS, WEIGHTS IN KILOGRAMS, PRESSURES AND ELASTIC MODULI IN NEWTONS PER SQUARE MILLIMETER, ANGLES AND SLOPES IN DEGREES, SURFACE ROUGHNESS IN MICRONS, SPEEDS IN REVOLUTIONS PER MINUTE, DENSITY IN GRAMS PER CUBIC CENTIMETER, KINEMATIC VISCOSITY IN CENTISTOKES AND THERMAL CONDUCTIVITY IN WATTS PER METER-DEGREE CENTIGRADE.

SOLUTION LEVEL = 2
THE MAXIMUM NUMBER OF FIT ITERATIONS ALLOWED IS 5 AND THE RELATIVE ACCURACY REQUIRED IS 0.00010

NUMBER	ROLLING ELEMENTS	ANGLE ORIENTATION	DIAMETER	CLEARANCE	ANGLE	SPEED	SPEED
1	12	0.000	65.024	0.160	25.300	30000.	0.

C A G E   D A T A

BEARING NUMBER	CAGE TYPE	CAGE POCKET CLEARANCE	RAIL-LAND WIDTH	RAIL-LAND DIAMETER	RAIL-LAND CLEARANCE	WEIGHT
1	OUTER RING LAND RIDING	0.750000	2.4400	71.5518	0.229	0.020000

S T E E L   D A T A

BRG.NO.	INNER RING TYPE	LIFE FACTOR	OUTER RING TYPE	LIFE FACTOR
1	440C	1.000	440C	1.000

R O L L I N G   E L E M E N T   D A T A
BEARING NUMBER (1)   TYPE - BALL BEARING

BALL DIAMETER	OUTER RACEWAY CURVATURE	INNER RACEWAY CURVATURE
11.1085	0.515	0.540

S U R F A C E   D A T A

BEARING NUMBER	CLA ROUGHNESS			RMS ASPERITY SLOPE		
	OUTER	INNER	ROLL. ELM.	OUTER	INNER	ROLL. ELM.
1	0.01	0.01	0.01	2.000	2.000	2.000

L U B R I C A T I O N   A N D   F R I C T I O N   D A T A
BEARING 1 IS OPERATING DRY WITH FRICTION COEFFICIENTS OF, RACE/R.E. 0.300 CAGE/R.E. AND CAGE/RING 0.100

F I T   D A T A   A N D   M A T E R I A L   P R O P E R T I E S

BEARING NUMBER	COLD FITS (MM TIGHT)		EFFECTIVE WIDTHS			
	SHAFT	HOUSING	SHAFT	INNER RING	OUTER RING	HOUSING
1	0.0356	-0.0660	33.8800	16.9200	16.9200	33.8800

EFFECTIVE DIAMETERS

BEARING NUMBER	SHAFT I.D.	BEARING BORE	INNER RING AVE. O.D.	OUTER RING AVE. I.D.	BEARING O.D.	HOUSING O.D.
1	19.050	44.988	56.410	73.980	83.894	95.500

BEARING NUMBER (1)

	SHAFT	INNER RING	ROLL. ELEM.	OUTER RING	HOUSING
MODULUS OF ELASTICITY	234200.0	212700.0	212700.0	212700.0	193200.0
POISSONS RATIO	0.2900	0.2900	0.2900	0.2900	0.2900
WEIGHT DENSITY	8.190	7.667	7.667	7.667	8.190
COEFF. OF THERMAL EXP.	0.00001440	0.00000929	0.00000929	0.00000929	0.00001440

GIVEN TEMPERATURES (C)

BRG	O.RACE	I.RACE	BULK OIL	FLNG.1	FLNG.2	FLNG.3	FLNG.4	CAGE	SHAFT	I.RING	ROLL.EL.	O.RING	HSG.
1	-133.00	-113.00	-145.00	-145.00	-145.00	-145.00	-145.00	-120.00	-120.00	-113.00	-65.00	-133.00	-145.00

LOADING IN THE X - Y PLANE

*   CONCENTRATED FORCE, FY   CONCENTRATED MOMENT ABOUT Z
                      4735.0 NEWTONS
                                                                                          0.0 NEWTON-MM.
LOADING IN THE X - Z PLANE

*   CONCENTRATED FORCE, FZ   CONCENTRATED MOMENT ABOUT Y
                      0.0 NEWTONS
                                                                                          0.0 NEWTON-MM.
THRUST LOAD FX =   5850.0 NEWTONS
**** ERROR MESSAGE FROM THE EQUATION SOLVING ROUTINE, AT ITERATION LOOP   3 ****
    THIS IS THE BEST WE CAN DO. IT MAY BE USEABLE.
    REL. ACCURACY 0.000100, ITERATION LIMIT 200 NUMBER OF UNKNOWNS   6
    ABSOLUTE ACCURACIES
          4.37342500E-07   4.37342500E-07   0.31415930   0.31415930   3.14159300E-02
          3.14159300E-02
    DAMPING FACTORS 1-5, OTHER STEP FACTORS 6-10
          1.0000000   1.0000000   1.0000000   1.0000000   1.0000000
          5.00000000E-04   1.00000000E-03   1.00000000E-06   0.10000000   1.00000000E-05
    MAXIMUM STEP FACTORS

```
U.10000000
CORRECTIONS OF THE X-ES FROM SIMQ
    0.13354410E-03 -0.31987950E-04  0.80727210E+03 -0.17866640E+04  0.15089600E+00  0.18040670E+03
NUMBER OF DERIVATIVES EXPECTED FOR EACH X
          -1           -1           -1           -1          -1          -1
X-VALUES
    0.20698840E-02  0.70372770E-02 -0.87402610E+04  0.21413380E+04 -0.25704960E+00  0.13153970E+04
CORRESPONDING EQ-VALUES
   -0.51844310E+00  0.12201910E+00  0.27360580E+03 -0.20542520E+01  0.21283190E+01 -0.17681570E+01
**** ERROR MESSAGE FROM THE EQUATION SOLVING ROUTINE, AT ITERATION LOOP   4 ****
THIS IS THE BEST WE CAN DO.  IT MAY BE USEABLE.
REL. ACCURACY 0.000100, ITERATION LIMIT 200 NUMBER OF UNKNOWNS  73
ABSOLUTE ACCURACIES
        4.37342500E-07        4.37342500E-07     0.31415930           0.31415930          3.14159300E-02
        3.14159300E-02        4.37342500E-07     4.37342500E-07       0.31415930           0.31415930
        3.14159300E-02        3.14159300E-02     4.37342500E-07       4.37342500E-07       0.31415930
        0.31415930            3.14159300E-02     3.14159300E-02       4.37342500E-07       4.37342500E-07
        0.31415930            0.31415930         3.14159300E-02       3.14159300E-02       4.37342500E-07
        4.37342500E-07        0.31415930         0.31415930           3.14159300E-02       3.14159300E-02
        4.37342500E-07        4.37342500E-07     0.31415930           0.31415930           3.14159300E-02
        3.14159300E-02        4.37342500E-07     4.37342500E-07       0.31415930           0.31415930
        3.14159300E-02        3.14159300E-02     4.37342500E-07       4.37342500E-07       0.31415930
        0.31415930            3.14159300E-02     3.14159300E-02       4.37342500E-07       4.37342500E-07
        0.31415930            0.31415930         3.14159300E-02       3.14159300E-02       4.37342500E-07
        4.37342500E-07        0.31415930         0.31415930           3.14159300E-02       3.14159300E-02
        4.37342500E-07        4.37342500E-07     0.31415930           0.31415930           3.14159300E-02
        3.14159300E-02        4.37342500E-07     4.37342500E-07       0.31415930           0.31415930
        3.14159300E-02        3.14159300E-02     3.85433100E-06
DAMPING FACTORS 1-5, OTHER STEP FACTORS 6-10
        1.0000000             1.0000000          1.0000000            1.0000000            1.0000000
        5.00000000E-04        1.00000000E-03     1.00000000E-06       0.10000000           1.00000000E-05
MAXIMUM STEP FACTORS
        0.10000000            0.10000000         0.10000000           1.0000000            1.0000000
        0.10000000            0.10000000         0.10000000           0.10000000           1.0000000
        1.0000000             0.10000000         0.10000000           0.10000000           0.10000000
        1.0000000             1.0000000          0.10000000           0.10000000           0.10000000
        0.10000000            1.0000000          1.0000000            0.10000000           0.10000000
        0.10000000            0.10000000         1.0000000            1.0000000            0.10000000
        0.10000000            0.10000000         0.10000000           1.0000000            1.0000000
        0.10000000            0.10000000         0.10000000           0.10000000           1.0000000
        1.0000000             0.10000000         0.10000000           0.10000000           0.10000000
        1.0000000             1.0000000          0.10000000           0.10000000           0.10000000
        0.10000000            1.0000000          1.0000000            0.10000000           0.10000000
        0.10000000            0.10000000         1.0000000            1.0000000            0.10000000
        0.10000000            0.10000000         0.10000000           1.0000000            1.0000000
        0.10000000            0.10000000         0.10000000           0.10000000           1.0000000
        1.0000000             0.10000000         0.10000000
CORRECTIONS OF THE X-ES FROM SIMQ
   -0.76636580E-06  0.93931020E-07 -0.27232920E+03 -0.13733530E+04  0.56528850E-01 -0.79875860E+01
   -0.10869850E-02  0.37811370E-03 -0.15512780E+04  0.89105820E+03 -0.16906240E+03  0.16033200E+03
    0.20927650E-02 -0.10244190E-02  0.77037960E+04 -0.14539900E+04 -0.80215570E+02 -0.10081070E+04
   -0.80525970E-03  0.58929240E-03 -0.20907520E+05 -0.12519760E+04  0.12708710E-02  0.93362810E+03
    0.16434570E-03 -0.41102280E-03  0.58080430E+04  0.50529380E+04 -0.71589620E+03 -0.13955130E+04
    0.82024600E-02 -0.83580420E-02  0.78168720E+04  0.93560580E+04  0.43923380E+01  0.92764920E+03
    0.45051720E-03 -0.59222970E-03  0.26060890E+04 -0.33576930E+04  0.21888820E-01 -0.66080940E+03
    0.10211940E-04 -0.17662990E-04 -0.35044770E+04 -0.37615760E+04  0.19378450E-01 -0.81257240E+02
    0.53461450E-03 -0.47624230E-03  0.35395490E+04 -0.46142740E+03 -0.45603790E+02 -0.88302560E+03
   -0.53851960E-05  0.13958710E-04 -0.20480650E+04 -0.18949890E+04 -0.15138840E+02  0.10552830E+03
    0.97506710E-03 -0.46485430E-03  0.38711450E+04 -0.13447140E+04 -0.26822040E+02 -0.76681150E+03
    0.21134460E-03 -0.68739600E-04  0.49399040E+03 -0.14192550E+04  0.31570350E+00  0.77544430E+02
   -0.10345540E-01
NUMBER OF DERIVATIVES EXPECTED FOR EACH X
        -1        -1        -1        -1        -1        -1        -1        -1        -1        -1
        -1        -1        -1        -1        -1        -1        -1        -1        -1        -1
        -1        -1        -1        -1        -1        -1        -1        -1        -1        -1
        -1        -1        -1        -1        -1        -1        -1        -1        -1        -1
        -1        -1        -1        -1        -1        -1        -1        -1        -1        -1
        -1        -1        -1        -1        -1        -1        -1        -1        -1        -1
```

103

```
U.20004250E-02   U.70383260E-02  -0.87220680E+04   0.21558360E+04  -0.87544100E-01   0.13151350E+04
0.22052130E-02   0.68257590E-02  -0.87228570E+04   0.23615250E+04  -0.11725190E+01   0.13161240E+04
0.21114250E-02   0.65373960E-02  -0.89030510E+04   0.24239490E+04  -0.15848230E+00   0.13529900E+04
0.19576660E-02   0.65217200E-02  -0.96484240E+04   0.24493530E+04  -0.18157410E-02   0.14497730E+04
0.30126050E-02   0.61474760E-02  -0.94006230E+04   0.38470850E+04  -0.14781220E+01   0.14894790E+04
0.43265050E-02   0.54135680E-02  -0.81719790E+04   0.54108330E+04  -0.53092510E+01   0.14624740E+04
0.48944170E-02   0.49892270E-02  -0.75431590E+04   0.59782930E+04  -0.22128720E-01   0.14481530E+04
0.43529490E-02   0.53860460E-02  -0.81337660E+04   0.53616890E+04  -0.22061830E-01   0.14621030E+04
0.30205070E-02   0.61408390E-02  -0.92556840E+04   0.38400770E+04  -0.40336340E+00   0.14800580E+04
0.19533220E-02   0.65248400E-02  -0.95894280E+04   0.24214150E+04  -0.57804080E-01   0.14499390E+04
0.21220090E-02   0.65321820E-02  -0.88271430E+04   0.24173570E+04  -0.14739850E+00   0.13441630E+04
0.22003980E-02   0.68277160E-02  -0.86918570E+04   0.23519320E+04  -0.34284480E+00   0.13175980E+04
0.60444180E-04
CORRESPONDING EQ-VALUES
-0.20197850E-01   0.84233690E-02   0.27142670E+03   0.99532680E+00   0.15376160E+01  -0.17445220E+01
-0.12476490E+01   0.80315050E+00   0.35118610E+03  -0.76890810E+00   0.14467410E+01  -0.18524010E+01
 0.40427150E-01   0.30698590E+00   0.31871790E+03  -0.29010790E+00   0.14092850E+01  -0.19843660E+01
 0.50650880E-01   0.11782910E+01   0.31188300E+03   0.22525730E+01   0.81138800E+00  -0.21340170E+01
-0.38437580E-01   0.64270390E+00   0.22843800E+03   0.24625490E+01   0.14681620E+01  -0.33644840E+01
 0.15204280E+01  -0.10732630E+01   0.15453420E+03   0.13009180E+01   0.34247870E+01  -0.44987670E+01
 0.84490890E-01   0.37332610E+00   0.10805630E+03   0.98220150E+00   0.40530420E+01  -0.52017740E+01
 0.31792340E-01   0.47985160E-01  -0.76601870E+01   0.35446380E+00   0.39347360E+01  -0.47140970E+01
 0.11423330E+00   0.54334360E-01  -0.14858720E+03   0.84224640E+00   0.22184730E+01  -0.34397290E+01
 0.56525240E-02   0.88203050E-01  -0.25426050E+03   0.12470050E+01   0.11174560E+01  -0.21158510E+01
-0.20059100E-01   0.50307030E+00  -0.21115330E+03   0.10011600E+01   0.99465260E+00  -0.19724600E+01
-0.23875220E+00   0.78179520E-01   0.40281460E+02  -0.28558710E+01   0.22368070E+01  -0.19150120E+01
 0.93154830E+02
```

B E A R I N G   S Y S T E M   O U T P U T

$F_{Z} = 4774$

```
         LINEAR (MM) AND ANGULAR (RADIANS) DEFLECTIONS        REACTION FORCES (N) AND MOMENTS (MM-N)
BRG.    DX      DY        DZ        GY        GZ        FX        FY        FZ        MY        MZ
 1   9.530E-02 0.130   4.345E-08 -7.662E-11 4.820E-03 5.855E+03 4.716E+03  739.     -224.     490.
        FATIGUE LIFE (HOURS)          H/SIGMA          LUBE-LIFE FACTOR     MATERIAL FACTOR
BRG.  O. RACE   I. RACE  BEARING   O. RACE   I. RACE  O. RACE  I. RACE  O. RACE  I. RACE
 1     85.1      9.01     8.39     0.000     0.000     1.00     1.00     1.00     1.00
        TEMPERATURES RELEVANT TO BEARING PERFORMANCE (DEGREES CENTIGRADE)
BRG  O.RACE  I.RACE BULK OIL FLNG.1  FLNG.2  FLNG.3 FLNG.4   CAGE    SHAFT   I.RING ROLL.EL.  O.RING   HSG.
 1  -133.00 -113.00 -145.00 -145.00 -145.00 -145.00 -145.00 -120.00 -120.00 -113.00  -65.00 -133.00 -145.00

        FRICTIONAL HEAT GENERATION RATE (WATTS) AND FRICTION TORQUE (N-MM)
BRG.  O. RACE  O. FLNGS. I. RACE   I. FLNGS. R.E.DRAG R.E.-CAGE  CAGE-LAND  TOTAL    TORQUE
 1   1.860E+03 0.000   3.970E+03 0.000    0.000    4.567E+04  0.303    5.150E+04 1.639E+04
EHD FILM THICKNESS, FILM REDUCTION FACTORS AND HEAT CONDUCTIVITY DATA FOR THE OUTER AND INNER RACEWAYS RESPECTIVELY
BRG.  FILM (MICRONS)     STARVATION FACTOR    THERMAL FACTOR ' MENISCUS DIST. (MM)  CONDUCTIVITY (W/DEG.C)
 1   0.000    0.000    0.000    0.000    0.000    0.000    0.000    0.000    17.7     11.1
        FIT PRESSURES (N/MM2)                   BEARING CLEARANCES (MM)    SPEED GIVING ZERO FIT PRESSURE
BRG. SHAFT-COLD, OPER.  HSG.-COLD, OPER.  ORIGINAL  CHANGE  OPERATING SHAFT-INNER RING (RPM)
 1   31.7    0.000    0.000    3.59     0.160  -4.222E-02 0.118     1.250E+04
C A G E   D A T A
(CAGE HAS ONE DEGREE OF FREEDOM)
        CAGE RAIL - RING LAND DATA            CAGE SPEED DATA
        TORQUE  HEAT RATE SEP.FORCE ECCENTRICITY EPICYCLIC SPEED    CALCULATED SPEED    CALC/EPIC CAGE/SHAFT
BRG.    (MM-N)  (WATTS)   (NEWTONS)  RATIO    (RAD/SEC)  (RPM)    (RAD/SEC)  (RPM)      RATIO     RATIO
 1     -0.215   0.303    6.049E-02  0.100    1.410E+03 1.347E+04  1.407E+03 1.344E+04  0.998     0.448
```

R O L L I N G   E L E M E N T   O U T P U T   FOR BEARING NUMBER 1

```
  AZIMUTH         ANGULAR SPEEDS (RADIANS/SECOND)              SPEED VECTOR ANGLES (DEGREES)    SPIN TO ROLL RATIO
ANGLE (DEG.)    WX        WY        WZ       TOTAL     ORBITAL  TAN-1(WY/WX)  TAN-1(WZ/WX)    OUTER    INNER
    0.00    -8722.068  2155.836   -0.088   8984.548  1315.135    166.12        -180.00       0.0023   0.1150
   30.00    -8722.857  2361.525   -1.173   9036.871  1316.124    164.85        -179.99       0.0038   0.1412
   60.00    -8903.051  2423.949   -0.158   9227.125  1352.990    164.77        -180.00       0.0017   0.3037
   90.00    -9648.424  2449.353   -0.002   9954.467  1449.773    165.76        -180.00       0.0013   0.5986
  120.00    -9400.623  3847.085   -1.478  10157.350  1489.479    157.74        -179.99       0.0030   0.6654
  150.00    -8171.979  5410.833   -5.309   9800.938  1462.474    146.49        -179.96       -.0044   0.5509
  180.00    -7543.159  5978.293   -0.022   9624.928  1448.153    141.60        -180.00       0.0001   0.4851
  210.00    -8133.766  5361.689   -0.022   9741.964  1462.103    146.61        -180.00       0.0028   0.5510
  240.00    -9255.684  3840.077   -0.403  10020.670  1480.058    157.47        -180.00       -.0016   0.6599
  270.00    -9589.428  2421.415   -0.058   9890.418  1449.939    165.83        -180.00       0.0017   0.6007
```

AZIMUTH	NORMAL FORCES (NEWTONS)			HZ STRESS (N/MM**2)		LOAD RATIO QASP/QTOT		CONTACT ANGLES (DEG.)	
ANGLE (DEG.)	CAGE	OUTER	INNER	OUTER	INNER	OUTER	INNER	OUTER	INNER
...	...	...	-0.141	9152.101	1344.105	164.66	-180.00	0.0016	0.5021
330.00	-8691.857	2351.932	-0.343	9004.441	1317.598	164.86	-180.00	0.0030	0.1417
0.00	0.911	3132.797	2837.124	2432.648	3291.686	0.0000	0.0000	16.3620	18.1103
30.00	658.799	2202.682	1911.996	2163.146	2885.944	0.0000	0.0000	17.9042	20.6585
60.00	1180.900	791.278	491.268	1537.723	1834.700	0.0000	0.0000	17.8992	29.6649
90.00	1223.592	570.489	240.417	1378.852	1445.820	0.0000	0.0000	16.7085	43.0913
120.00	776.689	701.332	389.038	1477.099	1697.421	0.0000	0.0000	26.1074	52.8317
150.00	284.229	1032.480	776.641	1680.334	2137.301	0.0000	0.0000	38.6317	57.6266
180.00	-59.991	1289.464	1056.275	1809.554	2368.015	0.0000	0.0000	44.4504	58.7892
210.00	-402.882	1012.086	754.358	1669.197	2116.661	0.0000	0.0000	38.9448	57.5068
240.00	-860.217	692.241	383.674	1470.689	1689.583	0.0000	0.0000	26.1913	52.7992
270.00	-1273.919	576.480	241.800	1383.661	1448.586	0.0000	0.0000	16.6660	43.1085
300.00	-1200.160	784.776	489.470	1533.500	1832.458	0.0000	0.0000	17.9966	29.6270
330.00	-651.686	2204.747	1911.459	2163.822	2885.674	0.0000	0.0000	17.8628	20.6749

F R I C T I O N A L   H E A T   G E N E R A T I O N   I N   C O N T A C T   E L L I P S E
R O L L I N G   E L E M E N T   N U M B E R   1

	INNER RACE				OUTER RACE		
# LAMINA	CONTACT AREA (MM**2)	SEMI-MAJOR AXIS (MM)	SEMI-MINOR AXIS (MM)	# LAMINA	CONTACT AREA (MM**2)	SEMI-MAJOR AXIS (MM)	SEMI-MINOR AXIS (MM)
20	1.293	1.582	0.2602	21	1.932	2.330	0.2639

WIDTH OF LAMINUM (MM)	HEAT GEN. PER LAM. (WATTS)	WIDTH OF LAMINUM (MM)	HEAT GEN. PER LAM. (WATTS)
0.1786409000	2.385	0.2249388000	21.922
0.1786409000	0.669	0.2249388000	49.798
0.1624784000	0.567	0.2249388000	61.029
0.1624784000	4.659	0.2249388000	60.482
0.1624784000	9.941	0.2249388000	52.282
0.1624784000	12.763	0.2249388000	39.855
0.1624784000	12.104	0.2249388000	25.911
0.1624784000	7.017	0.2249388000	11.927
0.1624784000	1.121	0.2249388000	2.073
0.1516899000	1.212	0.2249388000	0.065
0.1516899000	13.171	0.1340418000	0.001
0.1516899000	28.536	0.2275760000	0.068
0.1516899000	43.884	0.2275760000	2.202
0.1516899000	58.524	0.2275760000	12.651
0.1516899000	70.954	0.2275760000	27.093
0.1516899000	79.300	0.2275760000	41.617
0.1516899000	81.371	0.2275760000	54.598
0.1516899000	74.655	0.2275760000	63.189
0.1516899000	56.319	0.2275760000	63.793
0.1516899000	23.194	0.2275760000	52.081
0.0000000000	0.000	0.2275760000	22.940

M A X I M U M   S T R E S S * V E L O C I T Y   I N   C O N T A C T   E L L I P S E

BEARING NUMBER	ELEMENT NUMBER	STRESS VELOCITY (N/MM-S) INNER RACE	ELEMENT NUMBER	STRESS VELOCITY (N/MM-S) OUTER RACE
1	6	1.12404E+10	8	-1.18030E+10

S T R E S S   V E L O C I T Y   P R O F I L E   I N   C O N T A C T   E L L I P S E
R O L L I N G   E L E M E N T   N U M B E R   6
LAMINA POSITION FROM LOWER CONTACT ANGLE EDGE OF CONTACT ELLIPSE

	INNER RACE		OUTER RACE
LAMINA POSITION (MM)	STRESS VELOCITY (N/MM-S)	LAMINA POSITION (MM)	STRESS VELOCITY (N/MM-S)
5.21883E-02	-3.06789E+06	8.19662E-02	-9.15315E+05
1.56565E-01	-4.72015E+06	2.45899E-01	-1.21799E+06
2.60941E-01	-5.32757E+06	4.09831E-01	-1.17004E+06
3.65318E-01	-5.40168E+06	5.73763E-01	-9.88043E+05
4.69694E-01	-5.11248E+06	7.37696E-01	-7.55334E+05
5.74071E-01	-4.55019E+06	9.01628E-01	-5.18442E+05
6.78447E-01	-3.77482E+06	1.06556E+00	-3.06827E+05
7.82824E-01	-2.83257E+06	1.22949E+00	-1.39983E+05
8.87200E-01	-1.76297E+06	1.39343E+00	-3.06322E+04
9.91577E-01	-6.02750E+05	1.58298E+00	1.46770E+04
1.09427E+00	5.91865E+05	1.77426E+00	-3.15232E+04
1.19528E+00	1.78289E+06	1.94163E+00	-1.45044E+05
1.29630E+00	2.95171E+06	2.10901E+00	-3.19083E+05
1.39731E+00	4.05503E+06	2.27639E+00	-5.40509E+05
1.49832E+00	5.04086E+06	2.44377E+00	-7.88970E+05
1.59933E+00	5.84319E+06	2.61115E+00	-1.03355E+06

```
      1.70034E+00              6.37170E+06                      2.77853E+00                 -1.22542E+06
      1.80136E+00              6.48823E+06                      2.94590E+00                 -1.27695E+06
      1.90237E+00              5.93739E+06                      3.11328E+00                 -9.60485E+05
      2.00338E+00              3.98750E+06                      3.27828E+00                 -9.53132E+05
      2.06903E+00              2.85154E+04                      3.43572E+00                 -9.23879E+05
```

B A L L   E X C U R S I O N   F R O M   B A L L   P O C K E T   C E N T E R

POSITIVE FOR BALL LEADING THE CAGE

BALL NUMBER	BALL EXCURSION (MM)
1	-0.0015
2	-1.1108
3	-1.9911
4	-2.0631
5	-1.3096
6	-0.4792
7	0.1011
8	0.6793
9	1.4504
10	2.1479
11	2.0236
12	1.0988

```
Input data "card":
1ingl001
    30000.0    1    0    -5    00.000000000.000000000.00000000                            102
B1        440C                 0440C                0      1.00    1.00    0.00 0  BD1
    65.0240         12   0.16000     25.30                0.000
    11.1085
     0.51500    0.54000
     0.0140     0.0140     0.0140   -  2.00      2.00      2.00
        -1     71.5518     2.4400     0.2290    0.7500    0.0200          1
 0.0356000 -0.066000   33.88000   16.92000   16.92000   33.88000
   19.05000   44.98850   56.41000   73.98000   83.89370   95.50000
0.2342E+060.2127E+060.2127E+060.2127E+060.1932E+06
0.290000000.290000000.290000000.290000000.29000000
    8.19030    7.66700    7.66700    7.66700    8.19030
0.1440E-040.9290E-050.9290E-050.9290E-050.1440E-04
     0.0000     0.0000     0.0000.300000000.100000000.000000000.000000000.00000000
                      1
 -133.-113.-145.-145.-145.-145.-145.-120.-120.-113. -65.-133.-145.   0.   0.               TD2
  4735.0000    0.0000     0.0000     0.0000 5850.0000                                       LD1
```

APPROVAL

DETAILED STUDY OF OXIDATION/WEAR MECHANISM IN LOX TURBOPUMP BEARINGS

By T.J. Chase and J.P. McCarty

The information in this report has been reviewed for technical content. Review of any information concerning Department of Defense or nuclear energy activities or programs has been made by the MSFC Security Classification Officer. This report, in its entirety, has been determined to be unclassified.

J.P. MCCARTY
Director, Propulsion Laboratory